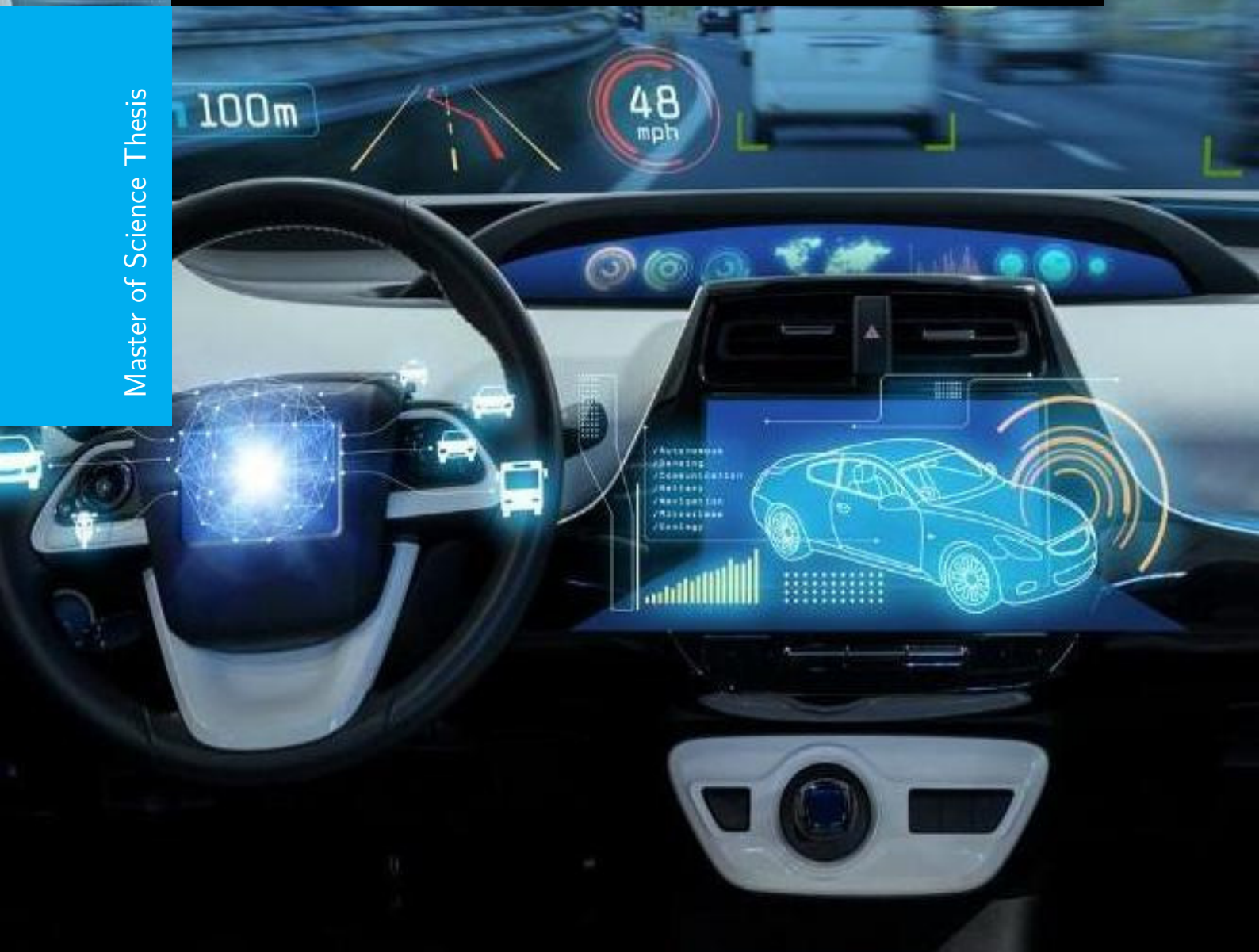


Automatic Steering Control for Path Following Vehicles

with a focus on higher order sliding mode control

A. Pandit

Master of Science Thesis



Automatic Steering Control for Path Following Vehicles

with a focus on higher order sliding mode control

MASTER OF SCIENCE THESIS

For the degree of Master of Science in Mechanical Engineering at Delft
University of Technology

A. Pandit

August 26, 2019

Faculty of Mechanical, Maritime and Materials Engineering (3mE) · Delft University of
Technology



DELFT UNIVERSITY OF TECHNOLOGY
DEPARTMENT OF COGNITIVE ROBOTICS (CoR)

The undersigned hereby certify that they have read and recommend to the Faculty of
Mechanical, Maritime and Materials Engineering (3mE) for acceptance a thesis
entitled

AUTOMATIC STEERING CONTROL FOR PATH FOLLOWING VEHICLES

by

A. PANDIT

in partial fulfillment of the requirements for the degree of
MASTER OF SCIENCE MECHANICAL ENGINEERING

Dated: August 26, 2019

Supervisor(s):

dr. Barys Shyrokau

ir. Yanggu Zheng

Reader(s):

prof.dr.ir. Martijn Wisse

dr.ir. Riender Happee

Abstract

Among the trends that are going to shape the automotive industry in the coming years, autonomous vehicles stand out as having the potential to completely change the automotive industry as we know it. One of the critical tasks in this framework includes robust execution of the steering control action to maintain a pre-defined path.

The main shortcomings of the state of the art steering controllers are controller robustness, cross-comparison and performance validation. To address this aspect, firstly, this study focuses on implementing a sensor model that geometrically measures the lateral and the heading error of the vehicle with respect to the path. Secondly, the focus was to implement existing lateral controllers like Stanley, Path Control with Preview (PCwP), Linear Quadratic Regulator (LQR), Immersion and Invariance (II), Passivity Based Control (PBC) and evaluate path-tracking performance.

The Sliding Mode Control (SMC) methodology has proven effective in dealing with complex dynamical systems affected by disturbances, uncertainties and unmodeled dynamics. However, the application of SMC and its algorithms to lateral control in vehicles is not effectively analysed. Finally, this master thesis includes a novel design of three variants of Sliding Mode Control; namely Sliding Mode Control with Super Twisting Algorithm, Modified Super Twisting Algorithm and Non-singular Terminal Modified Super Twisting algorithm. These algorithms were then tested against external disturbances such as localisation error, cross-wind, and parametric variations. This thesis successfully illustrates in detail, the aspects involved in path-tracking control. Results effectively suggest a betterment of the novel steering controllers designed, over the previously existing Sliding Mode Control Super Twisting algorithm and other bench-marking controllers at higher speeds. The work ends with vital conclusions and recommendations for future researchers in this domain to further increase robustness and achieve better performance.

Table of Contents

Acknowledgements	xi
1 Introduction	1
1-1 Background	1
1-2 Lane Keeping Systems	2
1-3 Research Objectives	3
1-4 Contribution of this thesis	4
1-5 Outline	4
2 Vehicle Modeling	7
2-1 Vehicle Coordinate System	7
2-2 Tyre Modeling	7
2-2-1 Linear Tyre Model	8
2-2-2 Pacejka's Magic Formula	8
2-3 Linear Bicycle Model	9
2-4 IPG CarMaker Vehicle Model	10
2-5 Steering Dynamics	12
2-6 Disturbance Modeling	12
2-6-1 Sensor Noise	12
2-6-2 Cross-wind	13
2-6-3 Changes in vehicle dynamics parameters	13
2-7 Model Validation	13
2-8 Error Dynamics Models	14
2-9 Summary	16

3	System Overview	17
3-1	Reference Path	17
3-2	Sensor Model	19
3-2-1	Lateral and Heading Error	19
3-2-2	Nearest Point Algorithm	20
3-3	The system	21
3-4	Summary	21
4	Bench-marking Steering Controllers	23
4-1	Stanley	23
4-2	PCwP	25
4-2-1	Vehicle Road Model	25
4-2-2	Gain determination	26
4-3	LQR	28
4-4	II	28
4-5	PBC	30
4-6	Summary	33
5	SMC	35
5-1	Introduction	35
5-2	Super Twisting Algorithm (STA)	36
5-2-1	Variant 1 - Literature	36
5-2-2	Variant 2 - Proposed Solution	38
5-3	Modified Super Twisting Algorithm (MSTA)	41
5-4	Non-singular Terminal Modified Super Twisting Algorithm (NSTMSTA)	43
5-5	Summary	44
6	Simulation Results and Comparisons	45
6-1	Vehicle Setup	45
6-2	Scenario	45
6-3	Results	45
6-3-1	Super Twisting Algorithm Variant 1 v/s Proposed	45
6-3-2	Modified Super Twisting vs Non-singular Modified Super Twisting Algorithm	51
6-3-3	Parametric Variations	57
6-3-4	Localisation error	58
6-3-5	Cross-wind	59
6-4	Summary	62
7	Conclusions and Recommendations	63
7-1	Conclusions	63
7-2	Recommendations	64

A	Vehicle Dynamics Parameters, Controller gains, Model Validation	67
A-1	Vehicle Dynamics Parameters	67
A-2	Controller Gains	68
A-3	Planar Vehicle Model Validation	68
B	Results - Bench-marking Controllers	73
C	Rate of lateral error estimation	81
	Bibliography	85
	Glossary	89
	List of Acronyms	89

List of Figures

1-1	Different areas to improve vehicle passenger safety	2
1-2	Block diagram of the subsystems involved in automatic steering	3
2-1	Vehicle Co-ordinate system with global and local frames of references with (X_g, Y_g, Z_g) being the global coordinates and (X_l, Y_l, Z_l) being the local coordinates	8
2-2	Approximate tyre model produced by Magic Formula	9
2-3	Bicycle model with relevant parameters used for vehicle modeling	10
2-4	Multi-body vehicle model in IPG CarMaker	11
2-5	Comparison of bicycle model - step steering input at 35 and 50 km/h	14
3-1	Reference Path Description	18
3-2	Nearest point and its relation with lateral error	20
3-3	Block Diagram of the implemented path-following vehicle	21
4-1	Bicycle Model with relevant parameters involved in Stanley steering control. Lateral error (in this case) is defined as the distance between the nearest point on the path (c_x, c_y) to the center of vehicle front axle.	24
4-2	Bicycle Model with look-ahead distance x_{la}	26
4-3	Inter-connection of systems	32
4-4	Block Diagram of passive systems from $\delta \rightarrow z$	32
5-1	Sliding Mode Dynamics	35
6-1	Sliding Mode Control - Super Twisting Algorithm (in literature) vs Super Twisting Algorithm (proposed solution) for velocity = 20 km/h	47
6-2	Sliding Mode Control - Super Twisting Algorithm (in literature) vs Super Twisting Algorithm (proposed solution) for velocity = 40 km/h	48
6-3	Sliding Mode Control - Super Twisting Algorithm (in literature) vs Super Twisting Algorithm (proposed solution) for velocity = 60 km/h	49

6-4	Sliding Mode Control - Super Twisting Algorithm (in literature) vs Super Twisting Algorithm (proposed solution) for velocity = 80 km/h	50
6-5	Sliding Mode Control - Modified Super Twisting Algorithm vs Non-singular Terminal Modified Super Twisting Algorithm for velocity = 20 km/h	52
6-6	Sliding Mode Control - Modified Super Twisting Algorithm vs Non-singular Terminal Modified Super Twisting Algorithm for velocity = 40 km/h	53
6-7	Sliding Mode Control - Modified Super Twisting Algorithm vs Non-singular Terminal Modified Super Twisting Algorithm for velocity = 60 km/h	54
6-8	Sliding Mode Control - Modified Super Twisting Algorithm vs Non-singular Terminal Modified Super Twisting Algorithm for velocity = 80 km/h	55
6-9	Effect of steering rate limiter with Non-singular Terminal Modified Super Twisting Algorithm at velocity = 80 km/h	56
6-10	Variation of s - sliding surface with Non-singular Terminal Modified Super Twisting Algorithm for velocity = 40 km/h	56
6-11	Robustness check against uncertainties in cornering stiffness of front and rear axles	57
6-12	Robustness check against localization error	58
6-13	Reference Path with cross-wind direction	59
6-14	Robustness check of the developed controllers against cross-wind disturbances . .	60
A-1	Validation of Planar Model - sine with dwell steering input at 60 kmph	70
A-2	Tyre Model Validation - Longitudinal Tyre Forces	71
A-3	Tyre Model Validation - Lateral Tyre Forces	72
B-1	Steering Wheel Angle at velocity = 20 km/h	73
B-2	Lateral acceleration at velocity = 20 km/h	73
B-3	Lateral error at velocity = 20 km/h	74
B-4	Heading error at velocity = 20 km/h	74
B-5	Steering Wheel Angle at velocity = 40 km/h	75
B-6	Lateral acceleration at velocity = 40 km/h	75
B-7	Lateral error at velocity = 40 km/h	76
B-8	Heading error at velocity = 40 km/h	76
B-9	Steering Wheel Angle at velocity = 60 km/h	77
B-10	Lateral acceleration at velocity = 60 km/h	77
B-11	Lateral error at velocity = 60 km/h	78
B-12	Heading error at velocity = 60 km/h	78
B-13	Steering Wheel Angle at velocity = 80 km/h	79
B-14	Lateral acceleration at velocity = 80 km/h	79
B-15	Lateral error at velocity = 80 km/h	80
B-16	Heading error at velocity = 80 km/h	80
C-1	Block Diagram of a Non-singular Terminal Modified Super Twisting Algorithm using a Modified Super Twisting Observer	81

List of Tables

3-1	Way-point attributes	18
6-1	Bench-marking controllers performance summary	61
6-2	Proposed controllers performance summary	62
A-1	Vehicle Dynamics Parameters - Toyota Camry	67
A-2	Stanley gains	68
A-3	Path Controller gains	68
A-4	LQR gains	68
A-5	Immersion and Invariance gains	69
A-6	Passivity Based Control	69
A-7	Sliding mode control gains - Variant 1 - ST	69
A-8	Sliding Mode Control gains - ST proposed	69
A-9	Sliding Mode Control gains - MST	69
A-10	Sliding Mode Control gains - NSTMST	70

Acknowledgements

I am greatly relieved to have finished my master thesis on time after being through numerous highs and lows over the past 9 months or so. This master thesis would not have been possible without the contribution of certain special people who have moulded me into the person I am today.

Firstly, I would like to thank my supervisor, Dr. Barys Shyrokau, for his constant assistance over the entire course of this thesis. He has been extremely supportive of my work and has helped me deliver weekly targets. His valuable advise on vehicle controls and Simulink saved a lot of time for me. Secondly, I would like to thank my daily supervisor, Yanggu Zheng for his critical observation and feedback regarding my implementation and simulation results. His suggestions at times were top-notch and incredibly accurate.

I am where I am today because of parents T.N.Vidyashankar and D.N.Gayathri, and my sister Dr. Aradhana Pandit. They have always supported my dreams and encouraged me to make decisions of my own. I shall forever remain indebted to them. I would like to mention these names: D.R.Krishnan, my uncle; Anuroop and Chandradeep, my brothers all of whom have encouraged me to pursue my dreams. My aunt Uma Krishnan has made cooking really easy with a variety of easy-to-cook Indian spice powders. Special thanks to her.

I would like to thank my friends and fellow batch mates - Anoosh, Laxmi, Vishrut, Nilay, Karan and Neel with whom I have spent my time working on assignments, discussing control strategies, vehicle dynamics and a lot of other interesting topics. I would like to thank Akilesh, Siddharth and Karthik for the disciplined gym sessions that helped me keep away from the hectic thesis work. Special thanks to the RH gang - Anurag, Arya, Samruddhi, Sharab, Sushanth and Varun for those memorable Friday nights which I thoroughly enjoyed.

Lastly, I would like to Prof. dr. ir. M. Wisse and dr. ir. R. Happee for making time to review my master thesis.

Delft, University of Technology
August 26, 2019

A. Pandit

“Calculus is the language God talks”

— *Richard Feynman*

Chapter 1

Introduction

1-1 Background

Since the invention of the first automobile by Nicolas Cugnot in 1769 [1], an enormous amount of work has been carried out in the field of automobiles concerning propulsion, performance, safety and comfort. However, over the past few decades, emphasis is mainly laid upon the automation of vehicles. With more than 320 million automobiles on the road [2], the quality of road transportation has changed drastically. As the number of automobiles increases, the need to take preventive measures to ensure there are no fatal accidents increases along with it. Thus, given the present day situation, the need for safe automobiles on the road is at its peak.

The global epidemic of road crash fatalities and disabilities is gradually being recognized as a major public health concern. Understanding such facts helps provide perspective and certain quantification of parameters seem helpful. According to the Association of Safe International Road Travel (ASIRT), nearly 1.25 million people die in road crashes each year, on average 3,287 deaths a day. Besides, there are 20-50 million people injured or disabled due to road accidents. Road crashes cost approximately \$518 billion globally, costing individual countries from 1-2% of their annual GDP [3].

Damena *et al.* reported that excessive speeding, reckless driving, driver impatience, overconfidence, dangerous overtaking and disregard for traffic rules are among the common causes of road traffic accidents in developing countries [4]. Statistics show that on German roads, 90% of registered accidents are caused by human error and the remaining 10% by technical defects [5, 6]. [7, 8] reports that 95% of accidents on Britain's roads involve human error.

On one front, some researchers believe that the best way forward is to completely reduce the effect of humans on driving. This is being put to test on roads off-late, transitioning towards SAE Level 4, Level 5 automation [9]. However, issues like trust, user acceptance, ethical and legal issues are still of concern [10]. On the other front, the introduction of vehicle safety systems, more particularly known as Advanced Driver Assistant Systems (ADAS) are an effective way to provide safety and combat accidents in an effective manner. In this case,

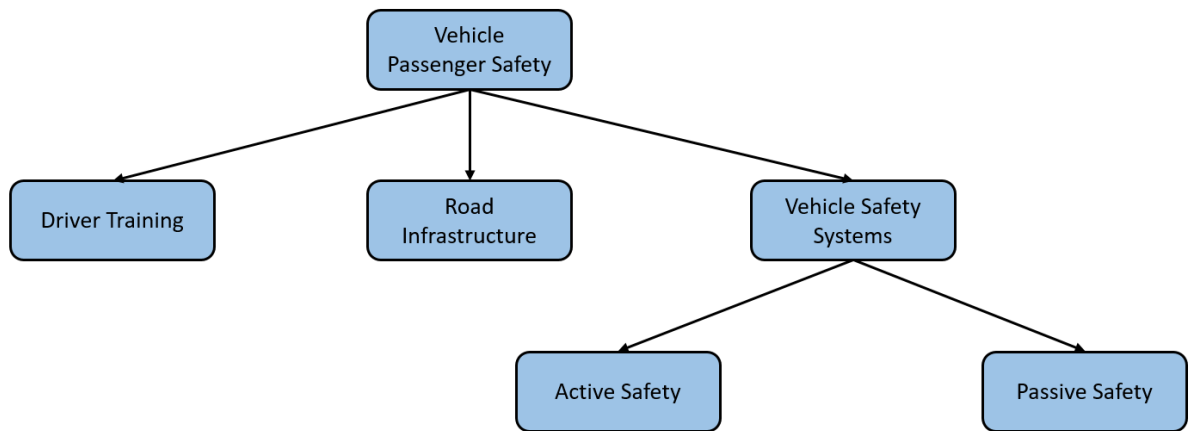


Figure 1-1: Different areas to improve vehicle passenger safety

the driver is still in control of the vehicle and the ADAS assists the driver in maintaining safety. Figure 1-1 give an idea of the different areas to improve vehicle passenger safety. ADAS features mainly come under the category of active and passive safety systems [11].

ADAS are systems developed to automate, adapt and enhance vehicle systems for safety and better driving. Some of the popular ADAS features include Adaptive Cruise Control (ACC), Anti-lock Braking Systems (ABS), Lane-centering systems and Collision Avoidance (CA) systems. ADAS relies on inputs from multiple data sources including automotive imaging, LiDAR, radar, image processing, computer vision, and in-car networking. ADAS also includes a reference generator and a controller. The reference generator generates reference values of the vehicle's parameters that are processed by the controller and the control action is realised using the available actuators.

1-2 Lane Keeping Systems

Lane Keeping Systems (LKS) is a type of ADAS that assists the driver by providing electronic steering support [12]. LKS is capable of supporting the driver in staying within a lane, however, does not provide all the steering torque required [13].

The potency of lane-keeping systems concerning real-world performance has been studied by a few researchers. Nodine *et al.* conducted a field trial with 16 vehicles equipped with Lane Departure Warning Systems and found a 33% reduction in near-crash events related to lane change and a 19% in those related to road departure [14]. Birrell *et al.* conducted a similar trial with 33 participants and observed a 12% reduction in lane deviations; however, this was not statistically significant [15]. Limited evidence for a reduction in collision rates with Lane Keeping systems has been identified. Sternlund *et al.* reported a reduction of 30% in head-on or single-vehicle crashes in a small sample of Swedish vehicles [16].

Although the work done on this front is significant, there is still room for improvement. The haptic interface as a Human Machine Interface (HMI) on the steering wheel in itself was not sufficient in itself. A multi-modal HMI was integrated to increase the driver's awareness about system operation. The HMI could incorporate a head-up-display in an appropriate position together with the haptic steering wheel [17]. There has been a constant effort to increase the complexity of the algorithm, but, the application on real vehicles includes challenges such as algorithm implementation in embedded processors and computational requirements; implying a trade-off between performance and cost [18].

To eliminate the drawbacks of LKS and moving towards SAE Level 3 and 4, there has been a significant amount of work carried out in the field of developing a robust control strategy for generating an automatic steering input for lateral control of vehicles [19–25]. The objectives of such a controller are to minimise the lateral distance between the vehicle and the predefined path, minimise the difference in the vehicle's heading and the defined path's heading, and limit steering inputs to smooth motions while maintaining stability. However, the steering controllers for path-tracking explained in literature are deterministic and do not account for disturbances.

Figure 1-2 depicts a block diagram of a typical closed-loop vehicle model with an automated steering controller. It is intuitive to realise that this approach is significantly different from LKS as the former boasts about taking control over the driver completely in contrast to steering assistance provided by LKS. Figure 1-2 shows all the key subsystems involved in modeling an automatically steered vehicle.

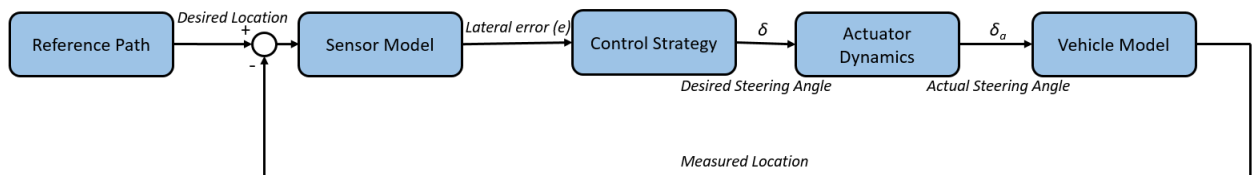


Figure 1-2: Block diagram of the subsystems involved in automatic steering

1-3 Research Objectives

In this thesis, automatic steering control systems are designed to control the lateral motion of a vehicle to maintain a predefined path. The control systems will be given full control of the vehicle to simulate an autonomous driving situation with the challenge being to make the controller more robust. Enhancement of the control system will enable path-following properties and generate robustness for a larger range of scenarios that will be explained in the subsequent sections. Furthermore, the aim was to create a certain standard benchmark for all the lateral controllers and to make a cross-comparison against each other.

An attempt is made to answer the following questions that are yet to be answered in literature. The research questions are as follows.

- Is it possible to utilise the advantages of Sliding Mode Control (SMC) for vehicle lateral control in path-following?
- What are the significant differences in lateral control strategies given in literature and SMC applied for the same purpose?
- Is it possible to develop other variants of SMC to get better performance in terms of robustness and accuracy concerning path-tracking?
- How is lateral error measured and is this measurement robust?
- What are the limitations of the existing lateral controllers explained in literature?
- Are the existing lateral controllers robust enough to handle parameter uncertainties?

It is ideal to define a problem statement before starting to work on a solution. A clear-cut problem was formulated and is as follows.

To minimise the lateral and heading deviation from the path by a continuous control action; and to be able to reject disturbances and handle parameter uncertainties

1-4 Contribution of this thesis

The main contribution of this thesis is the application of Sliding Mode Control with Super Twisting, Modified Super Twisting and Non-singular Terminal Modified Super Twisting Algorithm to automatic steering controllers. The work includes simulations for different scenarios and is aimed to create a simulation framework which encapsulates every subsystem that is required for vehicle lateral control in path-tracking*. A novel sensor model has been implemented that can measure lateral error based on geometric road profiles.

1-5 Outline

This thesis has been divided into seven chapters. Chapter 2 discusses a vehicle model that captures necessary lateral dynamics. This chapter also explains lateral error dynamics models that are crucial for path-tracking. Chapter 3 discusses the sensor model and the overall system that is implemented for path-tracking. This chapter also introduces reference path description and the nearest point algorithm.

Chapter 4 gives a clear picture of the different types of bench-marking steering controllers and necessary derivations of the steering law. Chapter 5 is the highlight of this thesis which contains key insights on SMC and its implementation for the objective of vehicle lateral control. This chapter talks about a certain variant of SMC explained in literature and its counter variant (a novel contribution presented in this thesis). Additionally, two other novel modifications to the twisting structure of SMC are presented with derivations of the same.

*In this thesis, the objectives of path-tracking is the same as that of automatic steering and the two words are used interchangeably

Chapter 6 involves simulation settings, results, and key inferences. This chapter addresses the effects of various parameters like wind, localization error, loss of friction, parametric uncertainties and includes different scenarios. Chapter 7 finally concludes the thesis by pointing out key conclusions and also talks about the scope for future work along with important recommendations for the same. The appendix chapters includes information about model parameters, controller gains, validation of planar model, performance of bench-marking controllers and a proposal for estimating rate of lateral error using a non-linear filter.

Chapter 2

Vehicle Modeling

To develop a control system for vehicle motion, it becomes imperative to understand the vehicle's dynamics and mathematically model them. This chapter introduces the vehicle models, tyre models and actuator dynamics used in simulations. Furthermore, to validate the robustness of the controller, disturbances in the form of sensor noise, crosswind, friction changes, and cornering stiffness changes are modeled. Finally, error dynamics models used in path-tracking are explained.

2-1 Vehicle Coordinate System

In order to quantify parameters associated with the localisation of the vehicle such as position, heading and lateral errors - coordinate systems are introduced. In this thesis, two main coordinate systems are chosen - namely the Global Coordinate System (GCS) and the Local Coordinate System (LCS). The GCS involves a frame of reference fixed at the vehicle Center of Gravity (CoG) at time t_0^* in a way such that the x axis points towards the heading of the vehicle. The LCS is a moving frame of reference that is fixed concerning the vehicle's CoG at all times. Figure 2-1 depicts these frames of references.

2-2 Tyre Modeling

All forces that act on a road vehicle are generated by the tyres, excluding aerodynamic and gravitational forces. Tyres are the only sources of contact between the vehicle and the ground. These forces act on the vehicle and a change in direction or velocity of the vehicle is seen upon control actuation. Therefore, it becomes crucial to represent the behaviour of the tyres accurately. In this thesis, two methods of tyre modeling have been introduced. For the sake of control system design, a simplified Linear Tyre Model is used. The multi-body vehicle on IPG CarMaker (plant to be controlled) has a list of tyre models that can be selected. For simulation purposes, a tyre model based on Pacejka's Magic Formula has been implemented.

* t_0 refers to the initial time

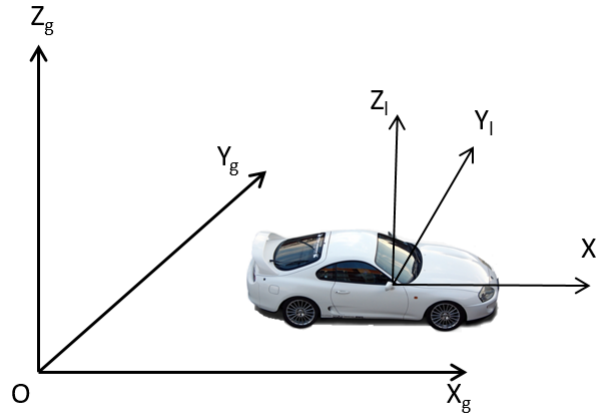


Figure 2-1: Vehicle Co-ordinate system with global and local frames of references with (X_g, Y_g, Z_g) being the global coordinates and (X_l, Y_l, Z_l) being the local coordinates

2-2-1 Linear Tyre Model

The forces from the tyres can be vectorised into two components namely - lateral and longitudinal forces. These forces produced by the tyres are non-linear and a function of parameters such as vertical load, slip angle, longitudinal slip ratio and friction. However, under normal driving conditions, when the slip angles and the slip ratios are small, it is safe to linearise the tyre forces. Considering pure slip, the linearisation becomes much simpler as the longitudinal force is purely a function of longitudinal slip and lateral force is purely a function of slip angle. Thus, the forces are written as,

$$F_{yi} = C_{\alpha i} \alpha_i \quad (2-1)$$

$$F_{xi} = C_{\kappa i} \kappa_i \quad (2-2)$$

where F_y and F_x represent the lateral and longitudinal tyre forces respectively. C_{α} and C_{κ} are the cornering stiffness and the longitudinal stiffness of the tyres. $i \in [fl, fr, rl, rr]$ is a variable used to indicate the tyre. α is the side slip angle and κ is the longitudinal slip.

2-2-2 Pacejka's Magic Formula

Since the inception of the Magic Formula, it has become an industry standard for vehicle handling simulations. It is shown to be adaptable at large camber angles, slip angles and robust to inflation pressure changes. The conventional Magic Formula based tyre model is a completely empirical mode that requires experimental tyre data. A smoothed curve is fit based on the collected data to model the tyres. Figure 2-2 illustrates the function produced by the revised Magic Formula.

The function used to empirically map the data is given by,

$$y(x) = D \left(C \tan^{-1} \left(Bx - E \left(Bx - \tan^{-1}(Bx) \right) \right) \right) \quad (2-3)$$

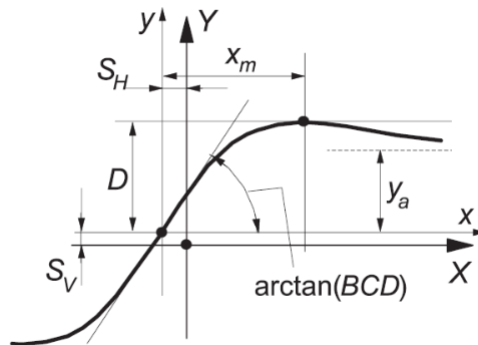


Figure 2-2: Approximate tyre model produced by Magic Formula [26]

where,

$$Y(x) = y(x) + S_v \quad (2-4a)$$

$$x = X + S_h \quad (2-4b)$$

where S_h and S_v are the shifting parameters. S_h is the horizontal shift and S_v is the vertical shift. These parameters provide the ability to model combined slip conditions along with pure slip. D is called the peak factor and controls the y-intercept as shown in figure 2-2. B is called the stiffness factor and determines the slope of the above curve at zero slip. E is called the curvature factor and affects the slip at which maximum peak occurs. C is called the shape factor and affects the stretching property of the curve in the x-direction.

There are several variations of the original Magic Formula present in literature. However, for this thesis, the conventional form as described in the above equations is used. The multi-body vehicle model on IPG CarMaker uses this kind of tyre model. However, for designing automatic steering control systems, linear bicycle model with linear tyres is used owing to its simplicity.

2-3 Linear Bicycle Model

In a lot of studies related to vehicle direction control, the Z direction is commonly not considered. The vertical Z-axis comes into play with pitch and roll dynamics. However, this thesis mainly focuses on lateral and longitudinal dynamics. This is a simplified model and the following assumptions are made.

- The model assumes a constant longitudinal velocity.
- Linear Tyre Model is used to model the tyres. Hence a linear cornering stiffness.
- The model assumes ideal steering effects and hence no steering actuator dynamics.
- Suspension effects are negated, i.e the suspension structure is considered to be rigid.

- The vehicle assumes to have small road wheel angles and hence small side slip and body slip angles.
- The small difference in the road wheel angle of the front tyres is neglected.
- Longitudinal and lateral load transfers are not considered.

A few of these assumptions seem important to be neglected. However, under normal driving circumstances and especially in the case of path-tracking/automatic steering, linear bicycle model is commonly used as it captures lateral behaviour of the vehicle - lateral acceleration a_y , body slip angle β , and yaw rate dynamics r .

The free-body diagram with lateral forces and other useful parameters on a bicycle model as shown in figure 2-3. By solving the Newton-Euler equations and simplifying further for steady-state conditions, a 2^{nd} order lateral dynamics model is derived [27].

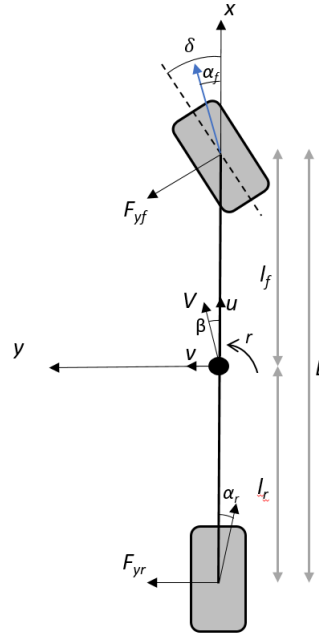


Figure 2-3: Bicycle model with relevant parameters used for vehicle modeling

$$\begin{bmatrix} \dot{v} \\ \dot{r} \end{bmatrix} = \begin{bmatrix} -\frac{C_{\alpha f} + C_{\alpha r}}{mu} & \frac{l_r C_{\alpha r} - l_f C_{\alpha f} - u}{mu} \\ \frac{l_r C_{\alpha r} - l_f C_{\alpha f}}{I_z u} & -\frac{l_f^2 C_{\alpha f} - l_r^2 C_{\alpha r}}{I_z u} \end{bmatrix} \begin{bmatrix} v \\ r \end{bmatrix} + \begin{bmatrix} \frac{C_{\alpha f}}{mu} \\ \frac{l_f C_{\alpha f}}{I_z} \end{bmatrix} \delta \quad (2-5)$$

2-4 IPG CarMaker Vehicle Model

Any control system that is developed for a purpose has to be implemented on higher order plant that is to be controlled. This allows one to check the performance of the control system designed. The IPG CarMaker is a virtual vehicle testing environment that has been developed as a simulation solution for modeling real-world scenarios. It contains a variety of modeling

options to represent the behaviour of vehicles, the driver and the environment including roads and traffic. The passenger vehicle models associated with this software captures realistic vehicle behaviour to the limits of vehicle dynamics. With respect to road modeling, it includes precise generation of customised tracks with options to include cambers, inclines and slopes. It is possible to generate random autonomous traffic with detailed traffic scenarios. This software comes with a detailed documentation and reference manual that give information with respect to models, frame of references, extracting useful vehicle parameters. Figure 2-4 shows the forces involved in the multi-body model of IPG CarMaker.

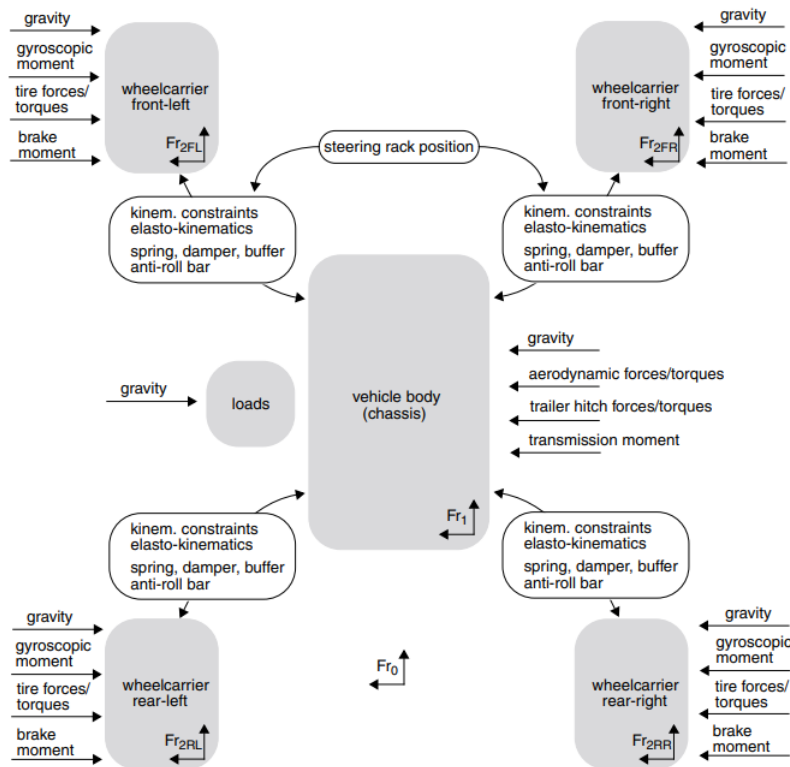


Figure 2-4: Multi-body vehicle model in IPG CarMaker [28]

IPG CarMaker includes automated test runs and helps in managing test maneuvers efficiently. It comes with visualisation tools like IPG Movie, IPG Control, and Instruments that provide detailed information regarding vehicle dynamics parameters and models. It is also possible for user interface modeling as it is linked to MATLAB/Simulink. This is one of the most useful features of this software. For control system development purposes, it proves handy to have access to the subsystems on Simulink and incorporate a user-defined block and run simulations.

All necessary vehicle parameters are available on IPG CarMaker as signals can be extracted during simulations. However, in reality, it might be the case that these parameters are not readily available as measurements. This is one of the main drawbacks of virtual testing. To give an example, the measurement of the sideslip angle is extracted as a measurement on the software. But, practically speaking, sensors cannot accurately measure the side slip angle; for

which sensor fusion and state estimators are made use of.

2-5 Steering Dynamics

The steering assembly converts a change in the radial position of the steering wheel to a change in the road wheel angle at the tyres. This steering assembly generally consists of a steering column, steering shaft, a rack and pinion gear assembly, an electric motor in the case of Electric Power-Assisted Systems (EPAS) for reducing driver effort, other linkages, and components. The input seen on the steering wheel is not instantaneously converted to a change in the road wheel angle. This happens gradually following the dynamics of the steering assembly.

For the sake of control system design, a constant steering ratio is assumed. This steering ratio is the ratio of turn in the steering wheel to that of the wheels (both in same units). It is mathematically represented as,

$$SR = \frac{\delta_{SWA}}{\delta_{RWA}} \quad (2-6)$$

where SWA and RWA refer to the steering wheel angle and road wheel angle respectively. where ω_n, ζ are the natural frequency and the damping ratio of the steering system. Furthermore, limits are set on the magnitudes of steering and the rate of steering to achieve smooth transitions.

Inequalities 2-7, 2-8 show the constraints on the road wheel angle. Longitudinal velocities are kept constant and tested for speeds ranging from 20 km/h to 80 km/h. In order to operate under stable limits, the longitudinal velocity varies by default (due to CarMaker's reference velocity tracker). This implies that the reference longitudinal velocity is a path curvature based parameter.

$$-20\text{deg} \leq \delta_{RWA} \leq 20\text{deg} \quad (2-7)$$

$$-25\text{deg/s} \leq \dot{\delta}_{RWA} \leq 25\text{deg/s} \quad (2-8)$$

2-6 Disturbance Modeling

2-6-1 Sensor Noise

It is a known fact that no sensor produces perfect measurements. These Electronic devices are highly prone to errors in the form of calibration errors, systematic errors, random errors. The lateral error being a key measurement in the case of automatic steering systems, it is important to check the performance of the control systems with sensor noise modeled. This also allows us to check the robustness of the controller and validate its performance and disturbance rejection capabilities.

In this thesis, measurement noise is added to the computed lateral error measurement. This noise is modeled as white noise with bounds of $\pm 0.005\text{m}$ and added at regular intervals.

2-6-2 Cross-wind

Cross-winds are a common source of disturbance in passenger vehicles. They create a force and a moment on the vehicle that can change the course of the vehicle. IPG CarMaker allows users to model winds at desired locations with the freedom to select the direction and speed at which they blow. The speeds chosen are of the range of 30,40,50 km/h perpendicular to vehicle motion during straight and left bend segments (Refer Chapter 6).

2-6-3 Changes in vehicle dynamics parameters

Parametric uncertainty is a common issue in physical systems and vehicles are no exception to this case. The system matrices of the reference vehicle model are a function of the cornering stiffnesses of the tyres and the longitudinal velocity of the vehicle. Cornering stiffness is a dynamic parameter and is also non-linear. The designed control system might work sufficiently well on an ideal plant model but, there is always a risk that the closed-loop system might not be stable if the model parameters change drastically.

The mass of the vehicle is also a dynamic parameter as it changes with change in passenger weights. Another dynamic parameter is the co-efficient of friction. Not all roads are perfectly behaving (co-efficient of friction variations) and it is crucial to check the controller's performance under different friction conditions.

2-7 Model Validation

The plant model that is to be controlled, i.e the multi-body model on IPG CarMaker is partly a black box model as the equations governing lateral, yaw and longitudinal are not completely known. During such circumstances, it is essential to model the behaviour of the plant - the aim is to capture the required dynamics of the plant model. In this case, since a steering controller is being developed, the focus is more on capturing lateral and yaw dynamics.

As the control design involves a linear bicycle model, the validation of bicycle model is important. In this process, the IPG CarMaker is validated against the linear bicycle model. Hence, a step steering input was considered for comparing behaviour of both models.

From figures 2-5a and 2-5b, it is seen that at 35 km/h, the behaviour of lateral dynamics of the vehicle is closely captured by the bicycle model. In the case of vehicle velocities higher than around 45 km/h, as seen in figure 2-5c and 2-5d, the the bicycle model tends to deviate from the behaviour of the IPG CarMaker plant. However, a linear bicycle model is good enough to capture lateral dynamics sufficiently at lower vehicle speeds and hence taken as the reference model for steering control design. The validation of planar vehicle model is reported in Appendix A. This is done to show that the planar model captures the behaviour of the plant at higher speeds more effectively than a bicycle model. The tyre forces for such a model are modeled by the Dugoff tyre model.

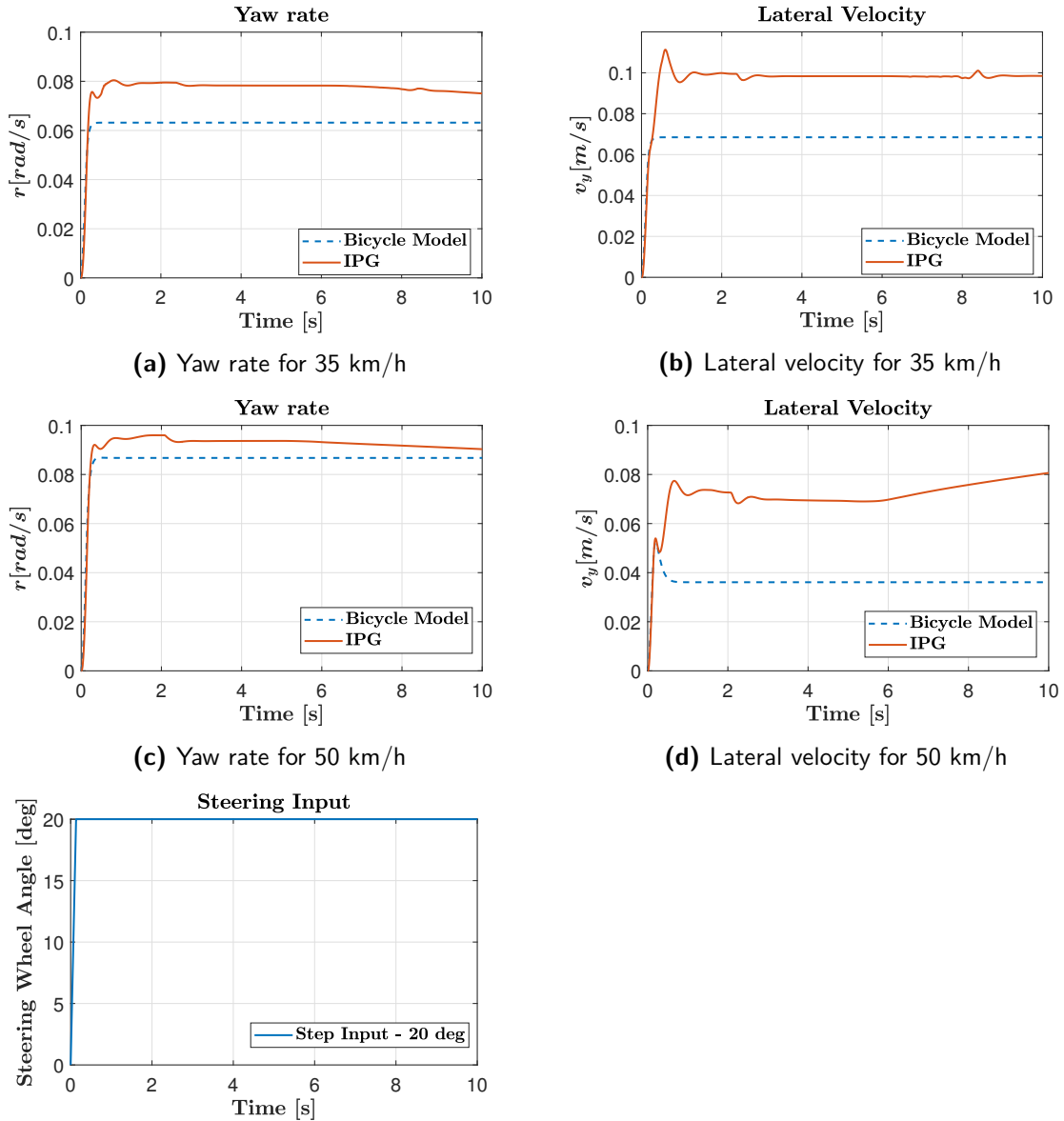


Figure 2-5: Comparison of bicycle model - step steering input at 35 and 50 km/h

2-8 Error Dynamics Models

In this section, three different error dynamics models are described. These variants differ mainly in the augmented states, however, the lateral error dynamics remains as one of the states in all three models. Concepts related to vehicle road models are adopted mainly from [29].

The following set of equations describe a method to model the lateral error and the heading error dynamics. Longitudinal velocity is assumed to be constant. The path is defined as a function of displacement s .

The yaw rate derived from the path $r(s)$ is defined as

$$r(s) = \kappa(s)u \quad (2-9)$$

where u is the longitudinal velocity and $\kappa(s)$ is the curvature of the path. The variables that are a function of s are defined with respect to the path.

The lateral acceleration derived from the path is given by,

$$\dot{v}_y(s) = \kappa(s)u^2 \quad (2-10)$$

Now, e_y is the lateral distance from the vehicle CoG to the path,

$$\begin{aligned} \ddot{e}_y &= (\dot{v}_y + ur) - \dot{v}_y(s) \\ &= \dot{v}_y + u(r - r(s)) \\ &= \dot{v}_y + u\dot{\theta}_e \end{aligned} \quad (2-11)$$

where r is the actual yaw rate of the vehicle. The difference $r - r(s)$ is represented by $\dot{\theta}_e$, that is treated as the heading error.

Substituting yaw rate and lateral velocity dynamics from linear bicycle model in 2-11, the following equations are obtained.

$$\ddot{e}_y - u\dot{\theta}_e = -\frac{C_f + C_r}{mu}(\dot{e}_y - u\theta_e) + \left(\frac{l_r C_r - l_f C_f}{mu} - u\right)(\dot{\theta}_e + r(s)) + \frac{C_f}{m}\delta \quad (2-12)$$

$$\ddot{\theta}_e + \dot{r}(s) = \frac{l_r C_r - l_f C_f}{I_z u}(\dot{e}_y - u\theta_e) - \frac{(l_f^2 C_f + l_r^2 C_r)}{I_z u}(\dot{\theta}_e + r(s)) + \frac{l_f C_f}{m}\delta \quad (2-13)$$

Thus, augmenting the lateral and heading error dynamics, the following state space structure is obtained.

- Variant 1:

$$\underbrace{\begin{bmatrix} \dot{e}_y \\ \ddot{e}_y \\ \dot{\theta}_e \\ \ddot{\theta}_e \end{bmatrix}}_{\dot{x}} = \underbrace{\begin{bmatrix} 0 & 1 & 0 & 0 \\ 0 & -\frac{C_f + C_r}{mu}\mu & \frac{C_f + C_r}{m}\mu & \frac{l_r C_r - l_f C_f}{mu}\mu \\ 0 & 0 & 0 & 1 \\ 0 & \frac{l_r C_r - l_f C_f}{I_z u}\mu & \frac{l_r C_r - l_f C_f}{I_z}\mu & -\frac{(l_f^2 C_f + l_r^2 C_r)}{I_z u}\mu \end{bmatrix}}_{A_1} \underbrace{\begin{bmatrix} e_y \\ \dot{e}_y \\ \theta_e \\ \dot{\theta}_e \end{bmatrix}}_x + \underbrace{\begin{bmatrix} 0 \\ \frac{C_f}{m}\mu \\ 0 \\ \frac{l_f C_f}{I_z}\mu \end{bmatrix}}_{B_1} \delta + \underbrace{\begin{bmatrix} 0 \\ \frac{l_r C_r - l_f C_f}{mu}\mu - u \\ 0 \\ -\frac{(l_f^2 C_f + l_r^2 C_r)}{I_z u} \end{bmatrix}}_{B_2} r_s \quad (2-14)$$

- Variant 2: This state space structure is derived from the lateral error dynamics augmented with lateral velocity and yaw rate dynamics as obtained from the linear bicycle

model[†].

$$\underbrace{\begin{bmatrix} \dot{v} \\ \dot{r} \\ \dot{e}_y \\ \dot{e}_\psi \end{bmatrix}}_{\dot{x}} = \underbrace{\begin{bmatrix} \frac{C_f+C_r}{mu} \mu & \frac{l_f C_f - l_r C_r}{mu} \mu - u & 0 & 0 \\ l_f C_f - l_r C_r & (l_f^2 C_f + l_r^2 C_r) & 0 & 0 \\ I_z u & I_z u & 0 & u \\ -1 & 0 & 0 & 0 \\ 0 & -1 & 0 & 0 \end{bmatrix}}_{A_2} \underbrace{\begin{bmatrix} v \\ r \\ e_y \\ e_\psi \end{bmatrix}}_x + \underbrace{\begin{bmatrix} -\frac{C_f}{m} \mu \\ -\frac{l_f C_f}{I_z} \mu \\ 0 \\ 0 \end{bmatrix}}_{B_3} \delta + \underbrace{\begin{bmatrix} 0 \\ 0 \\ 0 \\ u \end{bmatrix}}_{B_4} \rho \quad (2-15)$$

where ρ is the curvature of the path and the same as $\kappa(s)$.

- Variant 3: It is assumed that there is access to body slip and yaw rate measurements. Hence, the linear bicycle model is expressed in terms of these parameters and augmented along with lateral error dynamics. This variant is primarily used in Immersion and Invariance and Passivity Based Control which is explained in brief in the next chapter

$$\underbrace{\begin{bmatrix} \dot{\beta} \\ \dot{\psi} \\ \ddot{e}_y \\ \dot{e}_y \end{bmatrix}}_{\dot{x}} = \underbrace{\begin{bmatrix} -\frac{C_f+C_r}{mu} \mu & -\frac{l_f C_f - l_r C_r}{mu^2} \mu - 1 & 0 & 0 \\ l_f C_f - l_r C_r & (l_f^2 C_f + l_r^2 C_r) & 0 & 0 \\ I_z u & I_z u & 0 & 0 \\ -\frac{C_f+C_r}{m} \mu & -\frac{l_f C_f - l_r C_r}{mu} \mu & 0 & 0 \\ 0 & 0 & 1 & 0 \end{bmatrix}}_{A_3} \underbrace{\begin{bmatrix} \beta \\ \psi \\ \dot{e}_y \\ e_y \end{bmatrix}}_x + \underbrace{\begin{bmatrix} \frac{\mu C_f}{m} \\ -\frac{\mu l_f C_f}{I_z} \\ \frac{\mu C_f}{m} \\ 0 \end{bmatrix}}_{B_5} \delta + \underbrace{\begin{bmatrix} 0 \\ 0 \\ -u^2 \\ 0 \end{bmatrix}}_{B_6} \rho \quad (2-16)$$

2-9 Summary

The aim of this chapter was to introduce the types of vehicle modeling and motivate the reader to gain insight on the importance of vehicle dynamics modeling. Firstly, the types of tyre modeling were explained. The focus was laid on two types of tyre models namely - Linear Tyre Model and Pacejka's Magic Formula based empirical model. Secondly, a Linear Bicycle Model was introduced to capture the necessary lateral dynamics of the vehicle. IPG CarMaker was introduced as a virtual testing platform for vehicle control systems design and development. For this thesis, the IPG CarMaker model is used as the plant model for all simulations. The performance of the Linear Bicycle Model was checked as it proves to play a vital role in the design of control systems for path following. The steering actuator dynamics was introduced followed by the types of disturbances and how they are modeled. Finally, various error dynamics models were introduced; they augment the motion of the vehicle with the dynamics in reference trajectory. These models will be further used in Chapter 4 for steering control design.

[†] e_ψ is the same as θ_e , however they are used in different literature with the respective terminologies

Chapter 3

System Overview

In this chapter, the path-following control system is explained in detail. The main subsystems comprises of a reference path generator (in this case, a predefined path), a sensor model that outputs error measurements for the steering controller, the control logic itself and the multi-body vehicle model.

The three important aspects in the functioning of an autonomous vehicle are perception, planning, and control respectively [30]. This thesis mainly focuses on vehicle control. It is assumed that the vehicle has access to its location at every instant of time. Realistically, this is not the case generally as the measurements are inaccurate and noisy and hence, there is a need for state estimation methods such as Extended Kalman Filters and Particle Filters. However, these state estimation techniques are beyond the scope of this thesis.

Path planning provides safe and reliable manoeuvres under various driving environment, and it is the basis for an autonomous vehicle to drive without human intervention. The planning stage generally involves an algorithm which connects point A and point B with a certain continuous trajectory. The most commonly used algorithms that are available in the literature for such planning techniques are Rapidly exploring Random Trees (RRT), Optimal Rapidly Exploring Random Trees (RRT*), Probabilistic Road Maps (PRM), Dijkstra's algorithm. These algorithms generally do not include vehicle dynamics into account; however a lot of work is done on trying to model the vehicle's lateral behaviour in terms of steering capabilities.

3-1 Reference Path

In this thesis, localisation and planning stages are negated and the focus is laid completely on automatic steering which affects changes in the lateral motion of the vehicle. Thus, a predefined path is taken into consideration. All control techniques to be explained in the following chapter will be tested on this predefined path. This path is a collection of way-points at periodic intervals. Each way-point is a tuple containing path information in the

X Position	Y Position	Path Heading	Path Curvature	Length of the Path
x_1	y_1	θ_1	ρ_1	l_1
x_2	y_2	θ_2	ρ_2	l_2
x_3	y_3	θ_3	ρ_3	l_3
\vdots	\vdots	\vdots	\vdots	\vdots
x_{end}	y_{end}	θ_{end}	ρ_{end}	l_{end}

Table 3-1: Way-point attributes

form of path co-ordinates, path heading, path curvature, length of the path*. Table 3-1 represents the information available at each way-point.

All path attributes are represented with respect to the Global Coordinate System (GCS). The path coordinates represent the X and Y location of the way-points. The path heading represents the slope or the angle made by the tangent to the path at each way-point. The path curvature is defined as the reciprocal of the radius. The length of the path is the most crucial components that define a path. However, not a lot of emphasis is given to this particular parameter in literature. The length of the path governs how well the path is defined. In short, a shorter length of the path corresponds to a more distinct definition of the path. As this length increases, there is a loss of information between the way-points and this affects the controller performance which will be seen in the next section. The length of the path is somewhat equivalent to the sampling period in discrete-time systems.

Figure 3-1 illustrates a reference path represented by way-points. The length of the path is fixed to be $l_p = 0.1m$. It is assumed that the reference path remains smooth within this length. In cases where the reference path involves drastic dynamic manoeuvres, implying severe lateral accelerations, the length of the path has to be adjusted. However, 0.1m seems to be a fair assumption.

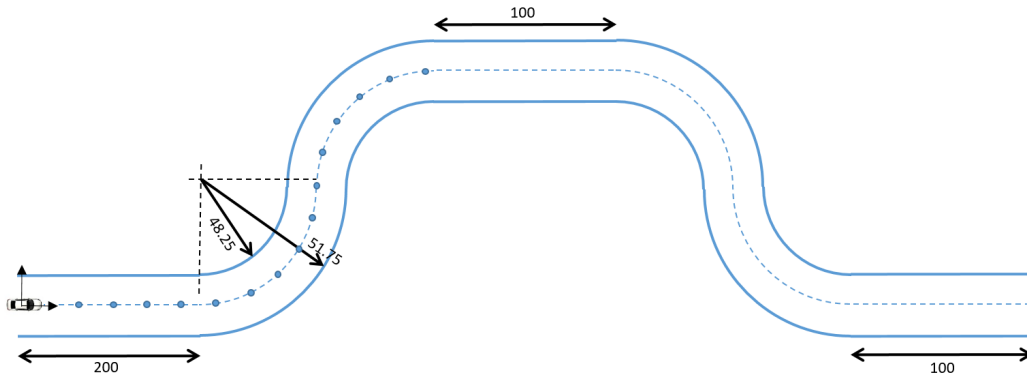


Figure 3-1: Reference Path Description

For this thesis, the controllers are compared against this reference path whose way-points are described by a piece-wise function as given in equation 3-1.

An important assumption here is that the length of the path is held constant throughout.

*All path attributes are represented in SI units for simulations

To achieve this, the way-points are to be in such a way that $\sqrt{(x_1 - x_2)^2 + (y_1 - y_2)^2}$ is held a constant. As a result, x_{ref} is not varied in a linearly. Since the segments are circular in nature, polar coordinates are made use of. By doing so, we can parameterise the way-point co-ordinates to the form $x = f(r, \theta)$ and $y = f(r, \theta)$. However the discretisation of θ has to be very fine to fulfill the above constraint. Furthermore, post-processing of these way-points is done to extract points that are exactly 0.1m apart. These intricacies involved in creating a reference path are essential to obtain a continuous and accurate lateral error measurement from the sensor model.

$$y_{ref} = \begin{cases} -1.75 & 0 \leq x_{ref} < 200 \\ 200 + r_1 \sin(\theta_1) & 200 \leq x_{ref} < 250 \\ 50 + r_2 \sin(\theta_2) & 250 \leq x_{ref} < 300 \\ 98.25 & 300 \leq x_{ref} < 400 \\ 50 + r_2 \sin(\theta_3) & 400 \leq x_{ref} < 450 \\ 50 + r_1 \sin(\theta_4) & 450 \leq x_{ref} < 500 \\ -1.75 & 500 \leq x_{ref} < 600 \end{cases} \quad (3-1)$$

where $r_i, i \in [1, 2]$ is radius of bend and $\theta_j, j \in [1, 4]$ is the angle of discretisation respectively.

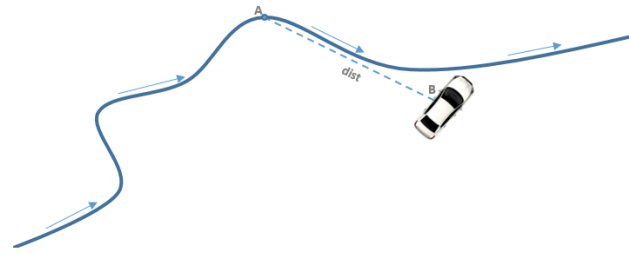
3-2 Sensor Model

The main objective of a reference tracking controller is to push the model states to the reference state and achieve asymptotic stability. Any such controller demands inputs mainly in the form of error signals. More often than not in the case of vehicles, modeling of error dynamics would not provide accurate results and it becomes vital to have measurements.

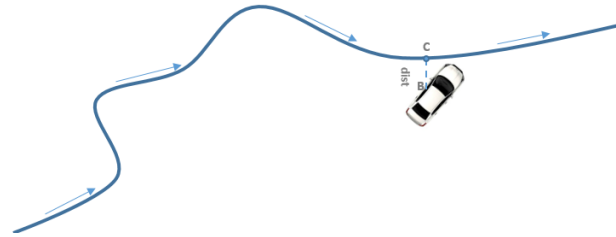
3-2-1 Lateral and Heading Error

In the case of path-following, the two cardinal error metrics are the lateral error and the heading error. Lateral error is defined as the distance from the nearest point to the vehicle on the path to the vehicle itself. Based on the requirement from the steering controller, this distance can be measured from the nearest point to the vehicle CoG or nearest point to the front axle. On the other hand, heading error is the difference between the vehicle heading and the path heading at the nearest point location. A key observation at this stage is that the lateral error is not always the perpendicular drawn from the path to the vehicle orientation. But, it is the normal drawn from the nearest point onto the vehicle. Figure 3-2 illustrates this concept with a clear example.

One of the main challenges and also a novelty about computing the lateral error was to eliminate the use of extrinsic functions as these functions do not support code generation on Simulink. Keeping this in mind, an algorithm was implemented to find the nearest path point to the vehicle. The path heading is achieved by interpolating the slopes at way-points on each side of the nearest point. This is done by solving for coefficients of a quadratic equation as extrinsic functions like 'interp' are not used. The heading error is then is computed by taking



(a) Perpendicular with respect to vehicle heading drawn on to the path



(b) Normal drawn from the nearest point on to the vehicle

Figure 3-2: Nearest point and its relation with lateral error

the difference between path heading and vehicle heading. Often, the heading error causes problems in robotic applications owing to the logic behind restricting its range between $[0 \leq e_\psi < \pi] \cup [0 > e_\psi \geq -\pi]$.

3-2-2 Nearest Point Algorithm

Consider a path described by a set of points called the way-points. These way-points are to be pre-processed in such a way that the way-points are equidistant from each other. A dynamic search is then made with respect to the CoG of the vehicle such that a circular boundary is created with the center of the circle kept at the CoG. This is done to keep the nearest point search restricted to a boundary around the vehicle rather than looking along the entire path.

The nearest index (i) or the way-point is then found out within the circular boundary. It has to be noted that this is not the nearest point on the path, but the nearest index. A small part of the path between indices ($i + 1$) and ($i - 1$) is then considered. Considering these indices as boundary conditions, a quadratic curve is fitted by solving for the coefficients of the quadratic polynomial. The choice of the polynomial is left to discretion; however since the distance between the two way-points was around 0.2m, a second-order polynomial was fitted. Furthermore, this portion of the path described by the line is cut into more segments. In this case, 200 points were interpolated. The choice on the number of points interpolated

is also left to discretion depending on the decimal accuracy of the computed distance to the actual value.

3-3 The system

In this section, the necessary subsystems that are essential for a path following vehicle are explained in brief. Although various lateral controllers are compared in detail in this thesis, longitudinal controllers have not been implemented. However, there is already a certain longitudinal velocity controller on IPG CarMaker that allows velocity tracking[†] to a certain extent. But, this being a black-box, there is limited knowledge on the type of longitudinal controller used. Figure 3-3 illustrates the overall picture of an autonomous steering controller with the sensor model and the vehicle model.

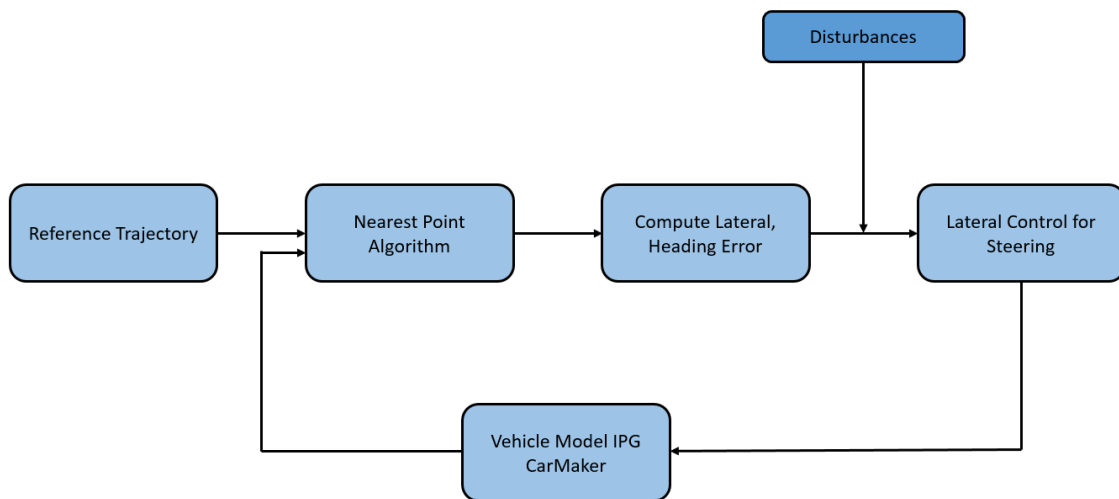


Figure 3-3: Block Diagram of the implemented path-following vehicle

As stated in the previous chapter, the main contribution of this thesis lie in the novel design of the lateral controllers.

3-4 Summary

This chapter explained the necessary components involved in path following for this thesis and also a generic structure of most path followers present in literature. To summarise, a reference path was chosen based on symmetry based on equidistant way-points and nominal total path-length (longer paths tend to take higher computational time and is not required for prototype development). A novel method to compute the nearest point algorithm was explained in detail. This is an unexplained/assumed concept in most literature. It is still

[†]It is because of this reason, 'trajectory' can be used interchangeably with 'path'

unknown to the author whether it is due to a simple implementation of such an algorithm or it's complexity. However, in this study, nearest point approach is clearly explained (without the use of extrinsic functions and hence, can be compiled as a C code) and the two main input signals - the lateral and the heading error were computed. Furthermore, the path following system was laid down as subsystems.

Bench-marking Steering Controllers

This chapter describes in detail the various control techniques deployed for path tracking. This chapter is divided into different sections, each section explaining a different control strategy. The methods explained here are widely known as geometric path trackers. The main idea of such a control strategy is to exploit geometric relations between the vehicle and the path and construct control laws for automatic steering.

4-1 Stanley

This type of geometry based control approach was incorporated by Stanford's robot Stanley that won the DARPA Defense Advanced Research Projects Agency (DARPA) challenge back in 2005 [31]. The steering controller accepts a trajectory generated by the path planner (in this case, a predefined path), the longitudinal velocity of the vehicle and the steering wheel angle. The function of the controller is to provide closed loop tracking of the desired vehicle path, as determined by the path planner.

The key error metric is the cross track error $e_y(t)$ which corresponds to the lateral error. The idea is to command the steering by a control law that allows $e_y(t)$ to converge to zero. Stanley steering controller is based on a nonlinear feedback function of the lateral error for which exponential convergence can be shown under certain assumptions [19]. Figure 4-1 depicts an illustration of a bicycle model with key terminologies for steering control design.

The steering control law is given by,

$$\delta(t) = \psi(t) + \tan^{-1}\left(\frac{ke_y(t)}{V(t)}\right) \quad (4-1)$$

In the above equation 4-1,

- $\psi(t)$ represents the heading error, in other words, the difference between the vehicle heading θ and the path heading θ_p .

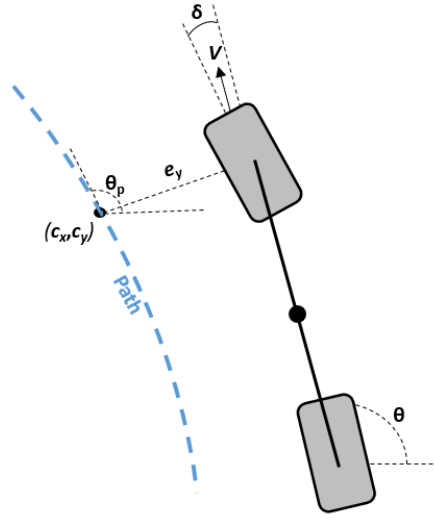


Figure 4-1: Bicycle Model with relevant parameters involved in Stanley steering control. Lateral error (in this case) is defined as the distance between the nearest point on the path (c_x, c_y) to the center of vehicle front axle.

- $V(t)$ represents the absolute vehicle speed at time t .
- k represents the rate of convergence parameter to be tuned.

Since stability and robustness is looked upon in this thesis, the asymptotic convergence of system trajectories of the closed loop system has to be studied. Assuming the tire stiffness coefficients are infinite with a linear bicycle model, the error dynamics is given by,

$$\begin{aligned} \dot{e}_y(t) &= -e_y(t) \sin\left(\tan^{-1}\left(\frac{ke_y(t)}{V(t)}\right)\right) \\ &= \frac{-ke_y(t)}{\sqrt{1 + \left(\frac{ke_y(t)}{V(t)}\right)^2}} \end{aligned} \quad (4-2)$$

Considering the lateral error is small, the solution of the above differential equation can be written as,

$$e_y(t) = y(0)e^{-kt} \quad (4-3)$$

Equation 4-3 proves that the lateral error decays to zero with a positive gain k

4-2 Path Control with Preview (PCwP)

This method is derived from an implementation of path control with look ahead distance as explained in [32]. The objective of this controller to push the vehicle to a reference lane by following a path that is previously known. However, unlike Stanley, lateral error at a preview distance is considered for feedback action on the steering. This type of control is implemented and tested on highways, where the radius of curvature is large. The performance of this control strategy here will be seen on smaller radius bends for a range of vehicle speeds.

4-2-1 Vehicle Road Model

To get a deeper insight as to how the control law is derived, the vehicle-road model as in equation 2-15

$$\underbrace{\begin{bmatrix} \dot{v} \\ \dot{r} \\ \dot{e}_y \\ \dot{e}_\psi \end{bmatrix}}_{\dot{x}} = \underbrace{\begin{bmatrix} \frac{C_f+C_r}{mu} \mu & \frac{l_f C_f - l_r C_r}{mu} \mu - u & 0 & 0 \\ l_f C_f - l_r C_r & (l_f^2 C_f + l_r^2 C_r) & 0 & 0 \\ I_z u & I_z u & 0 & u \\ 0 & -1 & 0 & 0 \end{bmatrix}}_{A_2} \underbrace{\begin{bmatrix} v \\ r \\ e_y \\ e_\psi \end{bmatrix}}_x + \underbrace{\begin{bmatrix} -\frac{C_f}{m} \mu \\ -\frac{l_f C_f}{I_z} \mu \\ 0 \\ 0 \end{bmatrix}}_{B_3} \delta + \underbrace{\begin{bmatrix} 0 \\ 0 \\ 0 \\ u \end{bmatrix}}_{B_4} \rho$$

where

- v represents the lateral velocity of the vehicle
- u represents the longitudinal velocity of the vehicle
- r represents the yaw rate of the vehicle
- C_f, C_r are the cornering stiffnesses on the front and rear axle respectively
- I_z represents the moment of inertia about the
- δ represents the road wheel angle
- l_f, l_r represent the distance of the CoG from the front and rear axle respectively
- m represents the mass of the vehicle and ρ represents the path curvature

Considering the vehicle road model described above,

$$\dot{x} = A_2 x + B_3 \delta + B_4 \rho$$

The aim of the lateral controller is to find a control law that pushes the 3rd and 4th states to zero. This problem then becomes a reference tracking problem which is solved by employing a state feedback strategy. The steering action can be written as,

$$\delta = \begin{bmatrix} 0 & 0 & k_{ye} & k_{\psi e} \end{bmatrix} x + \delta_{ff} \quad (4-4)$$

4-2-2 Gain determination

The feed-forward steering action is simply the curvature response gain from the bicycle model and is given by,

$$\delta_{ff} = \frac{L + K_{us}u^2}{R_{FF}} \quad (4-5)$$

To determine the feedback steering action, equation 4-4 is rewritten and further simplified,

$$\begin{aligned} \delta &= k_{y_e}y_e + k_{\psi_e}\psi_e + \delta_{ff} \\ &= k_{y_e}\left(y_e + x_{la}\psi_e\right) + \delta_{ff} \end{aligned} \quad (4-6)$$

The vehicle is assumed to move in a circular pattern while driving a certain velocity under steady state conditions, i.e $\dot{r} = 0$, $\ddot{r} = 0$ and $\dot{\delta} = 0$. The feedback gain is then solved for which reduces the lateral error at a look ahead distance to zero.

Figure 4-2 shows an illustration of the path preview scenario where the blue curve is the reference path and the orange curve is the circular arc the vehicle tries to follow in order to minimize the lateral error at a look ahead distance.

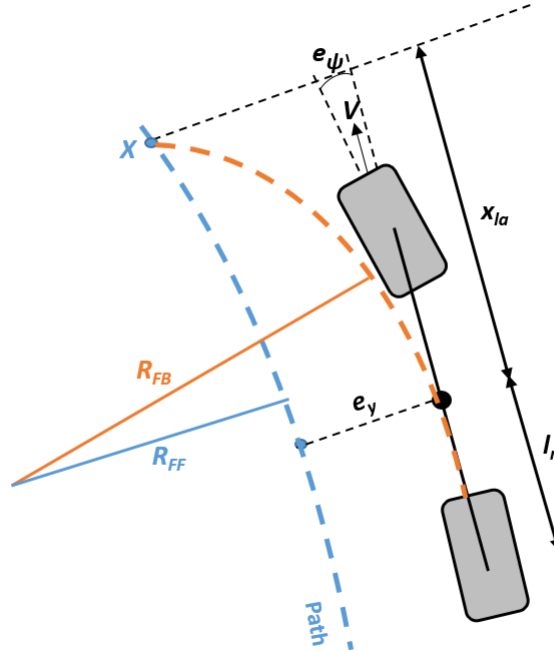


Figure 4-2: Bicycle Model with look-ahead distance x_{la}

The look ahead distance $x_{la} = ut_{la}$ is treated as a function of vehicle velocity. Hence, a look ahead time is defined which is treated as a tuning parameter. The distance to the look ahead point from the real axle is given by,

$$d_{la} = l_r + ut_{la}$$

At this point, it is interesting to observe that an important deduction between the lateral error at a look ahead distance y_{la} and the look ahead distance x_{la} itself.

With the vehicle moving in a circular radius, the lateral error equals the sagitta of the circular arc beginning from the rear axle. The look ahead distance is then the half chord length. One important assumption to arrive at the following relationship is that the sagitta is very small compared to the circular radius.

The relation between the sagitta s , the radius of the circular arc r and the half chord l is given by,

$$\begin{aligned} r^2 &= (r - s)^2 + l^2 \\ s^2 + l^2 &= 2rs \end{aligned}$$

Further dividing by s^2 throughout, an important result is made use of for further analysis of gain determination.

$$r = \frac{l^2}{2s} \quad (4-7)$$

On applying the above equation to the problem at hand, the radius that the vehicle has to traverse to minimise the lateral error at a look ahead distance becomes,

$$R_{FB} = \frac{d_{la}^2}{2(y_e + x_{la}\psi_e)}$$

The feedback steering law is given by

$$\delta_{FB} = \frac{2(l + K_{us}u^2)}{d_{la}^2} (y_e + ut_{la}\psi_e) \quad (4-8)$$

The overall steering law is given by

$$\delta = \frac{2(l + K_{us}u^2)}{d_{la}^2} (y_e + ut_{la}\psi_e) + \frac{L + K_{us}u^2}{R_{FF}}$$

where k_{FB} and k_{FF} are tuned during simulations to achieve better tracking.

4-3 Linear Quadratic Regulator (LQR)

Optimal control deals with the problem of finding a control law for a given system such that a certain optimality criterion is achieved. A control problem includes a cost functional that is a function of state and control variables. An optimal control is a set of differential equations describing the paths of the control variables that minimise the cost function. In this regard, the error dynamics model taking into account the vehicle-road dynamics as given by Chapter 3 is considered to design optimal gains.

$$\dot{x} = Ax + B_1\delta + B_2\dot{\psi}_{ref}$$

where $x = [e_y \ e_\psi \ \dot{e}_y \ \dot{e}_\psi]^T$ with usual notations

LQR is a type of optimal state feedback control where the gains are implemented by solving the Continuous-time Algebraic Riccati Equation (CARE) instead of pole placement techniques.

The objective function is given by

$$J = \int_0^\infty (x^T(t)Qx(t) + \delta^T(t)R\delta(t))dt$$

The solution X to this objective function can be obtained [33], and also the optimal gain

$$K = (R + B^T X B)^{-1} B^T X A$$

The control law is then given by,

$$\delta = -Kx \tag{4-9}$$

which drives the error dynamics to converge at zero

The gains Q and R are weights on the states and control input respectively and are to be tuned accordingly

4-4 Immersion and Invariance (II)

This type of control technique is a relatively newer method for constructing non-linear and adaptive controllers. This thesis explains key concepts involved in designing I&I type of steering controllers. However, detailed proofs are explained in [34]. Invariance is a concept of lyapunov stability. In other words, for any given dynamical system described by $\dot{x} = f(x, u)$, if the trajectories of the system remain in a certain set S for all times for all initial conditions in the same set S , then the set S is considered to be invariant.

The basic idea of immersion in control theory is to project the system under consideration into a system (often called the target system) with pre-specified properties. The stabilization problem of seeking for a state feedback control law such that the closed loop system is

locally (globally) asymptotically stable is considered. Immersion has been used in non-linear regulator theory to derive necessary and sufficient conditions for robust regulation.

However, an important step to design I&I controllers is to verify certain conditions about the system and the target dynamics.

Consider the system,

$$\dot{x} = f(x) + g(x)u$$

where $x \in R^n$ with an equilibrium point $x^* \in R^n$ and the control input $u \in R^m$. It is important that $p < n$ (implying the order of the target dynamics is lesser than the order of the system of interest). It is also assumed that a few mappings are available. The mappings are as follows,

- $\alpha(\cdot) : R^p \rightarrow R^p$
- $\pi(\cdot) : R^p \rightarrow R^n$
- $c(\cdot) : R^p \rightarrow R^m$
- $\phi(\cdot) : R^n \rightarrow R^{n-p}$
- $\psi(\cdot, \cdot) : R^{n*(n-p)} \rightarrow R^m$

The target system of the structure $\dot{\zeta} = \alpha(\zeta)$ with state $\zeta \in R^p$, has a global asymptotically stable equilibrium at $\zeta^* \in R^p$ and $x^* = \pi(\zeta^*)$

For all $\zeta \in R^p$ the condition

$$f(\pi(\zeta)) + g(\pi(\zeta))c(\pi(\zeta)) = \frac{\partial \pi}{\partial \zeta} \alpha(\zeta) \quad (4-10)$$

This constitutes the immersion condition.

The following identity,

$$x \in R^n | \phi(x) = 0 = x \in R^n | x = \pi(\zeta), \quad \zeta \in R^p \quad (4-11)$$

holds true.

The trajectories of the system

$$\dot{z} = \frac{\partial \phi}{\partial x} (f(x) + g(x)v(x, z)) \quad (4-12a)$$

$$\dot{x} = f(x) + g(x)v(x, z) \quad (4-12b)$$

are bounded and equation 4-12b as a globally asymptotically state equilibrium at $z = 0$

Then, x^* is a globally asymptotically stable equilibrium of the closed-loop system

$$\dot{x} = f(x) + g(x)v(x, \phi(x))$$

The proofs of the above conditions are explained in [35], [36]. More importantly, in the present case, the objective is to achieve $e_y = 0$ with respect to a given trajectory. The system of interest here is represented previously in equation 5-1. It is the vehicle error model augmented with side slip and yaw rate dynamics. The target dynamics is taken to be the dynamics of side slip and yaw rate. Furthermore, both the system and the target dynamics have a globally asymptotically stable equilibrium at the origin.

The target dynamics is given by,

$$\begin{bmatrix} \dot{\tilde{\beta}} \\ \dot{\tilde{\psi}} \end{bmatrix} = \begin{bmatrix} 0 & -1 \\ \frac{\mu C_r(l_f+l_r)}{I_z} & -\frac{\mu l_r C_r(l_f+l_r)}{I_z V_x} \end{bmatrix} \begin{bmatrix} \tilde{\beta} \\ \tilde{\psi} \end{bmatrix}$$

The manifold variable z is chosen to be, $z = \dot{e}_y + \lambda e_y$ such that $\lambda > 0$. In order to push the trajectories towards the manifold variable, $\dot{z} = -Kz$ is chosen to be the dynamics of the manifold variable. To modify the asymptotic convergence behaviour of the control law, an integral term was added was to the manifold dynamics resulting in the expression,

$$\dot{z} + K_1 z + K_2 \int_0^t z dt = 0 \quad \text{s.t.} \quad K_1 > 0, K_2 > 0 \quad (4-13)$$

Upon substituting the expression for the manifold variable and lateral error dynamics in the above equation 4-13 and further simplifying, we obtain the overall steering control.

The overall steering control is given by,

$$\delta_{II} = -\frac{m(K_1 + \lambda)}{\mu C_f} \dot{e} - \frac{m(K_1 \lambda + K_2)}{\mu C_f} e - \frac{m K_2 \lambda}{\mu C_f} \int_0^t e dt + \frac{C_f + C_r}{C_f} \beta + \frac{l_f C_f - l_r C_r}{C_f V_x} \dot{\psi} + \frac{m V_x^2}{\mu C_f} \rho$$

4-5 Passivity Based Control (PBC)

This type of steering control poses key advantages as explained in detail in [37]. Passive systems are a class of systems that involve physical or virtual energy, described by Lyapunov-like functions. The concept of passive systems is useful in stability analysis for interconnected systems. For a given system, its excess or deficit of passivity is quantified by the amount of feed-forward or feedback gain required to make it passive. But during its application to interconnected systems, the shortage of passivity in the model can be compensated by the excess of passivity in the controller, in order to ensure closed-loop stability. The main feature of this control technique is that it defines a control methodology that aim to make the closed-loop system passive. Furthermore, the passivity properties ensure closed-loop stability and robustness.

In literature, two approaches are used to design PBC controllers,

- An energy function that guarantees passivity of the closed-loop system and further selection of gains according to the energy function requirements

- Passivity properties of the model and controller are made use of to ensure closed-loop stability and robustness

A useful lemma which establishes the equivalence of passive properties with positive realness of the system in frequency domain; with input output relationship of the system in time domain is the Kalman-Yakubovich-Popov (KYP) lemma. The following conditions are as described in the KYP lemma,

- Consider the time domain characteristics, a system with an input u and an output y where $u(t), y(t) \in R^m$, is passive if there is a positive constant v such that

$$\int_0^T y^t(t)u(t)dt \geq v \quad \forall u \quad \text{and} \quad T \geq 0$$

- Any Linear Time Invariant (LTI) system of the form,

$$\begin{aligned} \dot{x} &= Ax + Bu \\ y &= Cx + Du \end{aligned}$$

with usual notations; is considered to be passive if the transfer function $H(s) = c(sI - A)^{-1}B + D$ is Positive Real (PR). Subsequently, if the transfer function $H(s)$ is strictly PR, then the system is strictly passive.

- In the frequency domain, consider a transfer function $G(s)$ mapping the input-output response of a system, where R is the operator returning the real part. $H(s)$ is considered PR if,

$$\begin{aligned} H(s) & \text{ is stable} \\ R[H(j\omega)] & \geq 0, \quad \forall \omega \in R \end{aligned}$$

It has to be noted that with the above definitions, unstable and non-minimum phase systems do not qualify for being positive real.

Interconnected Systems

In order to achieve closed-loop stability, the theory of interconnected systems is vital. Consider 2 systems as shown in figure 4-3.

Corollary 1 : For the feedback system shown in 4-3b, the overall transfer function is stable if either one of the following statements is true.

- G_1 is passive and G_2 is strictly passive
- G_1 is strictly passive and G_2 is passive

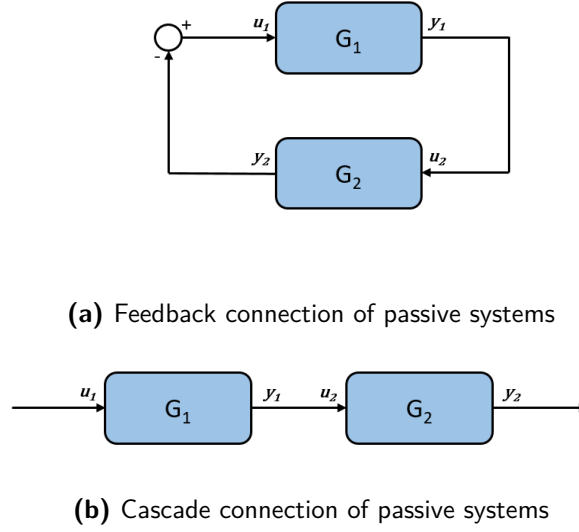


Figure 4-3: Inter-connection of systems

Corollary 2 : For the cascaded system shown in 4-3a, the overall transfer function is stable, if either one of the following statements is true.

- G_1 is passive and G_2 is strictly passive
- G_1 is strictly passive and G_2 is passive

Figure 4-4 represents a transfer function map of the steering control to the variable z .

By evaluating passive properties of each transfer function involved in the above mapping and verifying closed-loop stability by making use of the corollaries mentioned above, a control strategy for automatic steering is derived.

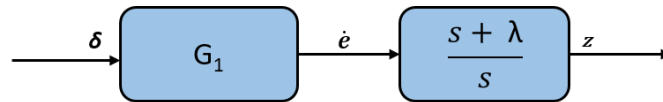


Figure 4-4: Block Diagram of passive systems from $\delta \rightarrow z$

Detailed analysis of the following arguments is explained clearly in [38].

Argument 1: The map $\delta \rightarrow \dot{e}$ is **strictly passive** for all $\mu > \mu_0$. The transfer function $P_0(s)$ that maps the quantities δ and \dot{e} is strictly positive real. This occurs as the individual co-efficients of the transfer function are physical parameters attributed to vehicle dynamics and are positive.

Argument 2: The map $\delta \rightarrow \dot{e}$ is **passive** for all $\mu > \mu_0$. The overall transfer function $P_1(s)$ is a cascaded connection of an integrator with $H_0(s)$. By making use of time domain characteristics of the individual transfer functions, it is proven that overall transfer function is passive.

Argument 3: The map $\delta \rightarrow z$ is **passive**. This map is a cascaded interconnection of $P_1(s)$ that is passive and $P_2(s)$ that is a strictly passive. The resulting map is then shown to be passive

A PI controller is further used to strengthen closed-loop passivity. However, in the presence of non-linearities (in this application, from the tire forces), the performance of such a PI controller may be deteriorated and hence an adaptive gain tuning mechanism is implemented.

$$\delta = -\left(k_I \int_0^t z dt + k_P z\right) k_e(e) \quad (4-14)$$

where $k_e(e)$ is the adaptive gain which is a non-linear function of lateral error, k_I and k_P are positive gains of the PI controller. The non-linear function is chosen such that the gain is proportional to the lateral error. High gains are provided away from the equilibrium state $e = 0$ to achieve quick response and the gains are low close the equilibrium state, thus preventing oscillatory behaviour.

The non-linear function of lateral error can be any function. However, For the present control design, $k_e(e)$ is given by,

$$k_e(e) = \frac{\exp(k_0 e_{sat}) + \exp(-k_0 e_{sat})}{2} \quad (4-15)$$

with e_{sat} being defined as,

$$e_{sat} = \begin{cases} e, & |e| \leq e_{max} \\ e_{max} \text{sign}(e), & |e| > e_{max} \end{cases} \quad (4-16)$$

where k_0 and e_{max} are tuning constants.

The overall steering command is given by,

$$\delta_{PBC-PI} = -k_I k_e(e) \int_0^t z dt - k_P k_e(e) z + (l_f + l_r) \rho + \frac{m V_x^2 (l_r C_r - l_f C_f)}{\mu C_f C_r (l_f + l_r)} \rho \quad (4-17)$$

4-6 Summary

This chapter explained Stanley, Path Control with Preview, Linear Quadratic Regulator, Immersion and Invariance, Passivity Based Control. The respective steering laws have been derived methodologically. These control strategies have been implemented in literature and gives a bench-marking platform for the controllers to be developed in the next chapter. This thesis accounts for a detailed cross-comparison with the above mentioned strategies. The focus now is on Sliding Mode Control - the main contribution of this thesis.

Sliding Mode Control (SMC)

5-1 Introduction

Variable Structure Control is a popular topic in the 1900's and has been mainly considered for continuous time systems in the form of SMC. SMC has been developed since 1950's and is one of the most reliable control techniques for robustness [39]. The objective of this control technique is to force the system states to reach a particular surface in the state space, called the sliding surface and eventually stay on this surface.

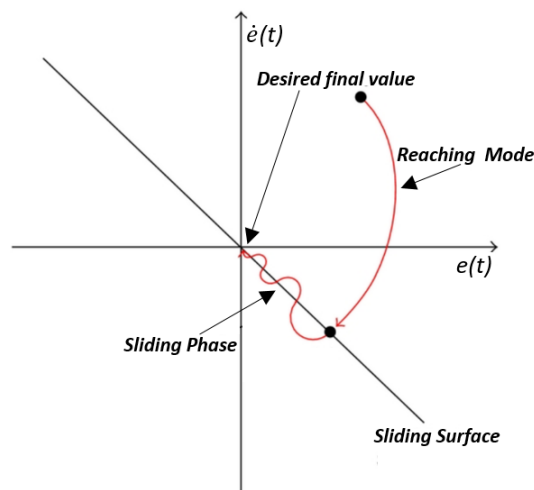


Figure 5-1: Sliding Mode Dynamics
[40]

Consider a nonlinear system whose dynamics are given by,

$$\begin{aligned}\dot{x} &= f(x) + g(x)u \\ y &= h(x)\end{aligned}$$

where y and u denote the output and the input variables, $x \in R^n$ denote the state variable. The control objective is to track a desired trajectory y_{ref}

Defining the output error given by, $e_y = y - y_{ref}$

To design any Sliding Mode Controller, the following steps have to be followed

- **Sliding surface design** : The first step is to construct a certain sliding surface that is a subset of the state space.

$$s(x) : R^n \rightarrow R$$

The function s should be chosen such that the solution to $s = 0$, gives a stable differential equation and eventually tend e_y to go to zero.

Typically, the sliding surface depends on a single scalar parameter, λ

$$s(x) = \left(\frac{d}{dt} + p \right)^{r-1} e_y$$

The integer r is based on the relative degree between y and u

- **Control input design** : A control law is sought for that steers the system trajectories onto the sliding surface. In other words, the control signal is able to steer the s variable to zero in finite time.
- **Stability and gain tuning** : The closed loop dynamics is then checked for stability based on lyapunov analysis. The gains are tuned based on a certain notion formed during stability analysis. The following sections gives an idea of how Sliding Mode Control is derived.

5-2 Super Twisting Algorithm (STA)

5-2-1 Variant 1 - Literature

Some of the key takeaways mentioned in [41] include development of robust path followers capable of handling parametric variations. This subsection describes about a Second Order Sliding Mode Control with Super Twisting algorithm applied to automatic steering of vehicles. Although the controller shows robustness (to be explained in the next chapter), there are a few modifications that are done to the control law in itself in order to get the desired results. These modifications are revealed in the following chapter based on simulation results.

Consider the lateral error dynamics equation given by,

$$\ddot{e}_y = -\frac{\mu(C_f + C_r)}{m}\beta - \frac{\mu(l_f C_f - l_r C_r)}{mV_x}\dot{\psi} - V_x^2\rho + \frac{\mu C_f}{m}\delta \quad (5-1)$$

The objective of the Sliding Mode Controller is to get the lateral error e_y to zero. As discussed, the first step is to choose a sliding surface followed by proposing a control law. To this end, the sliding surface is given by

$$s = \dot{e}_y + \lambda e_y$$

where λ is a positive constant. It has to be noted that upon pushing the sliding surface s to zero, we have asymptotic convergence with respect to the lateral error term e_y ; thus fulfilling our control objective.

On taking the first derivative of the sliding surface with time, we obtain

$$\dot{s} = \ddot{e}_y + \lambda \dot{e}_y$$

Upon substituting equation 5-1 in the above equation,

$$\dot{s} = -\frac{\mu(C_f + C_r)}{m}\beta - \frac{\mu(l_f C_f - l_r C_r)}{mV_x}\dot{\psi} - V_x^2\rho + \lambda \dot{e}_y + \frac{\mu C_f}{m}\delta \quad (5-2)$$

This equation can be represented in the form,

$$\dot{s} = \phi(t, s) + \psi(t, s)\delta$$

where $\phi(t, s)$ and $\psi(t, s)$ are derived from equation 5-2

On the assumption that there exists positive constants s_0 , b_{min} , b_{max} , C_0 such that $\forall x \in R^n$ and $|s(t, x)| < s_0$, the system satisfies the following conditions

$$\begin{aligned} |\delta| &\leq \delta_{max} \\ 0 < b_{min} &\leq |\psi(t, s)| \leq b_{max} \\ |\phi(t, s)| &< C_0 \end{aligned}$$

The super twisting structure mainly addresses the chattering phenomenon which is present in First Order Sliding Mode controllers. The common structure of the super twisting algorithm is to have a continuous signal and the integral of a discontinuous signal of the form

$$\begin{aligned} \delta_{ST} &= \delta_1 + \delta_2 \\ \delta_1 &= -\alpha_1 |s|^{\frac{1}{2}} \text{sign}(s) \\ \delta_2 &= -\alpha_2 \text{sign}(s) \end{aligned}$$

The final step of designing a sliding mode control is to tune gains according to stability analysis. The above super twisting structure is stable if,

$$\alpha_2 > \frac{C_0}{b_{min}}$$

$$\alpha_1 > \sqrt{\frac{4C_0(b_{max}\alpha_2 + C_0)}{b_{min}^2(b_{min}\alpha_2 - C_0)}}$$

The overall control input is a combination of the super twisting algorithm and the equivalent command. The equivalent command is obtained by solving the equation $\dot{s} = 0$. It is given by,

$$\delta_{EQ} = \frac{C_f + C_r}{C_f} \beta + \frac{l_f C_f - l_r C_r}{C_f V_x} \dot{\psi} + V_x^2 \rho - \frac{m\lambda}{\mu C_f} \dot{e}_y \quad (5-3)$$

$$\delta = \delta_{EQ} + \delta_{ST}$$

Simulations with respect to this Super Twisting structure are shown in the following chapter. However, the effect chattering still prevails; implying that the super twisting structure is not able to generate a continuous signal. The signum function used in the super twisting structure was replaced by a smooth function such as the hyperbolic tangent function to get rid of chattering. It must be noted that such an alteration does not guarantee stability in a theoretical sense. To address this issue found in literature, an alternate solution was proposed which is to be discussed in the following subsection.

5-2-2 Variant 2 - Proposed Solution

This method was adopted from a variant of twisting algorithm applied to flight control as mentioned in [42]. This solution of Sliding Mode Control proves stability without using alternative functions as explained in the first variant. The drawbacks of Super Twisting structure applied to vehicle lateral control propelled the author to further investigate the aspect of stability and gain tuning of the Super Twisting Control strategy.

The same lateral error dynamics equation given by 5-1 is considered,

$$\ddot{e}_y = -\frac{\mu(C_f + C_r)}{m} \beta - \frac{\mu(l_f C_f - l_r C_r)}{m V_x} \dot{\psi} - V_x^2 \rho + \frac{\mu C_f}{m} \delta + \zeta$$

where ζ includes both external disturbances and unmodeled dynamics.

A state vector z , where the individual components $z_1 = e_y$ and $z_2 = \dot{e}_y$ is introduced. This reduces the above equation to be written in a state space structure,

$$\dot{z}_1 = z_2 \quad (5-4a)$$

$$\dot{z}_2 = -\frac{\mu(C_f + C_r)}{m} \beta - \frac{\mu(l_f C_f - l_r C_r)}{m V_x} \dot{\psi} - V_x^2 \rho + \frac{\mu C_f}{m} \delta + \zeta(t, z) \quad (5-4b)$$

Consider the desired tracking references* for the two states given by z_{1_d} and z_{2_d} respectively. The new error dynamics is given by,

$$e = z_1 - z_{1_d} \quad (5-5a)$$

$$\dot{e} = \dot{z}_1 - \dot{z}_{2_d} \quad (5-5b)$$

The proposed Super Twisting Slide Mode Control strategy is given by the following equation,

$$\delta = \frac{C_f + C_r}{C_f} \beta - \frac{m\lambda}{\mu C_f} \dot{e} - \frac{k_1 m |s|^{\frac{1}{2}} \text{sign}(s)}{\mu C_f} - \frac{k_2 m}{\mu C_f} \int_0^t \text{sign}(s) d\tau \quad (5-6)$$

To prove closed-loop stability with the proposed control action, the first temporal derivative of the sliding surface is considered.

$$\begin{aligned} \dot{s} &= \ddot{e} + \lambda e \\ &= (\dot{z}_2 - \ddot{z}_{1_d}) + \lambda \dot{e} \end{aligned} \quad (5-7)$$

Equation 5-7 is substituted in the above equation to get,

$$\dot{s} = -k_1 |s|^{\frac{1}{2}} \text{sign}(s) - k_2 \int_0^t \text{sign}(s) d\tau + \zeta(t, z) \quad (5-8)$$

The above equation 5-8 describes the dynamics of the sliding surface. By substituting new variables g_1 and g_2 as,

$$\begin{aligned} g_1 &= s \\ g_2 &= -k_2 \int_0^t \text{sign}(s) d\tau + \zeta(t, z) \end{aligned} \quad (5-9)$$

On taking the time derivatives of these new variables and rearranging the terms, the dynamics of the sliding surface in 5-8 can be written as,

$$\begin{aligned} \dot{g}_1 &= -k_1 |g_1|^{\frac{1}{2}} \text{sign}(g_1) + g_2 \\ \dot{g}_2 &= -k_2 \text{sign}(g_1) + \dot{\zeta}(t, z) \end{aligned} \quad (5-10)$$

where $\dot{\zeta}(t, z)$ is the time derivative of the perturbation and is bounded. Thus, $|\dot{\zeta}| < \zeta^+ \in R^+$. Another set of variables is introduced to rewrite the above equation in a state space form. The new variables is represented as a state vector h given by,

$$h = \begin{bmatrix} h_1 & h_2 \end{bmatrix}^T = \begin{bmatrix} |g_1|^{\frac{1}{2}} \text{sign}(g_1) & g_2 \end{bmatrix}^T \quad (5-11)$$

On rewriting equation 5-10 in terms of the new state variables h_1 and h_2 ,

*In this application, z_{1_d} and z_{2_d} , the reference states are zero as the states already correspond to lateral error dynamics

$$\begin{aligned} \dot{h}_1 &= \frac{1}{2|h_1|}(-k_1 h_1 + h_2) \\ \dot{h}_2 &= \frac{1}{2|h_1|}(-2k_2 v_1) + \dot{\zeta}(t, z) \end{aligned} \quad (5-12)$$

To define the time derivative of ζ as a bounded signal, it is written as,

$$\dot{\zeta}(t, z) = \chi(t, z) \text{sign}(h_1) = \chi(t, z) \frac{h_1}{|h_1|} \quad (5-13)$$

where $\chi(t, z)$ is a bounded function such that $0 < \chi(t, z) < \zeta^+$

The above equation 5-12 is then condensed to be rewritten as,

$$\begin{bmatrix} \dot{h}_1 \\ \dot{h}_2 \end{bmatrix} = \underbrace{\frac{1}{2|h_1|} \begin{bmatrix} -k_1 & 1 \\ -2k_2 + 2\chi & 0 \end{bmatrix}}_{A(h_1)} \begin{bmatrix} h_1 \\ h_2 \end{bmatrix} \quad (5-14)$$

An important assertion at this stage is that if $h_1, h_2 \rightarrow 0$ in finite time[†], then $g_1, g_2 \rightarrow 0$ in finite time, and hence s reach 0. It can be observed that the above equation forms an autonomous system whose dynamics are governed by the matrix $A(h_1)$.

A Lyapunov function is introduced here to prove the convergence of h_1, h_2 in finite time.

$$V(h) = h^T P h \quad (5-15)$$

where P is a positive definite symmetric matrix given by,

$$P = P^T = \begin{bmatrix} \lambda_1 + \lambda_2^2 & -\lambda_2 \\ -\lambda_2 & 1 \end{bmatrix} \quad (5-16)$$

For any $\lambda_1 > 0$, it is seen that the matrix P is positive definite. Therefore, it is established that $V(h)$ is a positive definite function. The focus is now shifted towards the time derivative of the $V(h)$ given by,

$$\dot{V}(h) = h^T \left(P A(h_1) + A^T(h_1) P \right) h \quad (5-17)$$

On further simplification, $\dot{V}(h)$ is written as,

[†]The proofs for finite time is not provided in this thesis but can be observed in [42]

$$\dot{V}(h) \leq -\frac{1}{2|h_1|} h^T Q h \quad (5-18)$$

where Q is a symmetric matrix of the form,

$$Q = \begin{bmatrix} 2\lambda_1 k_1 + 2\lambda_2(\lambda_2 k_1 - 2k_2) + 4\lambda_2 \zeta^+ & \#^\ddagger \\ 2k_2 - \lambda_2 k_1 - \lambda_1 - \lambda_2^2 - 2\zeta^+ & 2\lambda_2 \end{bmatrix}$$

The Q matrix should also be a positive definite matrix for $V(h)$ to be negative semi-definite. Setting the gain $k_2 = \frac{1}{2}\lambda_2 k_1$, Q can be written as,

$$Q = \begin{bmatrix} 2\lambda_1 k_1 + 4\lambda_2 \zeta^+ & \# \\ -(\lambda_1 + \lambda_2^2 + 2\zeta^+) & 2\lambda_2 \end{bmatrix}$$

Therefore, Q will be positive definite if,

$$k_1 > \frac{(\lambda_1 + \lambda_2^2 - 2\zeta^+)^2 - 8\lambda_2 \zeta^+}{4\lambda_1 \lambda_2}$$

5-3 Modified Super Twisting Algorithm (MSTA)

One of the main drawbacks of the super twisting algorithm is the convergence time. The rate of convergence parameter λ is seen to have limited effect on the convergence rate in simulations. As a result, the sliding dynamics are modified in the following manner to achieve faster convergence. Consider again the equation for lateral error dynamics,

$$\ddot{e}_y = -\frac{\mu(C_f + C_r)}{m} \beta - \frac{\mu(l_f C_f - l_r C_r)}{m V_x} \dot{\psi} - V_x^2 \rho + \frac{\mu C_f}{m} \delta + \zeta \quad (5-19)$$

By introducing a new state vector z , where the individual components are $z_1 = e_y$ and $z_2 = \dot{e}_y$ the above equation can be rewritten as,

$$\dot{z}_1 = z_2 \quad (5-20)$$

$$\dot{z}_2 = -\frac{\mu(C_f + C_r)}{m} \beta - \frac{\mu(l_f C_f - l_r C_r)}{m V_x} \dot{\psi} - V_x^2 \rho + \frac{\mu C_f}{m} \delta + \zeta \quad (5-21)$$

As in the previous case, the first step is to define a sliding surface given by,

$$s = e + \lambda \dot{e}$$

The control objective is to design and implement a robust control signal u that can track

[‡]This entry is the same as the diagonal entry as Q is a symmetric matrix.

the path, in other words, can push the error dynamics to zero, in the presence of model uncertainty or external disturbances.

Consider the desired tracking references for the two states given by z_{1_d} and z_{2_d} respectively. The new error dynamics is given by,

$$\begin{aligned} e &= z_1 - z_{1_d} \\ \dot{e} &= \dot{z}_1 - \dot{z}_{2_d} \end{aligned} \quad (5-22)$$

Now, the first derivative of the sliding variable is considered,

$$\begin{aligned} \dot{s} &= \ddot{e} + \lambda e \\ &= (\dot{z}_2 - \ddot{z}_{1_d}) + \lambda \dot{e} \end{aligned} \quad (5-23)$$

A control law that stabilizes the open loop dynamics is proposed,

$$\begin{aligned} \delta &= \frac{m}{C_f} \left(\frac{\mu(C_f + C_r)}{m} \beta + \frac{\mu(l_f C_f - l_r C_r)}{m V_x} \dot{\psi} + V_x^2 \rho - \lambda \dot{e} - k_1 |s|^{\frac{1}{2}} \text{sign}(s) - k_2 s \right. \\ &\quad \left. - k_3 \int_0^t \text{sign}(s) d\tau - k_4 \int_0^t s d\tau \right) \end{aligned} \quad (5-24)$$

Substituting the above expression in equation 5-1, we have the dynamics of the sliding variable given by,

$$\dot{s} = -k_1 |s|^{\frac{1}{2}} \text{sign}(s) - k_2 s - k_3 \int_0^t \text{sign}(s) d\tau - k_4 \int_0^t s d\tau + \zeta(t, x) \quad (5-25)$$

By substituting,

$$v_1 = s \quad (5-26a)$$

$$v_2 = k_3 \int_0^t \text{sign}(s) dt - k_4 \int_0^t s dt \quad (5-26b)$$

We have,

$$\dot{v}_1 = -k_1 |v_1|^{\frac{1}{2}} \text{sign}(v_1) - k_2 v_1 + v_2 \quad (5-27a)$$

$$\dot{v}_2 = -k_3 \text{sign}(v_1) - k_4 v_1 \quad (5-27b)$$

$$V(v) = 2k_3 |v_1| + k_4 v_1^2 + \frac{1}{2} v_2^2 + \frac{1}{2} \left(k_1 |v_1|^{\frac{1}{2}} \text{sign}(v_1) + k_2 v_1 - v_2 \right)^2 \quad (5-28)$$

The time derivative of $V(v)$ is,

$$\begin{aligned}\dot{V} &= \frac{1}{|v_1|^{\frac{1}{2}}} \zeta^T Q_1 \zeta - \zeta^T Q_2 \zeta \\ Q_1 &= \frac{k_1}{2} \begin{bmatrix} (2k_3 + k_1^2) & 0 & -k_1 \\ 0 & (2k_4 + 5k_2^2) & -3k_2 \\ -k_1 & -3k_2 & 1 \end{bmatrix} \\ Q_2 &= k_2 \begin{bmatrix} (k_3 + 2k_1^2) & 0 & 0 \\ 0 & (k_4 + k_2^2) & -k_2 \\ 0 & -k_2 & 1 \end{bmatrix}\end{aligned}\quad (5-29)$$

A sufficient condition for \dot{V} to be negative definite is if $Q_1, Q_2 > 0$

$$4k_3k_4 > (8k_3 + 9k_1^2)k_2^2$$

5-4 Non-singular Terminal Modified Super Twisting Algorithm (NSTMSTA)

One of the main drawbacks of First Order Sliding Mode Control is the problem of chattering. Although this strategy is effective to track a certain trajectory in a reference tracking problem, they fail to produce a continuous control output. In order to ensure a continuous control signal is applied to the system in focus, Second Order Sliding Mode controls have gained popularity. However, there lie other problems in the existing Sliding Mode strategies for automatic steering applications. The choice of the right set of Lyapunov function was taken from an application of this type of sliding mode control to flight control as mentioned in [43–45].

The conventional form of Sliding Mode Control guarantees asymptotic convergence of the sliding variable to the sliding surface. However for real time applications where we need to arrive at the sliding surface in finite time. To address this issue, researchers have been working on Terminal Sliding Mode Control. This modification of the conventional Sliding Mode Control is based on having extra linear terms that are added to the Super Twisting algorithm as shown in the above section.

Another problem with respect to Second Order Sliding Mode strategies is the singularity issue. There might be possibilities that the Terminal Sliding Mode Control requires a control signal to be infinite in order to stay on the sliding surface. However, this is not practical and hence, a non-singular control approach is proposed. This Non-Singular Terminal control strategy involves the sliding surface to be a non-linear function.

Let us consider the equation 5-1 for lateral error dynamics and also the equation. The sliding surface is given by,

$$s = \dot{e} + \lambda_1 e + \lambda_2 (exp)^{-\alpha t} e^{1-2\beta} \quad (5-30)$$

where $\lambda_1 > 0$, $\lambda_2 > 0$, $\alpha > 0$, $0 < \beta < 1$. It has to be noted that the sliding surface is defined by a non-linear function to accelerate the convergence of the sliding variable to the sliding surface.

A control law is proposed that stabilizes the open loop dynamics give by,

$$\delta = \frac{m}{C_f} \left(\frac{\mu(C_f + C_r)}{m} \beta + \frac{\mu(l_f C_f - l_r C_r)}{m V_x} \dot{\psi} + V_x^2 \rho - \lambda \dot{e} - Z - k_1 |s|^{\frac{1}{2}} \text{sign}(s) - k_2 s - k_3 \int_0^t \text{sign}(s) d\tau - k_4 \int_0^t s d\tau \right) \quad (5-31)$$

where Z is defined as,

$$Z = \lambda_2 \exp^{-\alpha t} e^{-2\beta} \left((1 - 2\beta) \dot{e} - \alpha e \right) \quad (5-32)$$

To further prove stability of the closed-loop system with the proposed control action, the temporal derivative of the sliding surface is considered along with the lateral error dynamics given in equation 5-1.

$$\dot{s} = -\frac{\mu(C_f + C_r)}{m} \beta - \frac{\mu(l_f C_f - l_r C_r)}{m V_x} \dot{\psi} - V_x^2 \rho + \frac{\mu C_f}{m} \delta - \dot{z}_{2d} + \lambda_1 \dot{e} + Z \quad (5-33)$$

Upon substituting the proposed steering law in the above equation 5-33,

$$\dot{s} = -k_1 |s|^{\frac{1}{2}} \text{sign}(s) - k_2 s - k_3 \int_0^t \text{sign}(s) d\tau - k_4 \int_0^t s d\tau \quad (5-34)$$

This form of sliding surface dynamics was previously seen in Modified Super Twisting Algorithm. The proof follows from the previous section. Therefore, the Non-singular Terminal Modified Super Twisting algorithm yields finite-time convergence of the sliding surface $s = 0$, provided the gains are tuned as shown in the previous section.

5-5 Summary

This chapter proposed a new variant of Super Twisting algorithm for relatively easier gain tuning. Furthermore, a novel design for automatic steering based path following with Sliding Mode Control using Modified Super Twisting and Non-singular Terminal Modified Super Twisting Algorithm is explained. Having explained such wide variety of path following control systems, the focus is now on simulation results.

Simulation Results and Comparisons

To evaluate the performance of the bench-marking steering controllers with the novel variants of Sliding Mode Control developed (refer section 5-2 onwards), a high fidelity multi-body model is used on IPG CarMaker. Comparisons are made for different type of disturbances and key performance matrices are tabulated.

6-1 Vehicle Setup

All simulations were carried out for Toyota Camry vehicle model. The vehicle dynamics parameters of this model is given in Appendix A. Tire model based on Pacejka's Magic Formula was used. It was observed that steering dynamics played a huge role in influencing vehicle lateral behaviour. To check validity of the controllers at simpler conditions at first, a static steer ratio is initially chosen and steering dynamics are not included.

6-2 Scenario

The reference path used for simulations is mentioned in Chapter 3. The path is kept symmetrical for ease of analysing the performance parameters. The radius of the bends were chosen to arrive at lateral accelerations in the linear range for the simulated longitudinal velocities.

6-3 Results

6-3-1 Super Twisting Algorithm Variant 1 v/s Proposed

As an alternate control design to the already existing ST algorithm (Variant 1), another variant of the ST algorithm (ST-proposed) was designed based on stability analysis. This proposed controller was tested for Toyota Camry at different vehicle speeds under different

conditions. Figures 6-1, 6-2, 6-3 and 6-4 show the comparison between the two ST algorithms at different vehicle speeds. It is seen that the ST-proposed performs much better with respect to lateral and heading error. The gains of the proposed ST controller was kept the same at all velocities. However, at 40 km/h it is seen that the peak-to-peak lateral errors is fairly greater than ST Variant 1. The gain tuning for ST-proposed is done keeping in mind that the lateral error should not exceed $\pm 0.5\text{m}$.

The main issue of ST Variant 1 is that there is no stability proofs shown in the literature for the constraints held on its gains. This led to a lot of chattering in the control signal (steering input). As such, there are a lot of issues with Sliding Mode Control, in general, in generating high frequency chattering output signals which is not really recommended in an application like steering due to passenger comfort problems. To rectify this issue, the discontinuous signum function of the ST Variant 1 that caused the chattering effect was replaced by a tangent hyperbolic function - a continuous function. Although there are no stability analysis proofs for such a 'hack', it worked well. However, to look at this issue, the ST algorithm was redesigned (ST proposed) and the results are shown in the following plots.

This ST algorithm designed is based on a simple linear bicycle model based on body slip and yaw rate dynamics. The reference path is described as a function of constant longitudinal velocity. Although, this mismatch between the model chosen for control design and the actual plant on IPG CarMaker is negligible at lower speeds for the purpose of reference trajectory tracking (Refer lateral error at 20 km/h). At higher speeds, quite obviously, as shown in Chapter 2, there is a significant mismatch between plant and model behaviour. However, the controller is able to do sufficiently well fulfilling the objective of keeping the vehicle as close to the lane center as possible. From the lateral error plots of 6-2, 6-3 and 6-4, it is shown that after the vehicle makes a left and a right turn and reaches the straight segment of the track, there is a certain offset. Ideally, there should have been zero lateral error at this juncture as shown in the lateral error plot of figure 6-1. This is clearly a plant-model dynamics mismatch and is something to be looked into. The advantages of ST-proposed are however that it performs better than its alternative and the peak-to-peak lateral error ± 40 cm. This performance on having minimal lateral error can however be greatly improved with better gain tuning. However, this comes at a cost of having a greater overshoot in steering wheel angle. The ST controller is highly sensitive to the convergence rate parameter λ , which dictates the rate at which the the controller pushes the sliding dynamics back to the plane $s = 0$. An increase in λ is seen to increase the overshoot in the steering angle. In these simulations λ is tuned accordingly - to have lesser lateral error and lesser overshoot.

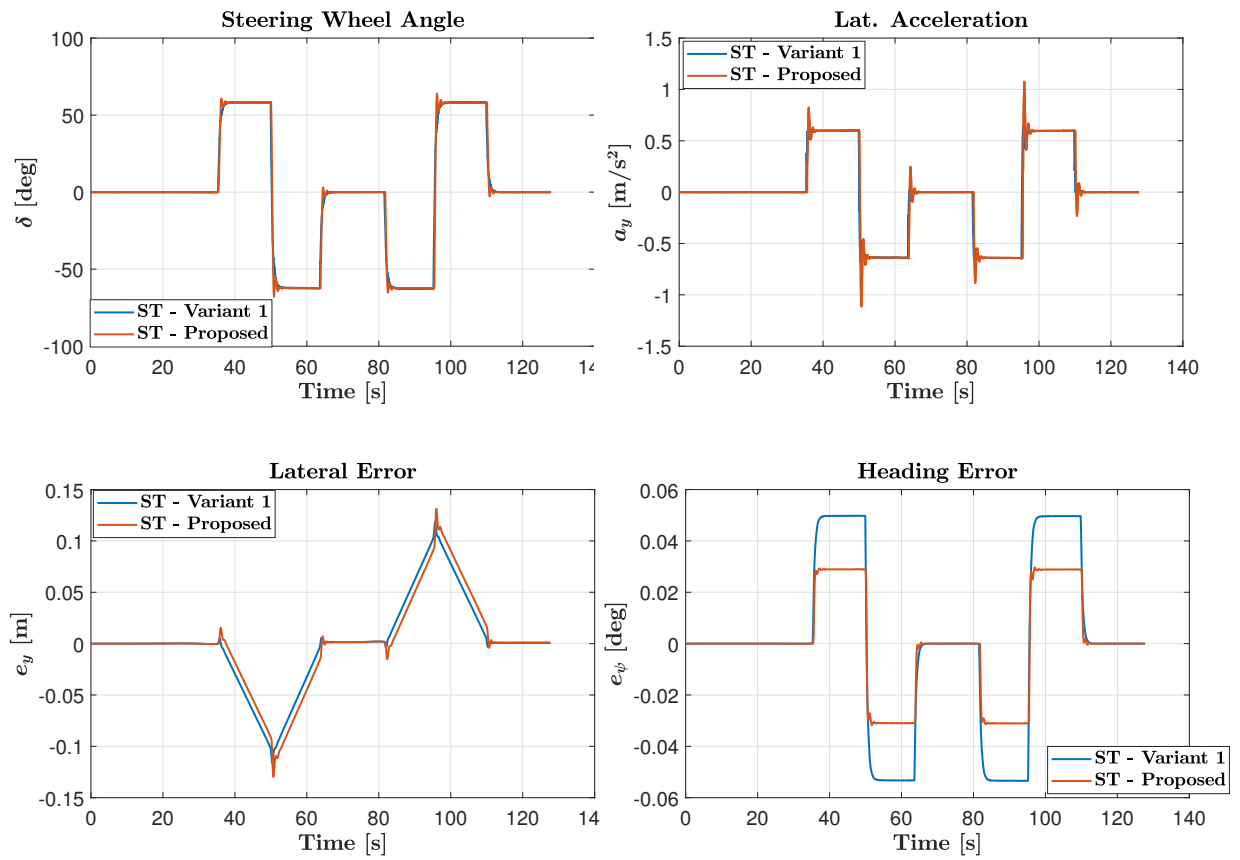


Figure 6-1: Sliding Mode Control - Super Twisting Algorithm (in literature) vs Super Twisting Algorithm (proposed solution) for velocity = 20 km/h

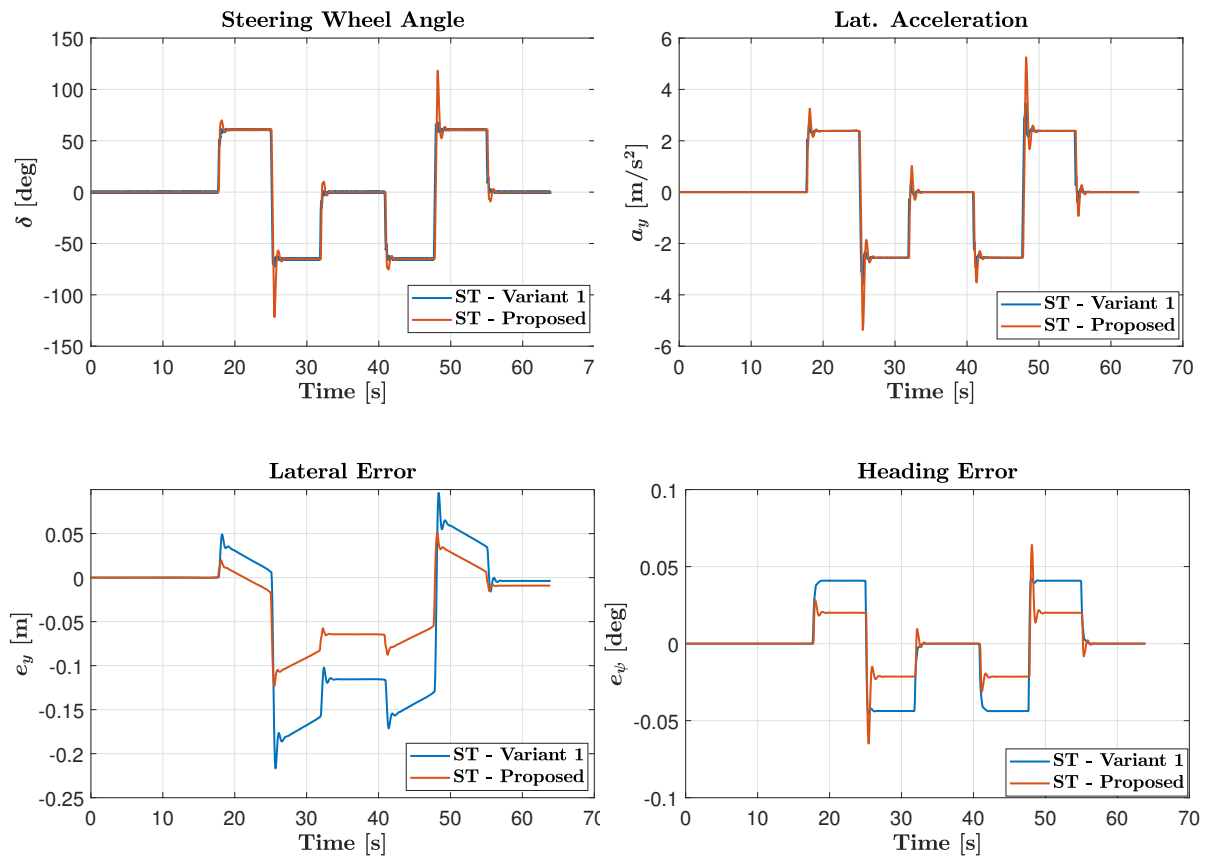


Figure 6-2: Sliding Mode Control - Super Twisting Algorithm (in literature) vs Super Twisting Algorithm (proposed solution) for velocity = 40 km/h

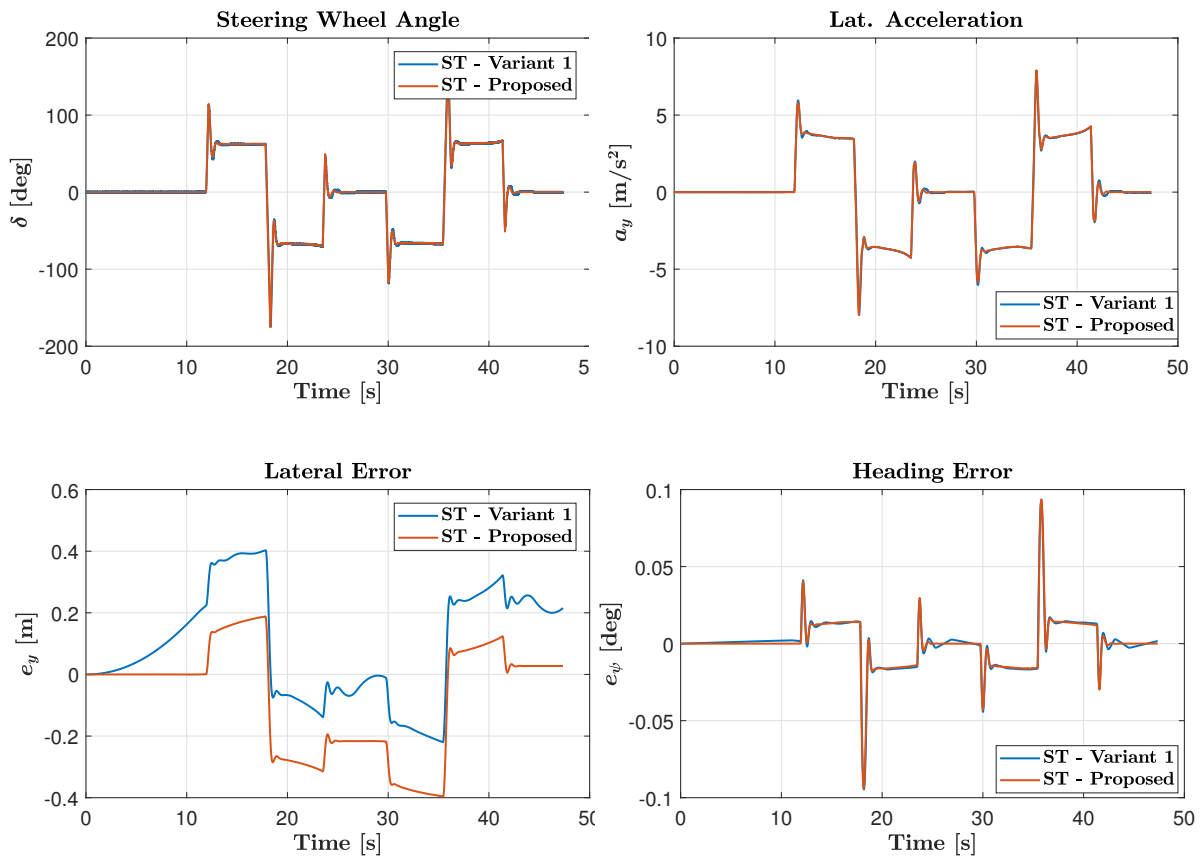


Figure 6-3: Sliding Mode Control - Super Twisting Algorithm (in literature) vs Super Twisting Algorithm (proposed solution) for velocity = 60 km/h

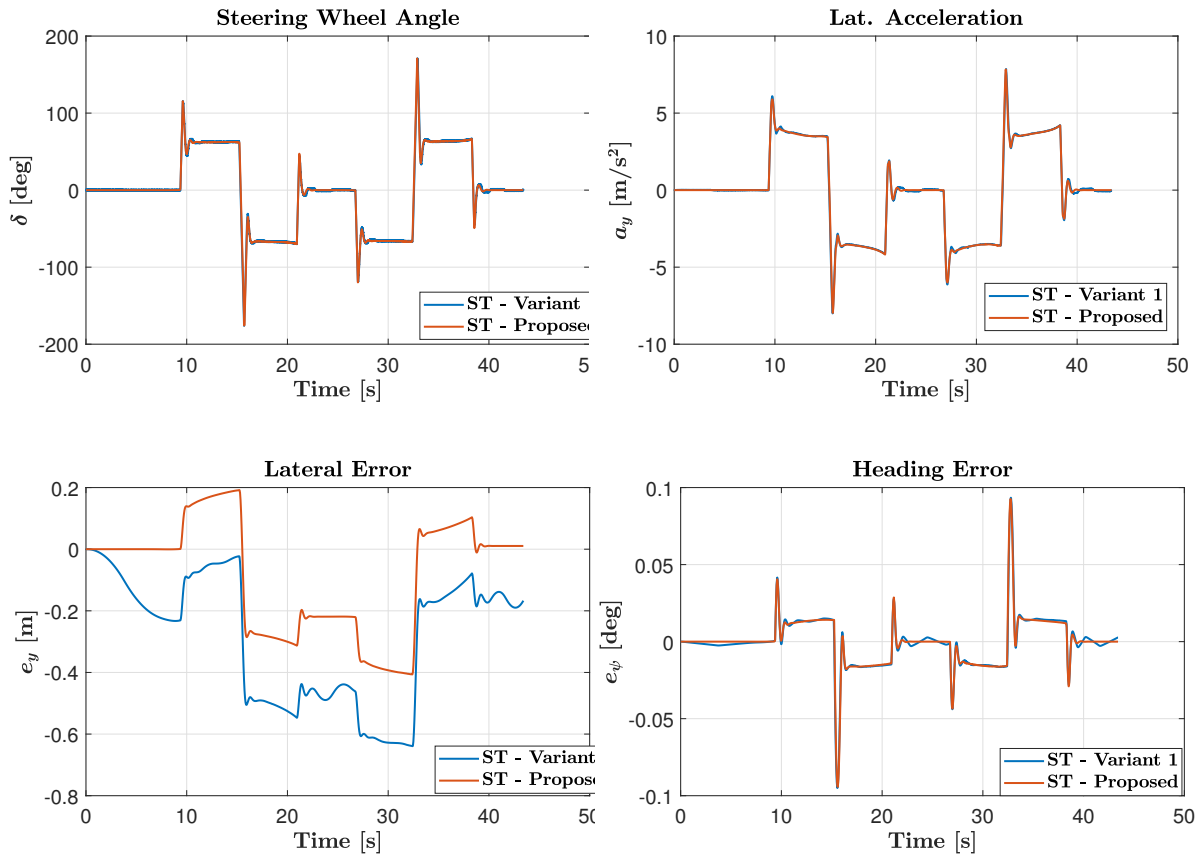


Figure 6-4: Sliding Mode Control - Super Twisting Algorithm (in literature) vs Super Twisting Algorithm (proposed solution) for velocity = 80 km/h

6-3-2 Modified Super Twisting vs Non-singular Modified Super Twisting Algorithm

Figures 6-5, 6-6, 6-7 and 6-8 show the comparison between key parameters involved in reference tracking. Mathematically, the main advantages of MSTA and NSTMSTA are its finite time convergence to the sliding surface. Sliding Mode Control, by default, boasts about convergence to the plane $s = 0$, hence proving the result, $\dot{e}_y = -\lambda e_y$, and thereby proving asymptotic convergence. It should be noted that in an application like autonomous steering, asymptotic convergence is not sufficient. The vehicle has to react very quickly to changes in road curvature and speed profiles. Therefore, finite time convergence is looked at, instead of asymptotic convergence. In this regard, both MST and NSTMSTA are capable of finite time convergence.

In comparing with the ST-proposed controller, the performance of NSTMSTA is much better at higher speeds. Although, this can be attributed to better tuning of gains in the case of NSTMSTA, it cannot be known for certain unless optimal gains are mathematically proven. Comparing MST and NSTMSTA, the latter performs much better in terms of having a lower peak-to-peak lateral error. However, the peak-to-peak heading error is lower in the case of MST. This is attributed to the control logic used in NSTMSTA. The nearest point algorithm used in the control logic with NSTMSTA was calculated based on the distance between the center of front axle and not the CoG. This tweak was done to arrive at a low peak-to-peak lateral error. It is still not certain as to why this occurs.

Just like the previous scenarios with ST algorithms, the parameter λ in the case of MSTA, the parameters λ_1, λ_2 are highly influential in fine tuning of lateral error. The controller gains k_1, k_2, k_3, k_4 have limited scope of tuning concerning performance in steering wheel/ change in lateral error. However, these controller gains make sure that stability is proven, which is of utmost importance.

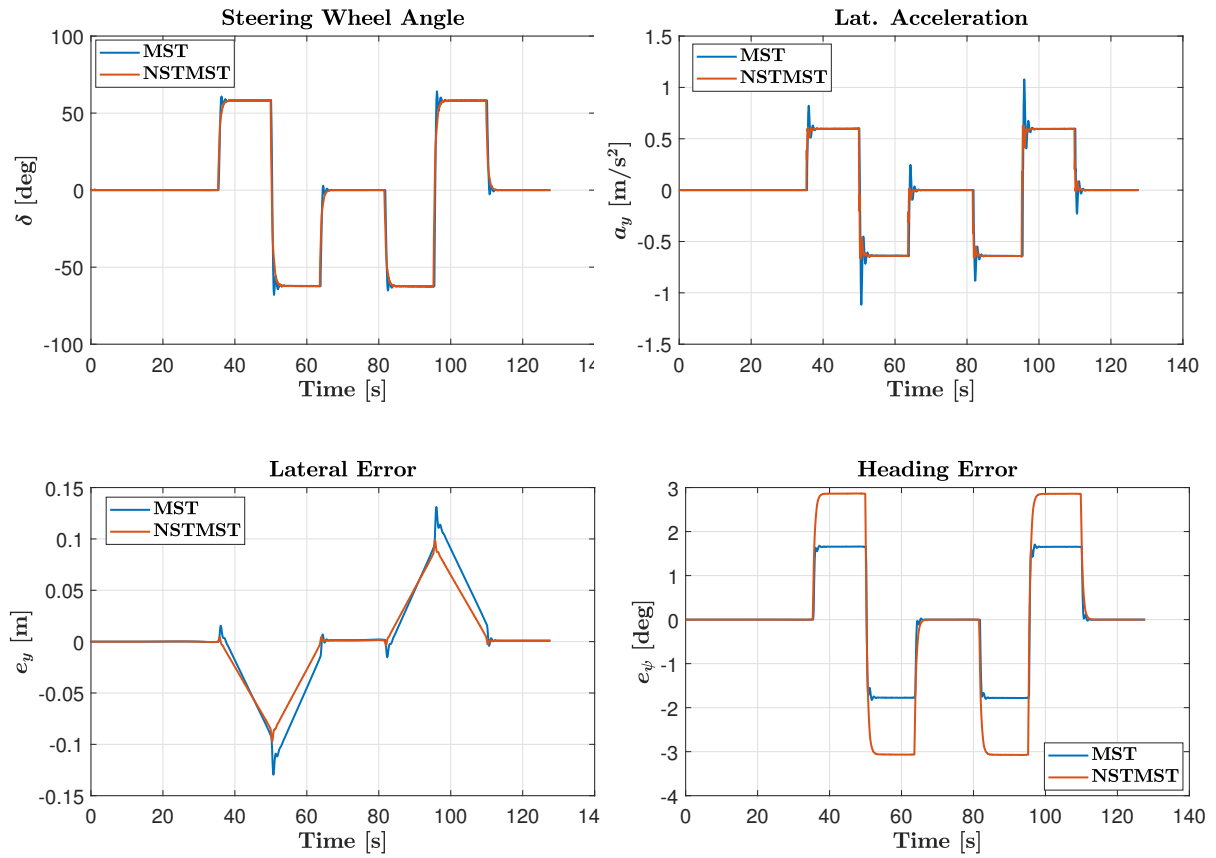


Figure 6-5: Sliding Mode Control - Modified Super Twisting Algorithm vs Non-singular Terminal Modified Super Twisting Algorithm for velocity = 20 km/h

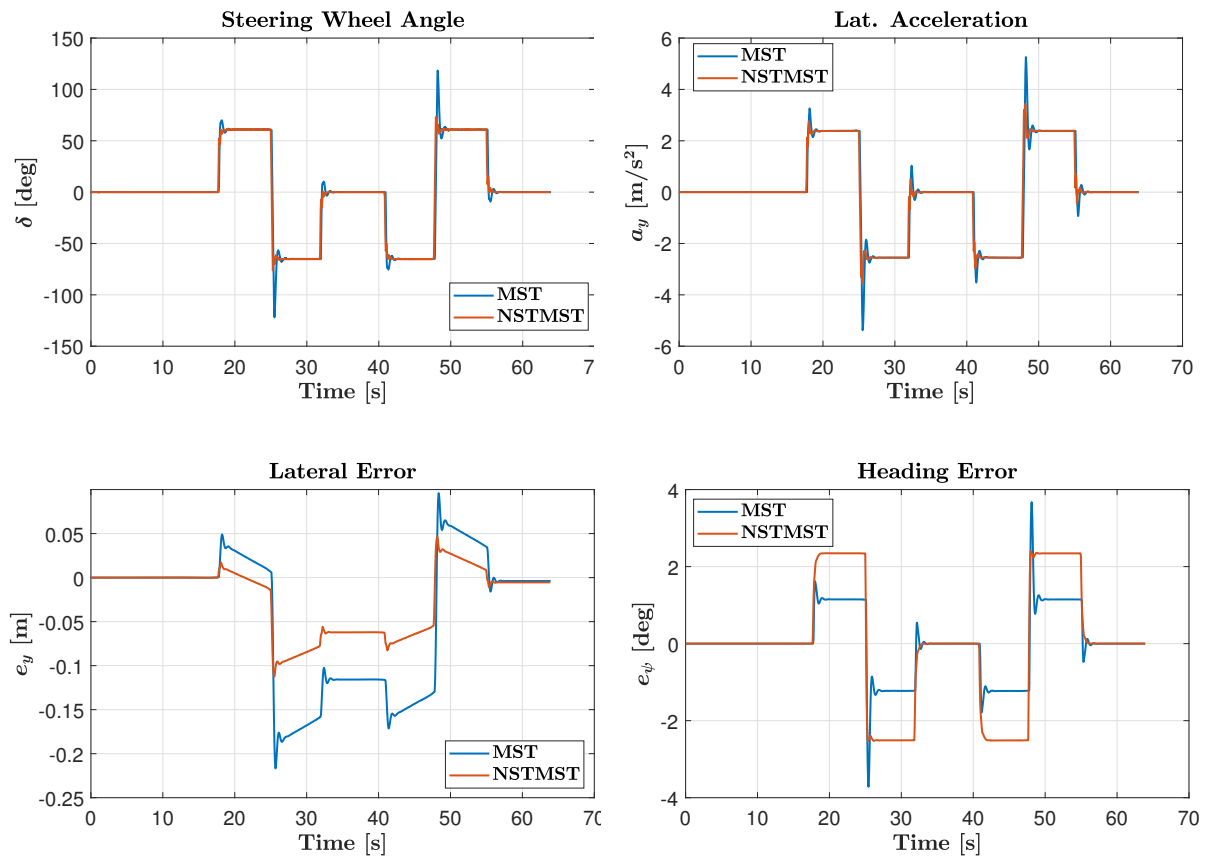


Figure 6-6: Sliding Mode Control - Modified Super Twisting Algorithm vs Non-singular Terminal Modified Super Twisting Algorithm for velocity = 40 km/h

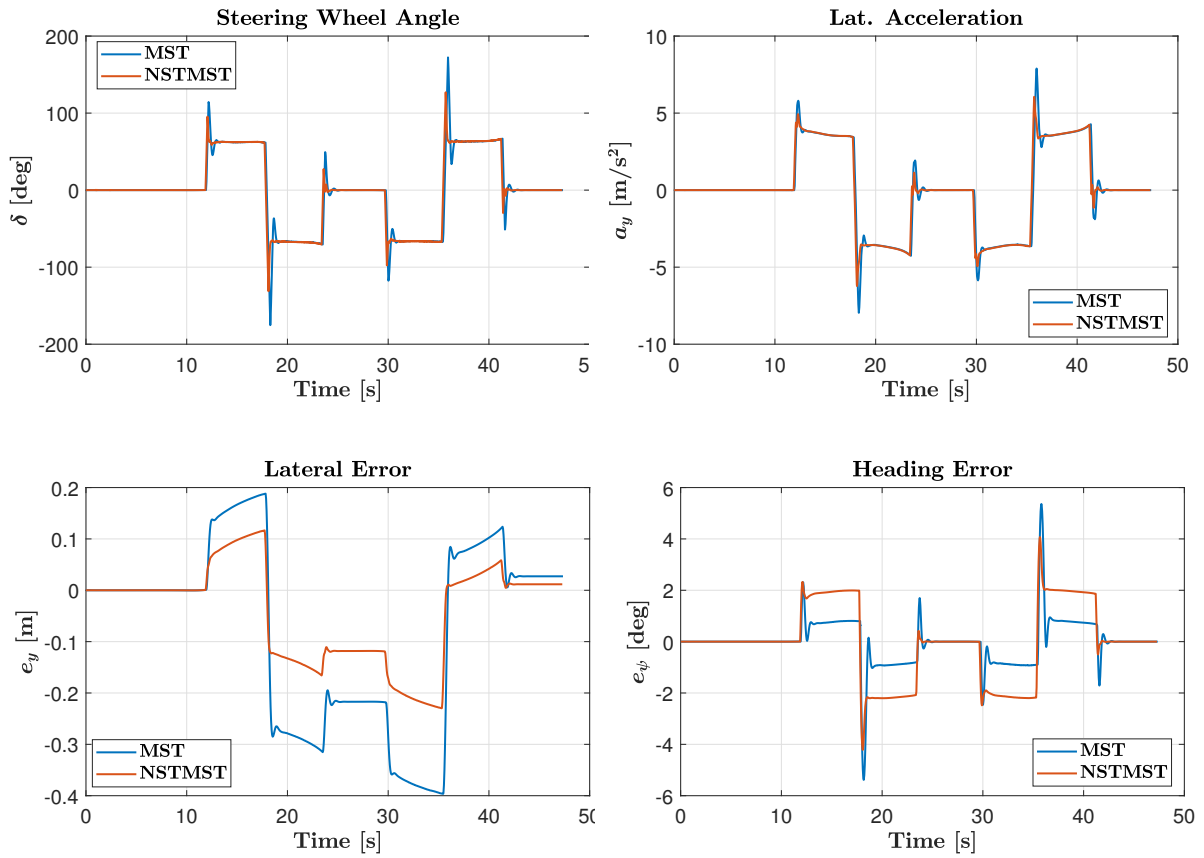


Figure 6-7: Sliding Mode Control - Modified Super Twisting Algorithm vs Non-singular Terminal Modified Super Twisting Algorithm for velocity = 60 km/h

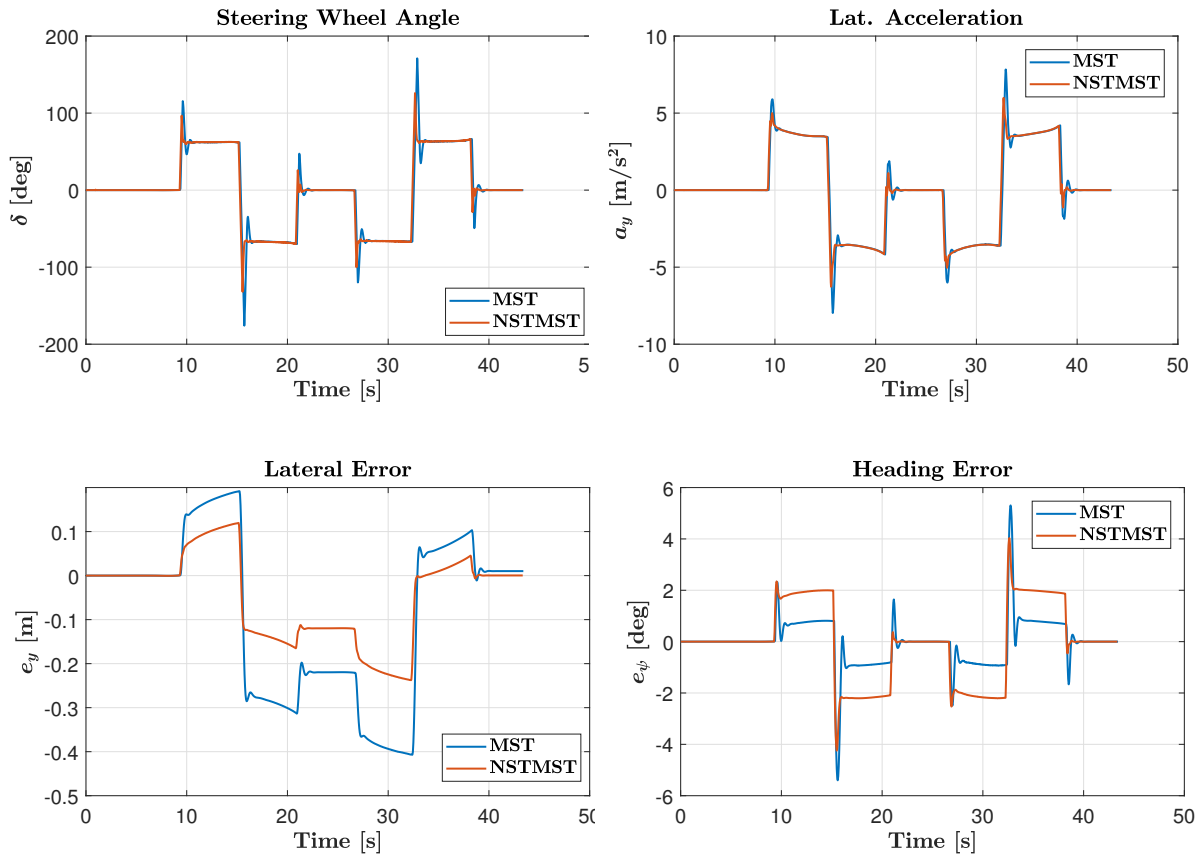


Figure 6-8: Sliding Mode Control - Modified Super Twisting Algorithm vs Non-singular Terminal Modified Super Twisting Algorithm for velocity = 80 km/h

A drawback of the Sliding Mode Controllers is their performance at higher speeds. As reported earlier, this is due to a mismatch in plant and model. Another critical aspect is the sudden and abrupt changes in the steering wheel angle during turns (Refer to Steering wheel angle plots of figures of ST, MST, NSTMST). Figure 6-9 shows a comparison between the difference in road wheel angle before and after rate saturation, in the case of NSTMST. Unlike other benchmarking controllers (PCwP, LQR) that perform well at higher speeds, the Sliding Mode Controllers are influenced by the convergence rate parameter λ ; which causes the steering angle/road wheel angle to jump higher than the value suggested by the rate limiter. Thus, the steering angle proposed by the controller is not being applied and the controller underperforms. However, NSTMST shows significant improvements over the ST structure at higher speeds.

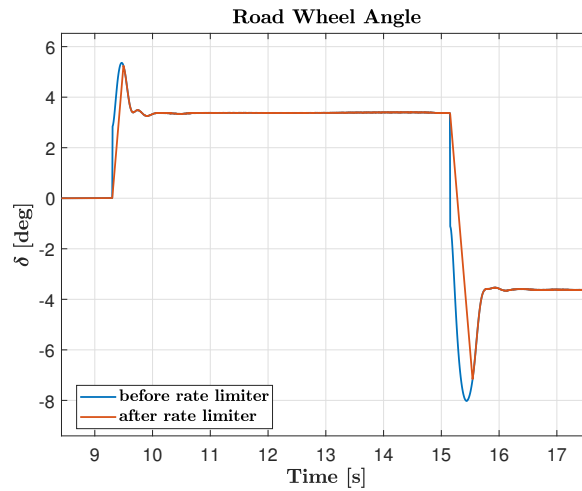


Figure 6-9: Effect of steering rate limiter with Non-singular Terminal Modified Super Twisting Algorithm at velocity = 80 km/h

Figure 6-10 shows the variation of the sliding variable over the course of the reference path. Chattering being a frequent issue in Sliding Mode Control, the ability of the implemented NSTMSTA controller to push the sliding surface to the plane $s = 0$ becomes crucial to investigate. Figure 6-10a shows that the controller is able to push the dynamics to the plane $s = 0$ rather quickly. The peaks that are shown are the time instants when the vehicle encounters a right/left turn. Figure 6-10b shows a zoomed in view of the sliding surface. It can be seen clearly that the fluctuations are of the order of 10^{-5} and hence, it is negligible. Any fluctuations of the order of 10^{-3} will cause a high frequency oscillatory behaviour of the steering wheel.

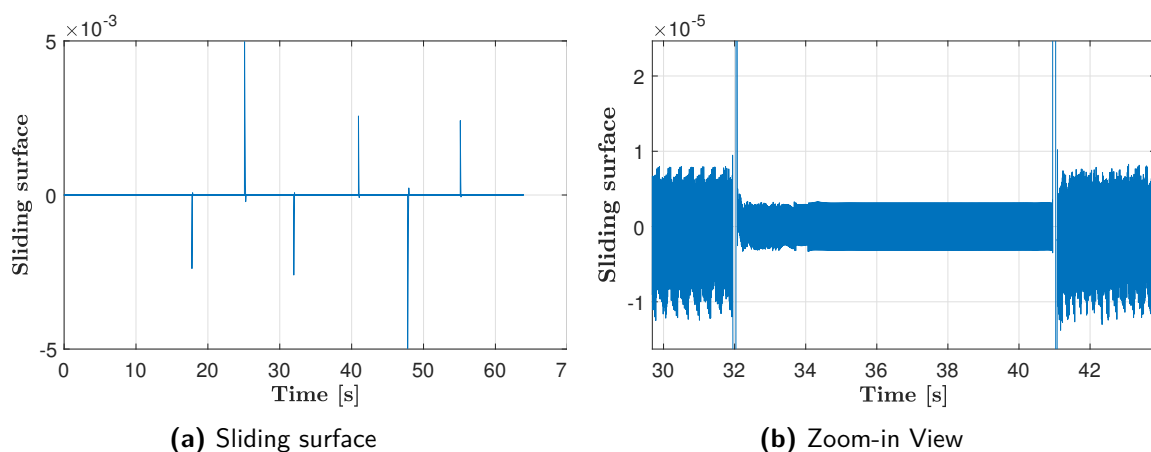
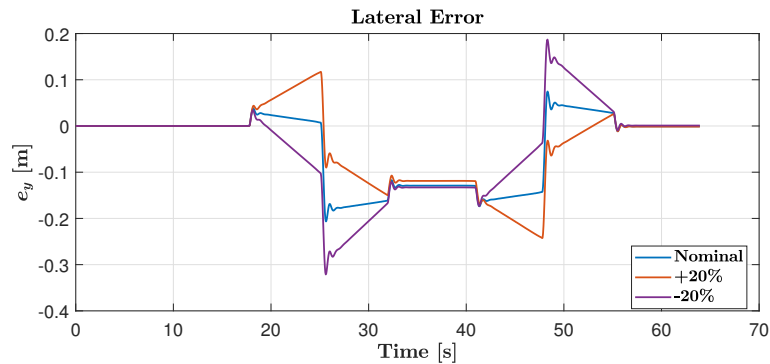


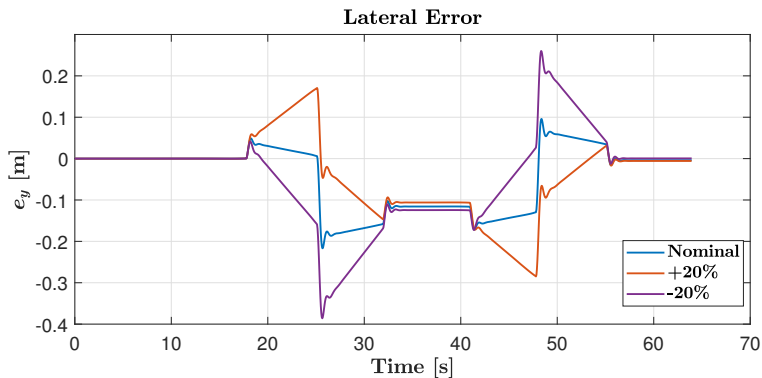
Figure 6-10: Variation of s - sliding surface with Non-singular Terminal Modified Super Twisting Algorithm for velocity = 40 km/h

6-3-3 Parametric Variations

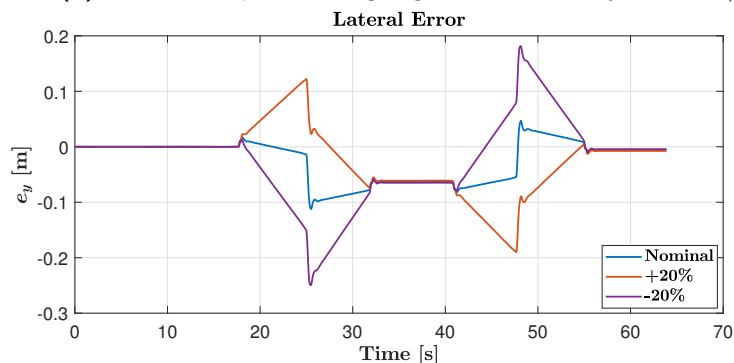
The main vehicle parameters that change dynamically over the course of drive are the mass of the vehicle, the cornering stiffnesses of the tires and the co-efficient of friction. The developed controllers are tested for +/- 20% change in cornering stiffness values. Mass and co-efficient friction variations are not considered for this study. Figure 6-11c shows the change in lateral error over time for the proposed controllers. The velocity for all robustness tests is kept at 40 km/h.



(a) Proposed Solution for Super Twisting Algorithm at velocity = 40 km/h



(b) Modified Super Twisting Algorithm at velocity = 40 km/h



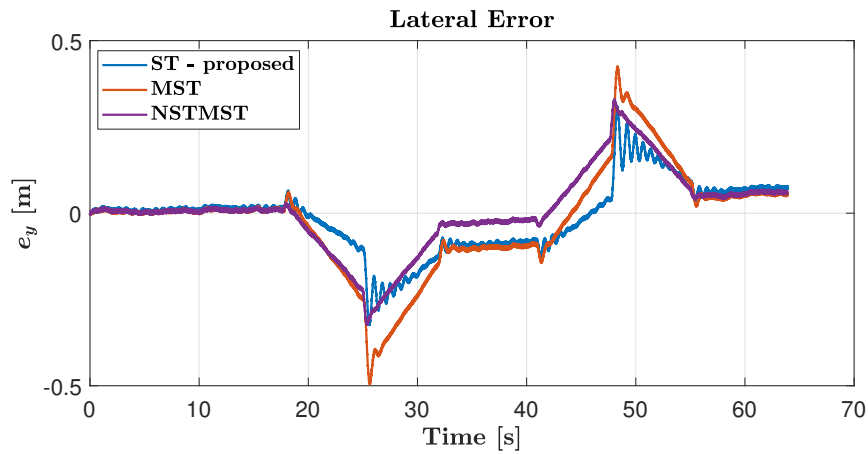
(c) Non-singular Terminal Modified Super Twisting Algorithm at velocity = 40 km/h

Figure 6-11: Robustness check against uncertainties in cornering stiffness of front and rear axles

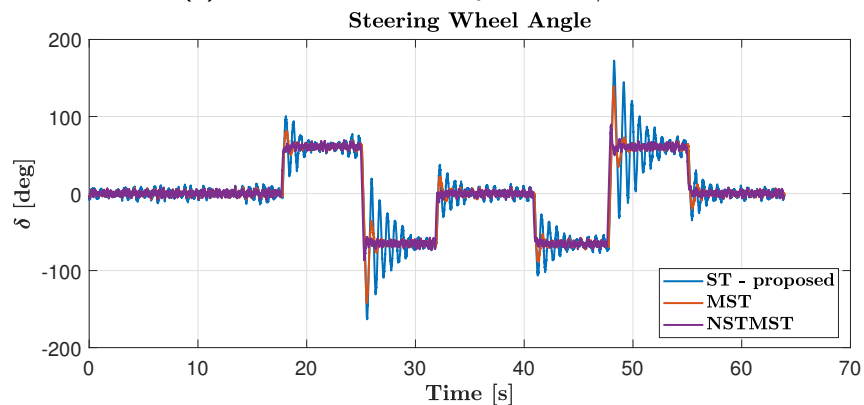
Based on the above figures, it is clear that the deviation in lateral error is quite small for $\pm 20\%$ change in cornering stiffness values. ST-proposed performs the best out of three with a peak-to-peak lateral error of about 0.7m, followed by NSTMSTA which is about 0.8m. MSTA shows a variation of more than 1m which is above the control objective limit ($\pm 0.5\text{m}$). It is to be noted that the gains are kept constant during the simulation runs.

6-3-4 Localisation error

All measurements are noisy and hence it is important to test controller performance considering the fact that lateral error measurements are noisy. To model the vehicle localization noise, a white mean uniformly distributed noise signal with a co-variance of 0.005 is considered. In addition, the mass of the vehicle was altered to be 20% more than the actual value. This is done as an added parametric uncertainty.



(a) Lateral error at velocity = 40 km/h



(b) Steering Wheel Angle at velocity = 40 km/h

Figure 6-12: Robustness check against localization error

Figures 6-12a and 6-12b shows the lateral error and steering wheel angle plots for the proposed controllers. ST-proposed is not able to reject measurement noise and the effect of such a noise, seen on the steering wheel angle as it oscillates to arrive at a steady state value. Meanwhile, MSTA is able to reject disturbances without having much effect on the steering wheel angle. But one of the drawbacks is high peak-to-peak lateral error. NSTMSTA on the other hand, having a lateral error of about $\pm 0.3\text{m}$, clearly outperforms the other 2 controllers. This is one of the important advantages of SMC over the other proposed controllers and also benchmarking controllers. The ability to reject bounded disturbances is crucial with real-time applications and SMC stands out to be an important candidate.

6-3-5 Cross-wind

Figure 6-13 shows the direction of the modeled wind with respect to the reference path. Wind speeds of 30,40,50 km/h are tested respectively. The controller's robustness is checked at different vehicle speeds.

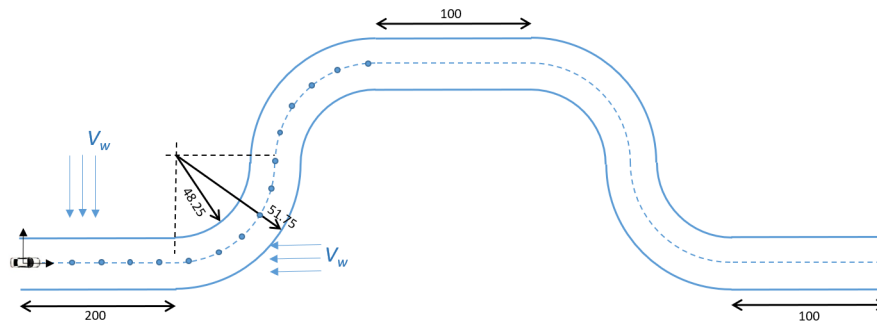
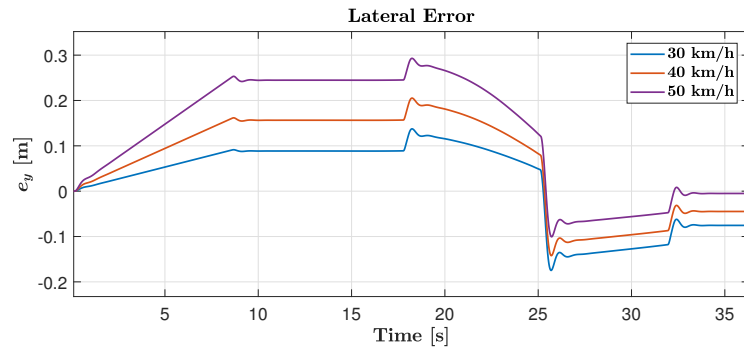
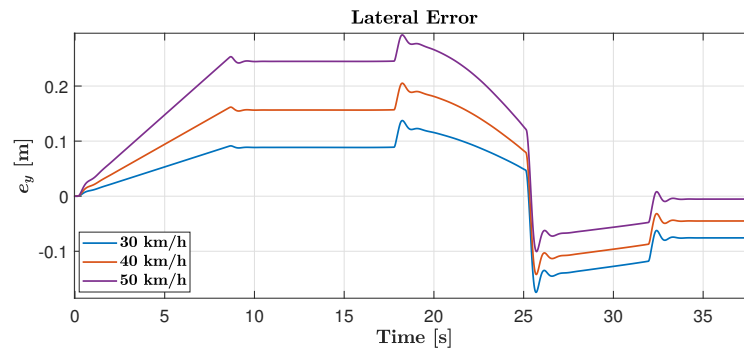


Figure 6-13: Reference Path with cross-wind direction

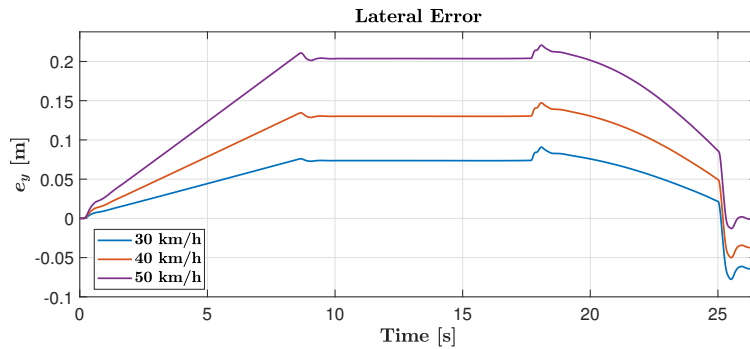
Figures 6-14a, 6-14b and 6-14c show the effect of cross-wind on the performance of path-tracking with the proposed controllers. The initial straight segment and the first left bend were the regions of cross-wind. There is a slight deviation due to the presence of wind, however, this lateral error is negligible (of the order of 0.03m), with the lowest error in the case of NSTMSTA.



(a) Proposed Solution for Super Twisting Algorithm at velocity = 40 km/h



(b) Modified Super Twisting Algorithm at velocity = 40 km/h



(c) Non-singular Terminal Modified Super Twisting Algorithm at velocity = 40 km/h

Figure 6-14: Robustness check of the developed controllers against cross-wind disturbances

Table 6-1 summarises the set of performance metrics to evaluate the performance of the bench-marking controllers. The numbers tabulated are for the simple case - which does not include localisation error, parametric variations and cross-wind. In an ideal scenario, it is clear that Stanley performs the best*.

Table 6-1: Bench-marking controllers performance summary

Vehicle Speed (km/h)	Controller	Lateral error (m)		Heading error (deg)	
		Absolute mean	Absolute max	Absolute mean	Absolute max
20	Stanley	0.0016	0.0173	1.3045	3.1361
	PCwP	0.0026	0.0224	1.9644	1.9644
	LQR	0.0179	0.0489	0.8068	4.4438
	II	0.0087	0.0290	1.3031	3.1493
	PBC	0.1089	0.4270	0.7821	5.199
40	Stanley	0.0304	0.0734	1.0874	2.9470
	PCwP	0.0061	0.2122	3.3708	3.6708
	LQR	0.0340	0.1601	0.5708	3.6321
	II	0.0093	0.1211	1.0546	2.9692
	PBC	0.0376	0.1035	0.5426	2.441
60	Stanley	0.0752	0.1907	1.0563	4.3293
	PCwP	0.0207	0.4608	5.3820	5.3820
	LQR	0.0452	0.3883	0.5165	5.3135
	II	0.0289	0.2531	0.9646	4.2408
	PBC	-	-	-	-
80	Stanley	0.0822	0.1967	1.1479	4.3317
	PCwP	0.0224	0.4632	5.4047	5.4047
	LQR	0.0492	0.3918	0.5606	5.3302
	II	0.0314	0.2591	1.0487	4.2485
	PBC	-	-	-	-

*PBC at high speeds produced a lot of low frequency oscillating steering could not be tuned

Table 6-2 summarises the set of performance metrics to evaluate the performance of the proposed SMC controllers. The numbers tabulated are for the simple case again. At low speeds, ST-proposed performs well, however, at higher speeds, NSTMST is seen to work better.

Table 6-2: Proposed controllers performance summary

Vehicle Speed (km/h)	Controller	Lateral error (m)		Heading error (deg)	
		Absolute mean	Absolute max	Absolute mean	Absolute max
20	ST - V1	0.0243	0.1184	1.2733	3.0619
	ST - Proposed	0.0249	0.1319	0.7516	1.8192
	MSTA	0.0248	0.1311	0.7510	0.8249
	NSTMSTA	0.0202	0.0990	1.2788	3.074
40	ST - V1	0.0315	0.1232	1.0609	2.6016
	ST - Proposed	0.0593	0.2168	0.5579	3.7180
	MSTA	0.0593	0.2162	0.5580	3.7184
	NSTMSTA	0.0294	0.1124	1.0636	2.5279
60	ST - V1	0.1697	0.4027	0.3442	3.4228
	ST - Proposed	0.1421	0.3958	0.5028	5.3839
	MSTA	0.1419	0.3964	0.5030	5.3837
	NSTMSTA	0.0737	0.2297	0.5560	3.7117
80	ST - V1	0.2846	0.6392	1.1479	4.2462
	ST - Proposed	0.1497	0.4067	0.5456	5.3994
	MSTA	0.1498	0.4069	0.5459	5.3998
	NSTMST	0.0781	0.2376	1.1142	4.2442

6-4 Summary

In a case where there is no measurement noise and uncertainties, Stanley and PCwP work the best with a mean lateral error and mean heading error of 0.0822m and 4.33 deg at about 80 km/h. In this regard, the best Sliding Mode Control - NSTMSTA has a mean lateral and heading error of 0.0781m and 1.1142 deg at 80 km/h. At lower speeds, both ST-proposed and NSTMSTA performed the best with a mean lateral error of around 0.03m. However, controller robustness is the main issue of concern and the proposed controllers were tested at different scenarios of disturbances. It was observed that NSTMSTA was the best controller when measurement noise was considered. With parametric variations, ST-proposed performed well as the changes in fluctuation of the lateral error was the least.

Conclusions and Recommendations

7-1 Conclusions

Firstly, a thorough study and implementation of bench-marking steering controllers is carried out. However, disturbances hamper the performance of such simple control laws and there is no possibility of disturbance rejection. A main requirement for such type of controllers is the nearest point algorithm which is implemented as a MATLAB function. A second order polynomial was fit between the nearest indices that allows accurate computation of the nearest point. However, for this computation, the way-points have to be equidistant from each other to generate a continuous lateral error signal.

To further improve the performance of Sliding Mode Control, three variants namely: Super Twisting Algorithm, Modified Super Twisting Algorithm, Non-singular Terminal Modified Super Twisting Algorithm were implemented. The gains of these controllers were tuned such that the lateral error was bounded between $\pm 0.5\text{m}$. However, there the chosen gains are not optimal and can be improved.

Furthermore, robustness characteristics of ST, MSTA and NSTMSTA were evaluated. With measurement noise being added as localisation error, the performance of NSTMSTA was clearly the best. A low frequency oscillatory behaviour of the steering wheel angle was observed in the case of ST-proposed which is clearly not desirable. The performance with respect to steering was found to be much better in the case of NSTMSTA and MSTA. Between the two, the former had better performance concerning lateral error.

Under parametric uncertainties, the cornering stiffness values were varied by $\pm 20\%$ and the controllers were evaluated based on their performance. In this regard, all controllers fared well with effective path tracking, ST outperforming the other two variants. The presence of cross-wind acts as a type of localisation error - a constant error rather than a uniformly fluctuation error. However, the difference in performance was minimal at 0.2m deviation for wind speeds upto 50 km/h with NSTMSTA performing the best. In addition, the proposed controllers had sufficient path-tracking for 20% increase in vehicle mass.

In conclusion, the domain of developing the best autonomous steering controller is vast and in this study, an attempt was made to design the best steering controller possible under external disturbances and uncertainties. Stanley - in the no disturbance case (deterministic) and ST-proposed and NSTMSTA were the stand out controllers for the given reference trajectory. The existing ST- Variant 1 is not effective at all, compared to the proposed controllers and gain tuning is extremely difficult. NSTMSTA can effectively deal with measurement uncertainties.

7-2 Recommendations

One of the main challenges concerning vehicle control for path-tracking is robustness and performance - in terms of computation time and accuracy in achieving the required control objective. To implement a controller on a real vehicle is not easy owing to measurement noise, hardware and software compatibility issues. The following suggestions in order of importance (highest first) are suggested by the author for researchers interested in taking this study forward.

1. Plant and model mismatch

The controllers developed in this thesis including the bench-marking controllers make use of a linear bicycle model for control design. This comes with a few disadvantages. Firstly, it is known that the tire forces are non-linear in nature. This implies that the expression $F_y = C_{\alpha f}\alpha$ is no longer valid for $\alpha > \alpha_0$ where α_0 is the slip angle at maximum lateral force. Secondly, this type of model is valid at lower vehicle speeds. In scenarios involving limit handling, one suggestion would be to use a force-based automatic steering system. If the forces could be measured/estimated accurately at every instant of time, it would then be possible to devise a control law that is a function of lateral forces instead of the cornering stiffness values.

Measuring forces on the tires are quite expensive and would be difficult with today's technological limitations. An alternate suggestion would be to use a higher DoF (Degrees of Freedom) vehicle model in place of a linear bicycle model. The non-inclusion of tire transient lateral forces affects brings in unmodeled lateral dynamics and hence affects the closed-loop behaviour. Planar vehicle model with Dugoff tyre model seems to capture lateral dynamics more accurately than a linear bicycle model as shown in Appendix B. An area of future work is to devise a steering controller based on planar vehicle model equations rather than a linear bicycle model.

2. Effect of longitudinal velocity on lane keeping

Many works of literature involving the study of automatic steering controllers treat the task of lane-keeping completely independent of longitudinal velocity. Although the steering controllers are tuned for different velocities, it can be said that it is not yet sufficient based on simulation results of the bench-marking controllers and Sliding Mode controllers shown in this thesis. The equation 2-9 shows that the reference path assumes a constant velocity in expressing the reference yaw rate. However, the vehicle in IPG CarMaker adjusts its longitudinal velocity based on the g-g diagram - maximum longitudinal and lateral accelerations. This is an important parameter during bends as there are restrictions on lateral accelerations - hence affecting longitudinal velocities. A solution would be to use the concept of 'trajectory'* instead of 'path'. This would further lead to a lateral dynamics model accounting for changes in longitudinal velocity.

3. Robustness capabilities of Sliding Mode Control

It is proven that Sliding Mode Control can handle unmodeled dynamics, parametric variations and external disturbances. Considering the equation, $\dot{x} = f(x, u) + h(x, u)u + \zeta$ where ζ is the term that accounts for unmodeled dynamics, the cardinal requirement is for this parameter to be a Lipschitz continuous function [†]. In other words, the bound ζ^+ is to be known to prove the derivative $\dot{\zeta}(t, \zeta_0)$ is bounded. Therefore, it becomes crucial to have more information about ζ . One suggestion would be to validate the vehicle model for control design significantly accurately and then add a known noise signal whose derivative is bounded and is known.

4. Sampling frequency

The nature of an automatic steering system is that the plant to be controlled evolves continuously. The steering controller is required to generate steering inputs that fulfill the required objective - in this case, reducing the lateral error to zero. However, the tested controllers in this thesis are continuous in nature. In other words, simulation frequency of 1000 Hz is used (except for a lone case of testing the controller at lower sampling period). For real-life implementation, however, much lower sampling rates of the rate of 25-50 Hz is required. This becomes a tricky issue at higher vehicle speeds. For example, for speeds in the range of 25m/s and a sampling period of 0.04 seconds(25 Hz), the vehicle moves 1m every time step. In the simulations considered for this thesis, the vehicle moves about 0.02m for speeds of 80km/h. Therefore, it is important to add sampling periods and evaluate controller performance.

*In literature, a trajectory is defined as a path with known reference longitudinal velocity at each way-point

[†]A real-valued function $f : R \rightarrow R$ is called Lipschitz continuous if there exists a positive real constant K such that, for all real x_1 and x_2 , $|f(x_1) - f(x_2)| \leq K|x_1 - x_2|$ is satisfied.

Appendix A

Vehicle Dynamics Parameters, Controller gains, Model Validation

A-1 Vehicle Dynamics Parameters

Parameter	Value
Overall mass of the vehicle (m)	1620 Kg
Distance of CoG from front axle (l_f)	1.075 m
Distance of CoG from rear axle (l_r)	1.725 m
Vehicle moment of inertia about Z-axis (I_z)	2253 Kgm ²
Co-efficient of friction (μ)	1
Height of CoG (h_{cg})	0.589 m
Steering Ratio (SR)	19.2
Cornering Stiffness of front axle ($C_{\alpha f}$)	150000 N/rad
Cornering Stiffness of rear axle ($C_{\alpha r}$)	110000 N/rad
Effective radius of the wheel (r_w)	0.3 m
Track Width (B)	1.52

Table A-1: Vehicle Dynamics Parameters - Toyota Camry

A high pass filter was used to compute the derivative of the lateral error. The continuous and discrete time transfer functions of such a filter are given by equations A-1 and A-2

Continuous Time:

$$G_c = \frac{s}{0.03183s + 1} \quad (\text{A-1})$$

Discrete Time:

$$G_d = \frac{31.42z - 31.42}{z - 0.9691} \quad (\text{A-2})$$

A-2 Controller Gains

Longitudinal Velocity u Kmph	k_{stan}
10	2
20	2
40	2
60	2
80	2

Table A-2: Stanley gains

Longitudinal Velocity u Kmph	Look-ahead time t_{la} (s)	k_{ff}
10	0.4	0.5
20	0.4	0.5
40	0.4	0.5
60	0.35	0.52
80	0.4	0.54

Table A-3: Path Controller gains

$$Q = \begin{bmatrix} 1.2 & 0 & 0 & 0 \\ 0 & 0 & 0 & 0 \\ 0 & 0 & 1.2 & 0 \\ 0 & 0 & 0 & 0 \end{bmatrix}$$

Longitudinal Velocity (u)	R	k_{stan}
10	10	0.6
20	20	0.6
40	40	0.6
60	60	0.75
80	80	0.8

Table A-4: LQR gains

A-3 Planar Vehicle Model Validation

Longitudinal Velocity u Kmph	K_1	K_2	λ
10	0.9831	0.0427	3.5169
20	0.9835	0.0498	4.0165
40	0.9851	0.0598	5.0149
60	1.2048	0.1021	4.8952
80	1.2945	0.1319	5.3055

Table A-5: Immersion and Invariance gains

Parameter	Value
Proportional gain k_P	0.01
Integral gain k_I	0.0009
Reduction rate k_0	5
Max. admissible error e_{max}	0.1
Convergenve rate λ_{PBC}	2

Table A-6: Passivity Based Control

Longitudinal Velocity u Kmph	Convergence rate λ_{ST}	C_0
10	5	0.08
20	5	0.08
40	6	0.2
60	8	0.8
80	9	0.9

Table A-7: Sliding mode control gains - Variant 1 - ST

Parameter	Value
λ_1	0.1
λ_2	0.1
λ	10
ζ^+	0.005

Table A-8: Sliding Mode Control gains - ST proposed

Parameter	Value
k_1	0.1
k_2	1.2
k_3	0.05
k_4	3.728
λ	10

Table A-9: Sliding Mode Control gains - MST

Parameter	Value
Convergence rate λ_1	10
Convergence rate λ_2	0.1
α	0.8
β	0.28
k_1	0.1
k_2	1.2
k_3	0.05
k_4	3.728

Table A-10: Sliding Mode Control gains - NSTMST

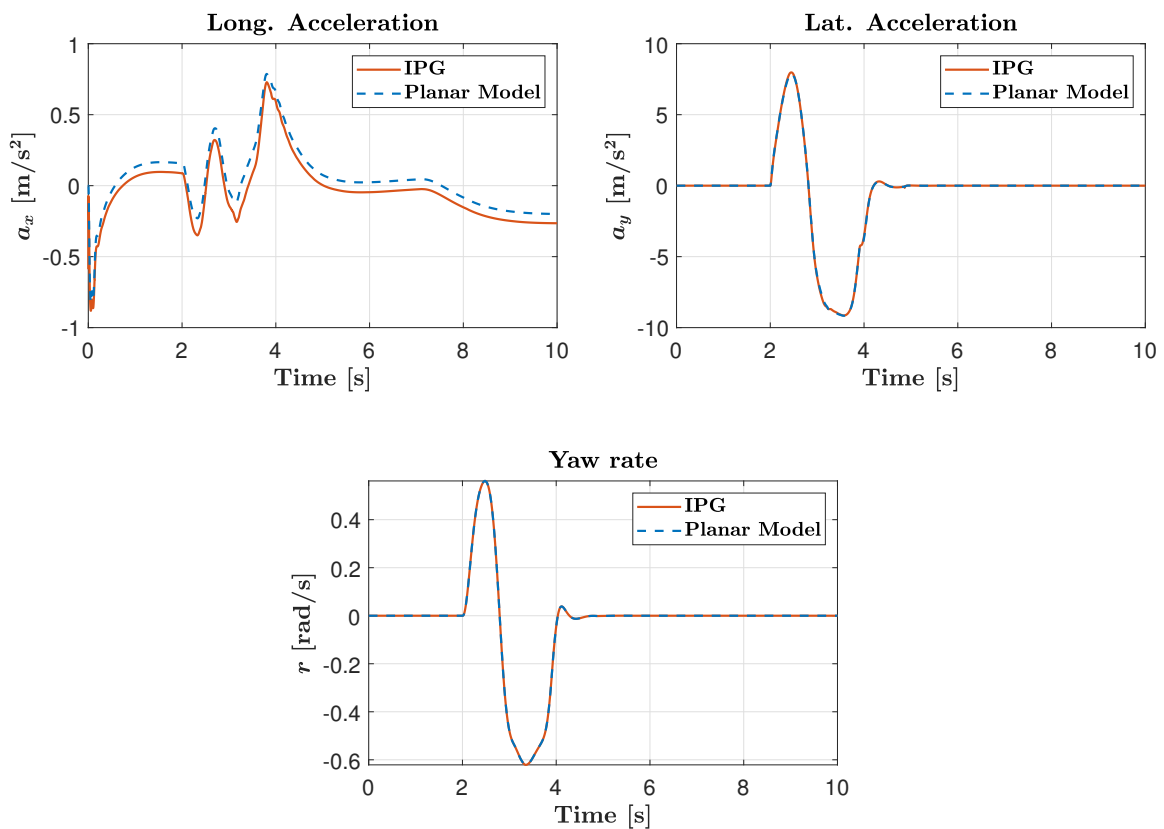


Figure A-1: Validation of Planar Model - sine with dwell steering input at 60 kmph

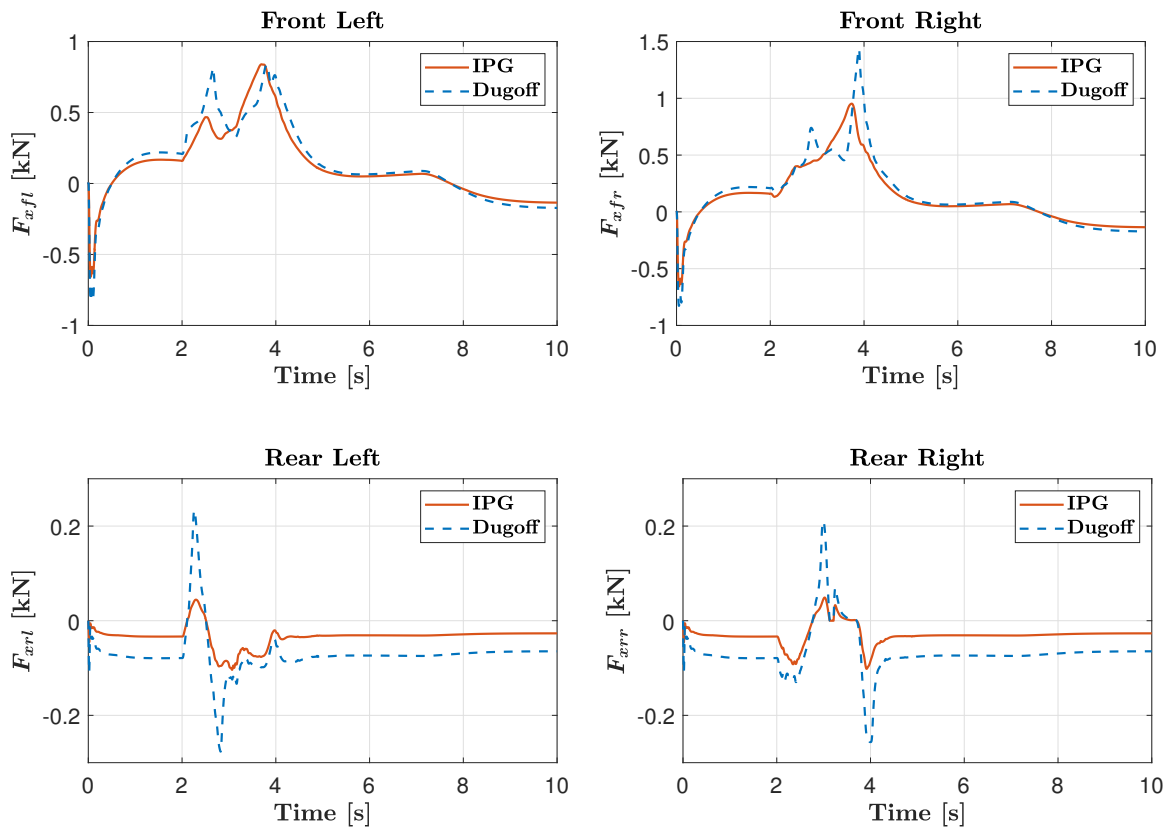


Figure A-2: Tyre Model Validation - Longitudinal Tyre Forces

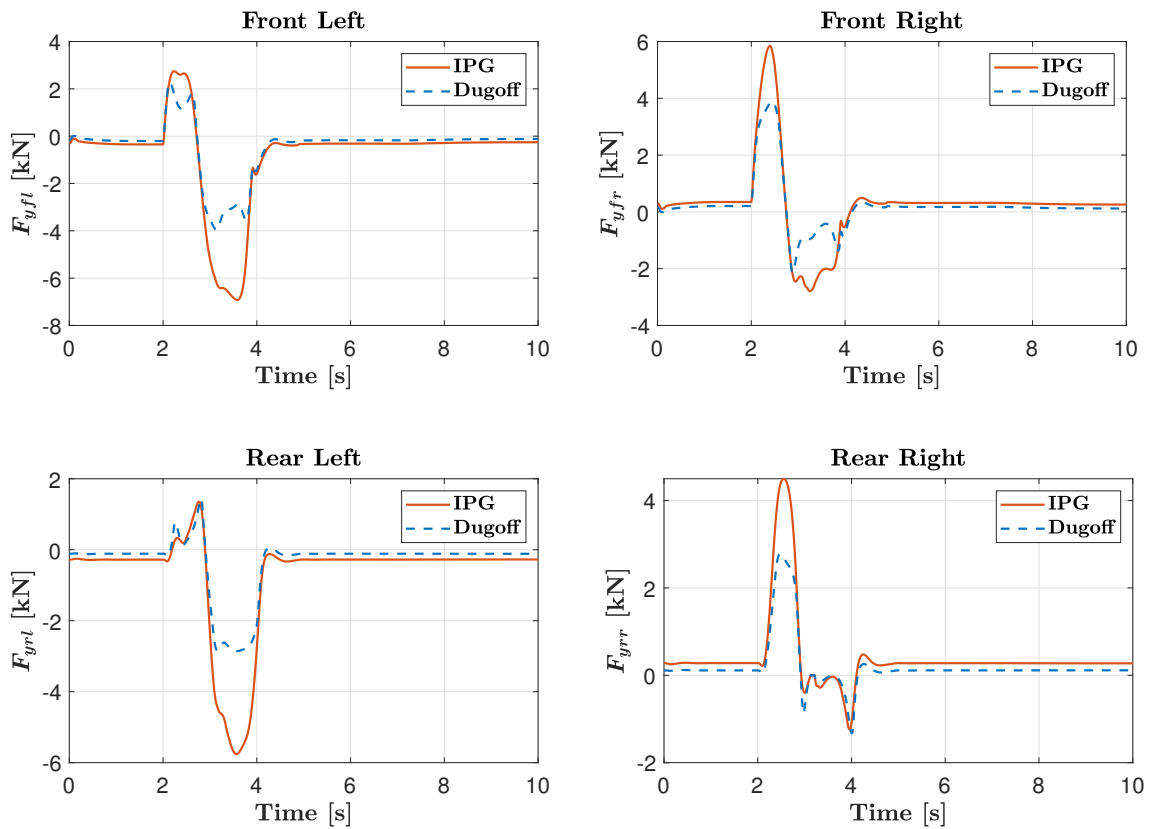


Figure A-3: Tyre Model Validation - Lateral Tyre Forces

Results - Bench-marking Controllers

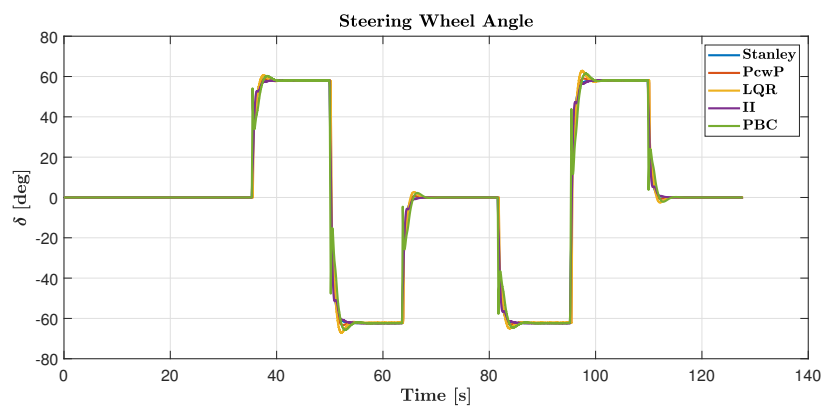


Figure B-1: Steering Wheel Angle at velocity = 20 km/h

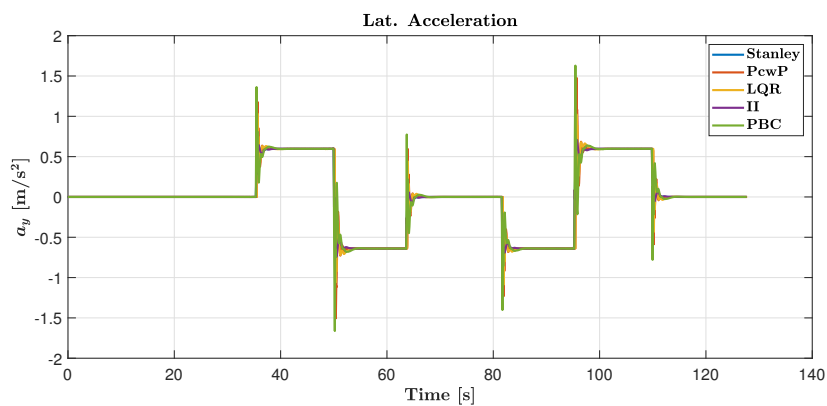


Figure B-2: Lateral acceleration at velocity = 20 km/h

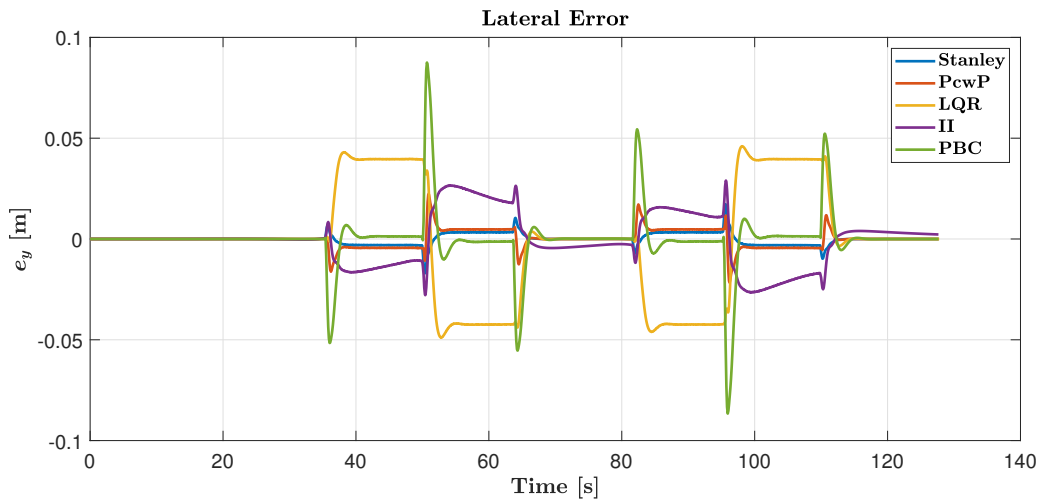


Figure B-3: Lateral error at velocity = 20 km/h

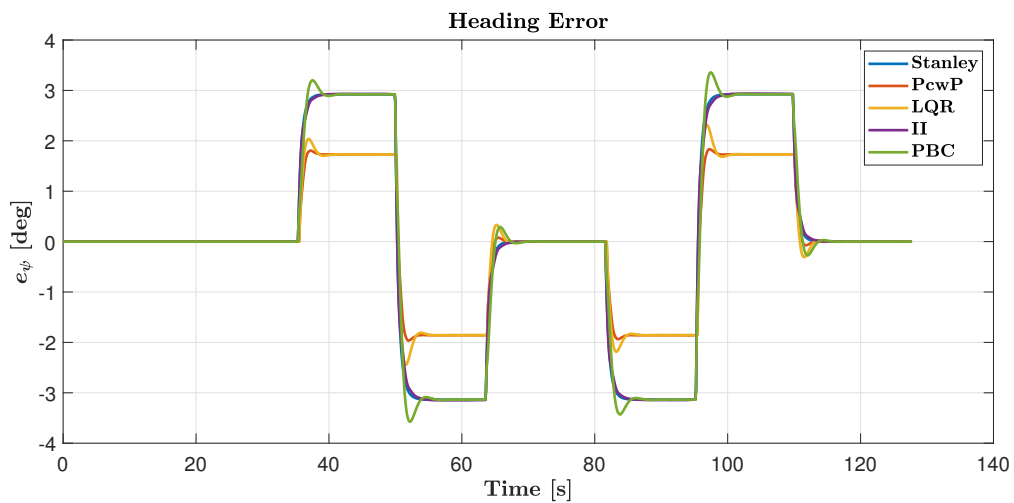


Figure B-4: Heading error at velocity = 20 km/h

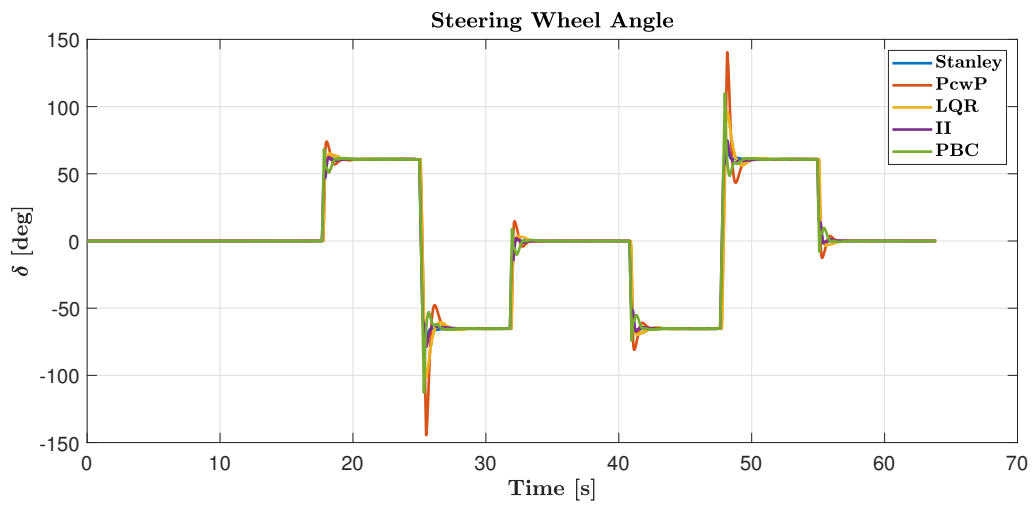


Figure B-5: Steering Wheel Angle at velocity = 40 km/h

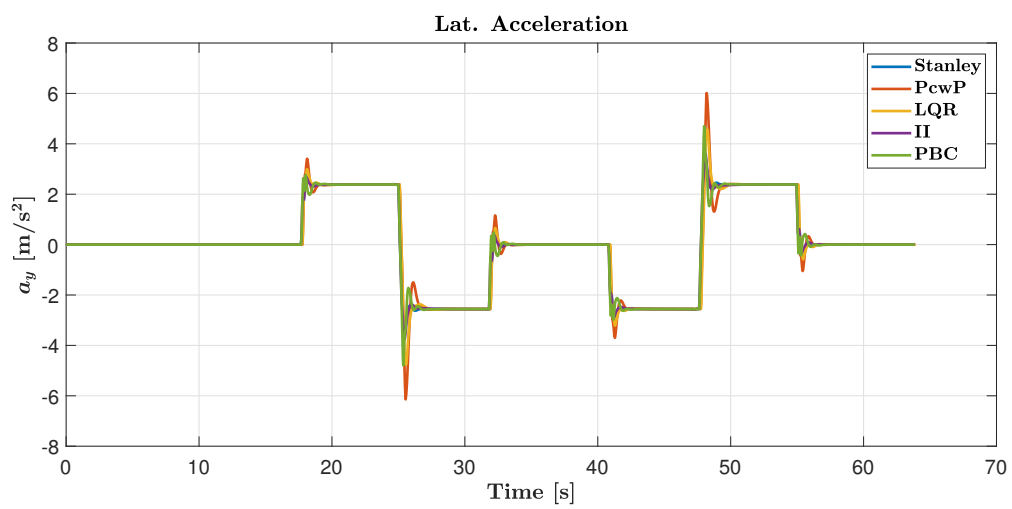


Figure B-6: Lateral acceleration at velocity = 40 km/h

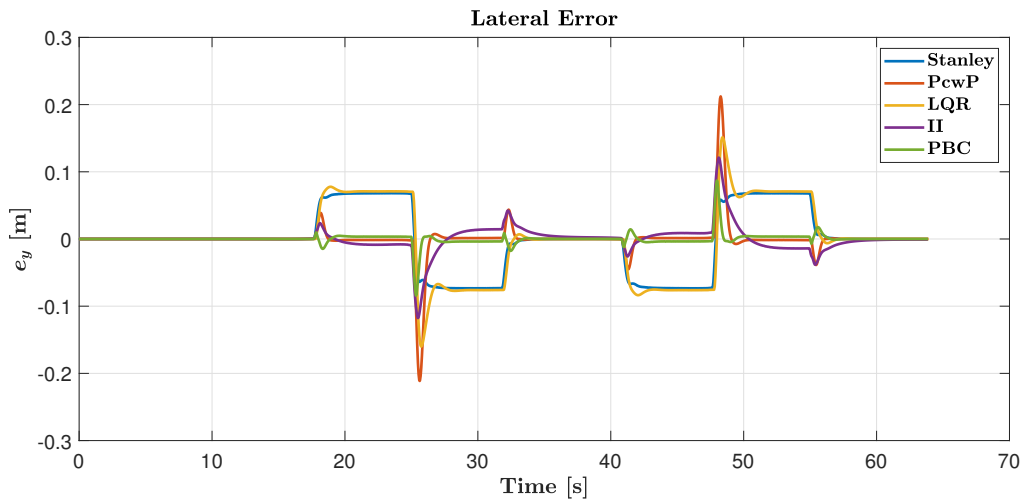


Figure B-7: Lateral error at velocity = 40 km/h

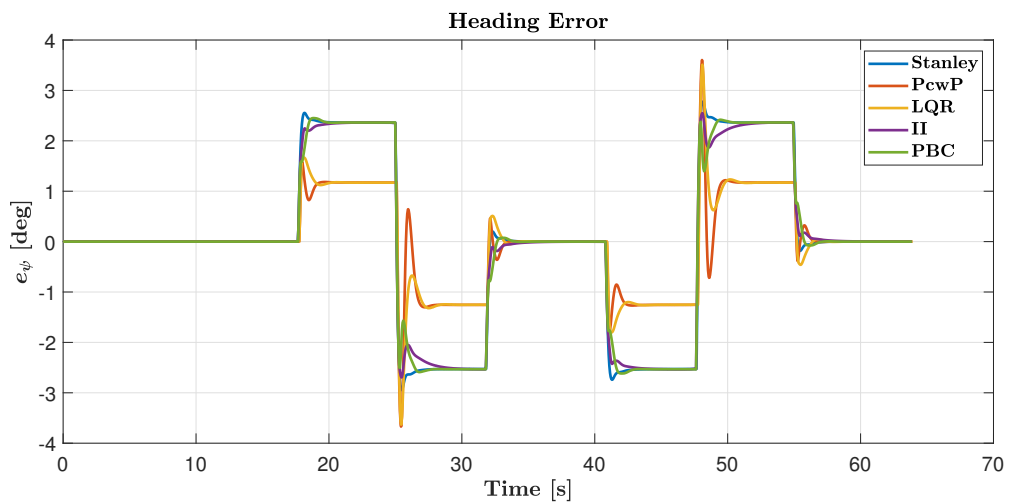


Figure B-8: Heading error at velocity = 40 km/h

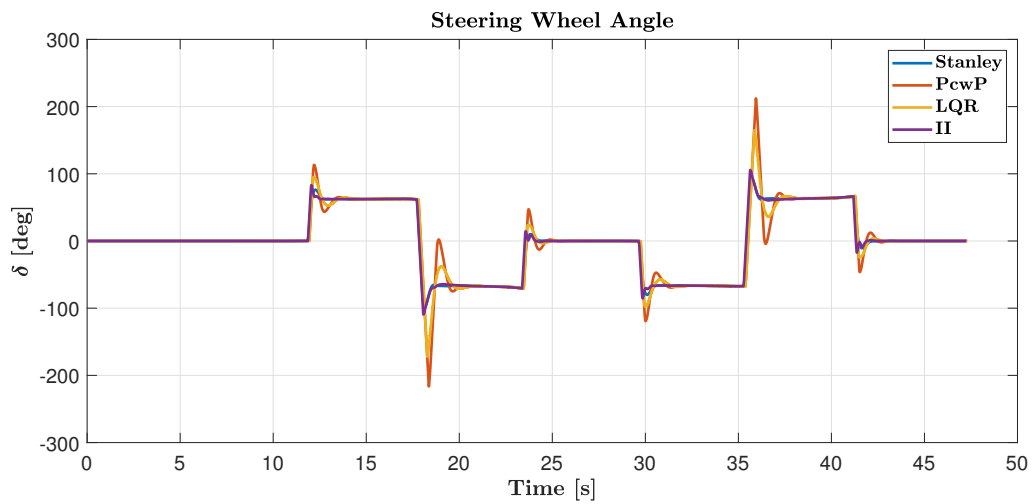


Figure B-9: Steering Wheel Angle at velocity = 60 km/h

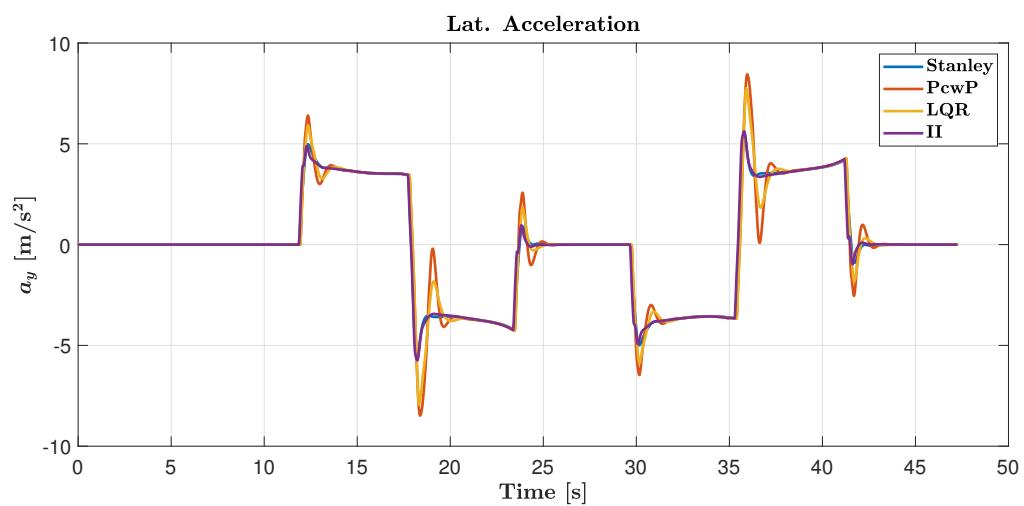


Figure B-10: Lateral acceleration at velocity = 60 km/h

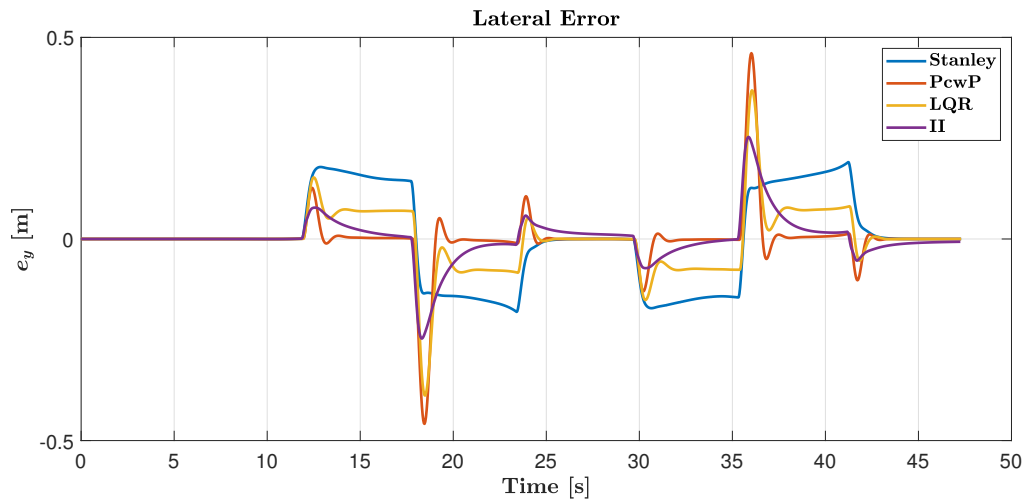


Figure B-11: Lateral error at velocity = 60 km/h

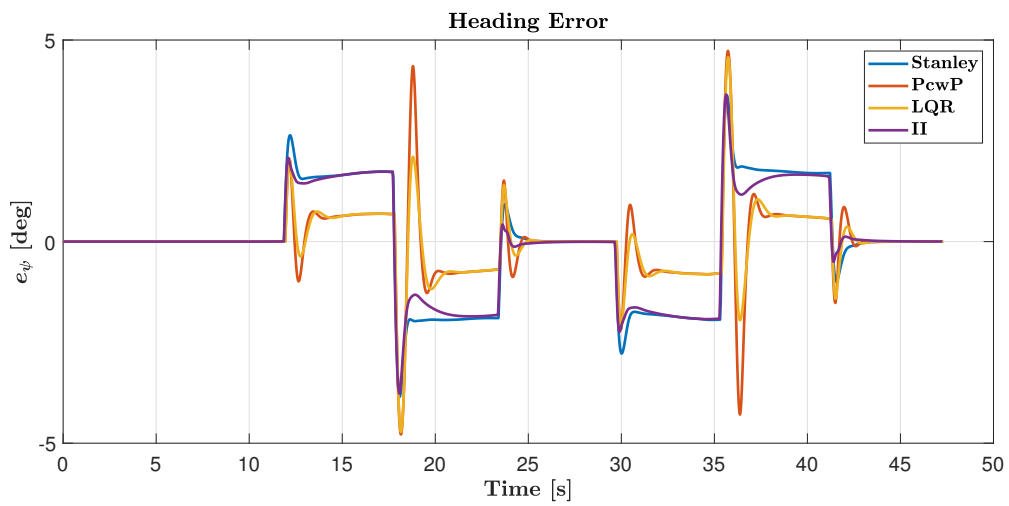


Figure B-12: Heading error at velocity = 60 km/h

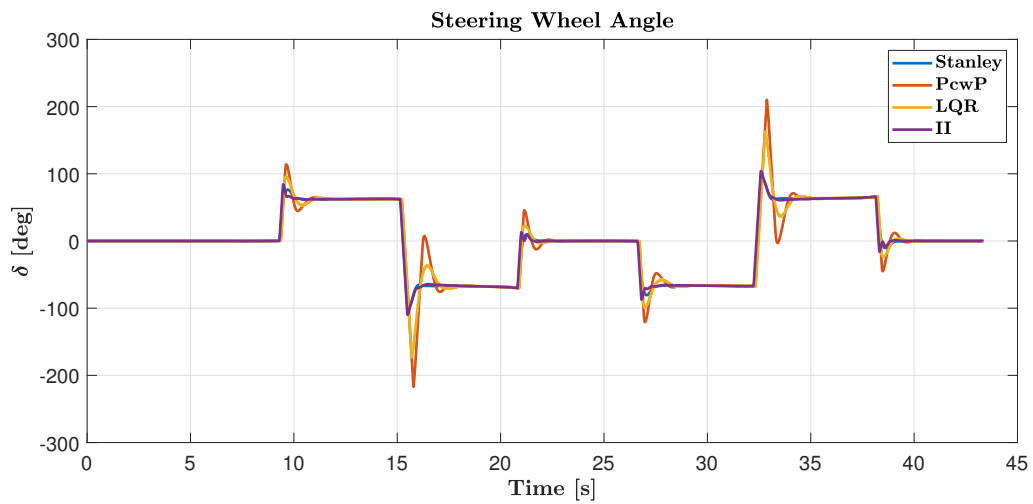


Figure B-13: Steering Wheel Angle at velocity = 80 km/h

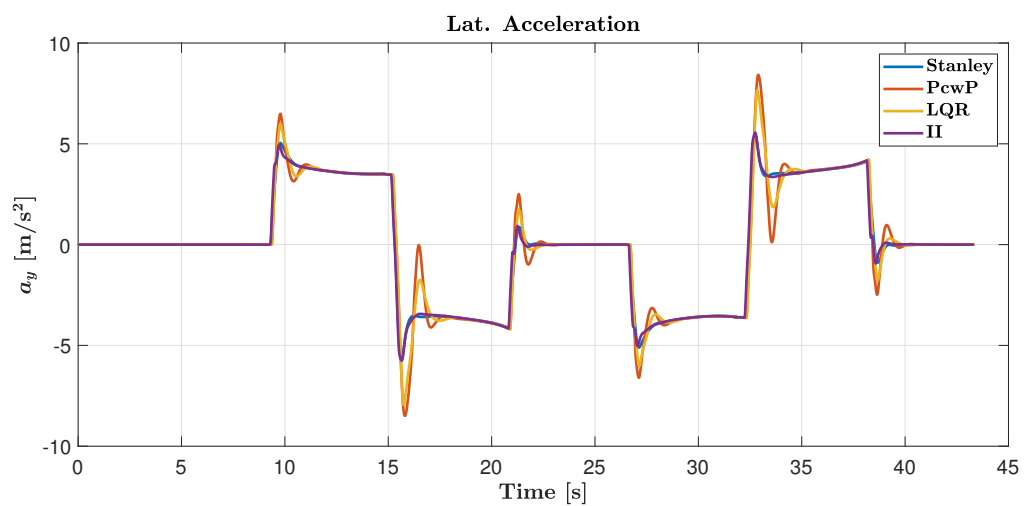


Figure B-14: Lateral acceleration at velocity = 80 km/h

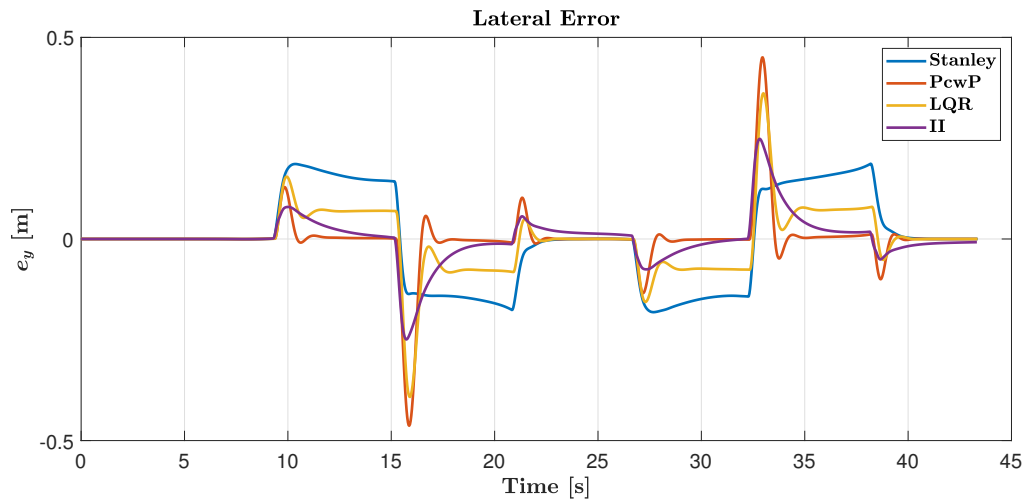


Figure B-15: Lateral error at velocity = 80 km/h

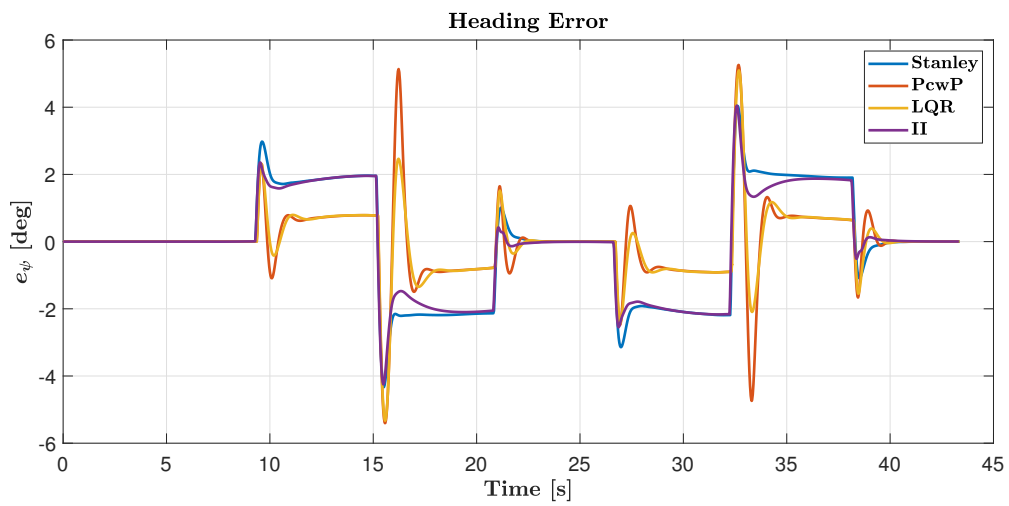


Figure B-16: Heading error at velocity = 80 km/h

Rate of lateral error estimation

In this section, a method to estimate the rate of lateral error accurately is described. The method explained here is by using a non-linear observer that estimates the rate of lateral error. It is found in literature that one of the requirements of Higher Order Sliding Mode Controllers is the access of information about higher order derivatives of the error measurement. In the case of vehicle lateral control for a path follower, a first order derivative is required. It is found that the linear filter implemented in this thesis produces a small amount of chattering. To curb this issue, a non-linear filter based on Modified Super Twisting Observer is summarized. Figure C-1 represents a block diagram of the observer and the controller.

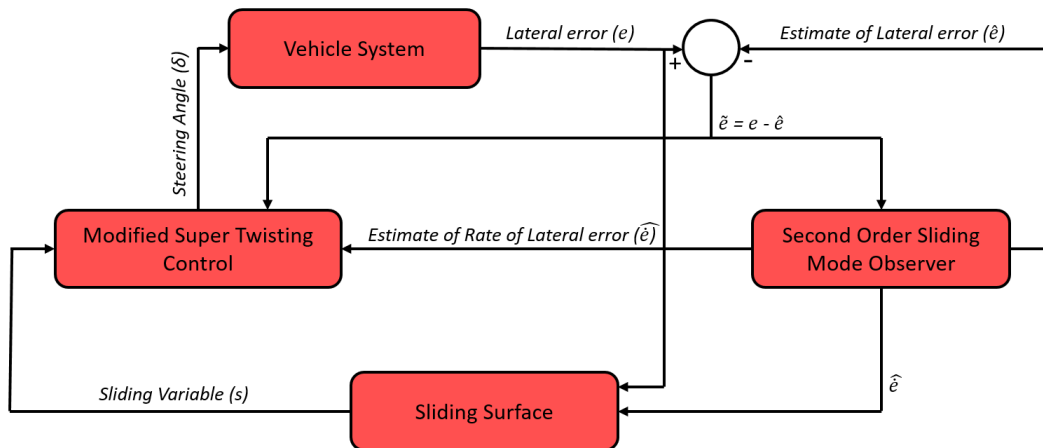


Figure C-1: Block Diagram of a Non-singular Terminal Modified Super Twisting Algorithm using a Modified Super Twisting Observer

The same lateral error dynamics equation given by 5-1 is considered,

$$\ddot{e}_y = -\frac{\mu(C_f + C_r)}{m}\beta - \frac{\mu(l_f C_f - l_r C_r)}{mV_x}\dot{\psi} - V_x^2 \rho + \frac{\mu C_f}{m}\delta$$

$$\dot{z}_1 = z_2 \quad (\text{C-1})$$

$$\dot{z}_2 = \underbrace{-\frac{\mu(C_f + C_r)}{m}\beta - \frac{\mu(l_f C_f - l_r C_r)}{mV_x}\dot{\psi} - V_x^2 \rho}_{f(\theta)} + \underbrace{\frac{\mu C_f}{m}}_{h(\theta)} \delta \quad (\text{C-2})$$

Considering that there is access to the measurement e_y in real world scenarios, a sliding mode observer based on modified super twisting algorithm is proposed as follows. This observer is supposed to mimic the plant dynamics and estimate derivatives of the plant states, thereby estimating \dot{e}_y .

Considering an observer whose dynamics are given,

$$\dot{\hat{z}}_1 = \hat{z}_2 + l_1 \quad (\text{C-3})$$

$$\dot{\hat{z}}_2 = f(\theta) + h(\theta)\delta + l_2 \quad (\text{C-4})$$

where the quantities l_1 and l_2 are given by,

$$l_1 = k_1 |\tilde{z}_1|^{\frac{1}{2}} \text{sign}(\tilde{z}_1) + k_2 \tilde{z}_1 \quad (\text{C-5})$$

$$l_2 = k_3 \text{sign}(\tilde{z}_1) + k_4 \tilde{z}_1 \quad (\text{C-6})$$

The equations shown above in C-5 and C-6 has the same structure as the equations given in 5-27a and 5-27b. Based on the proof given as per Chapter 5-3, the above equations are asymptotically stable provided that $4k_3k_4 > (8k_3 + 9k_1^2)k_2^2$ is satisfied. However, the estimate z_2 has to be accounted in the sliding surface. Furthermore, the modified super twisting controller has to be redesigned accordingly.

Consider the new sliding surface,

$$s = \dot{e} + \lambda e$$

with,

$$e = z_1 - z_{1_d}$$

$$\dot{e} = \hat{z}_2 - z_{2_d}$$

where λ is a positive constant. On considering the first derivative of the surface surface with time,

$$\begin{aligned} \dot{s} &= \ddot{e} + \lambda \dot{e} \\ &= \dot{\hat{z}}_2 - \dot{z}_{2_d} + \lambda(\dot{z}_1 - \dot{z}_{1_d}) \end{aligned} \quad (\text{C-7})$$

Assuming that after a certain time $t_0 \geq T_0$, it results that $z_1 = \hat{z}_1, z_2 = \hat{z}_2, \dot{z}_1$ can be interchanged with \dot{z}_2 which results as follows.

$$\begin{aligned}\dot{s} &= \dot{\hat{z}}_2 - z_{2_d} + \lambda \hat{z}_2 - \lambda z_{1_d} \\ &= \lambda \hat{z}_2 - \lambda z_{1_d} - z_{2_d} + f(\theta) + h(\theta)\delta + k_2 \text{sign}(\tilde{z}_1) + k_4 \tilde{z}_1\end{aligned}\quad (\text{C-8})$$

C-8 is arrived upon substituting C-4 and C-6. In order push the sliding variable s to zero, the sliding dynamics has to be fed by a control law that asymptotically stabilises the closed-loop system. The same control law will further track the reference trajectory. It should be kept in mind that z_{1_d} and z_{2_d} are zeros since lateral error dynamics is being considered. A control law is proposed using Modified Super Twisting seen in Chapter 5 earlier.

$$\begin{aligned}\delta &= \frac{1}{h(\theta)} \left(-f(\theta) - \lambda \hat{z}_2 - m_1 |s|^{\frac{1}{2}} \text{sign}(s) - m_2 s - k_2 \text{sign}(\tilde{z}_1) - k_4 \tilde{z}_1 \right. \\ &\quad \left. m_1 |s|^{\frac{1}{2}} \text{sign}(s) - m_2 s - m_3 \int_0^t \text{sign}(s) d\tau - m_4 \int_0^t s d\tau \right)\end{aligned}\quad (\text{C-9})$$

Substituting the equation C-9 in sliding surface dynamics C-8, the following closed loop system is obtained.

$$\dot{s} = -m_1 |s|^{\frac{1}{2}} \text{sign}(s) - m_2 s - m_3 \int_0^t \text{sign}(s) d\tau - m_4 \int_0^t s d\tau \quad (\text{C-10})$$

Referring to the proof of Modified Super Twisting Algorithm as derived in Chapter 5, the above closed loop dynamics is stable for $4m_3 m_4 > (8m_3 + 9m_1^2)m_2^2$. Hence the proposed control law is stable. This entire formulation is called "Sliding Mode Control using Modified Super Twisting Algorithm using Modified Super Twisting Observer".

Bibliography

- [1] “Nicholas-joseph cugnot and the automobile.” <http://scihi.org/nicholas-joseph-cugnot-and-the-automobile/>. Accessed: 2015-09-25.
- [2] “Global car sales.” <https://www.statista.com/statistics/200002/international-car-sales-since-1990/>. Accessed: 2019-07-12.
- [3] “Road safety facts.” <https://www.asirt.org/safe-travel/road-safety-facts/>.
- [4] M. Damena, D. K. Geleta, and T. Gobena, *Trend of Road Traffic Collision Fatality and Associated Factors in South West Shoa Romia Ethiopia*. PhD thesis, Haramaya University, 2017.
- [5] “Advanced driver assistant systems.” https://ec.europa.eu/transport/road_safety/sites/roadsafety/files/ersosynthesis2016-adas15_en.pdf/. Accessed: 2015-09-25.
- [6] G. Lehmann and A. Cheale, “The contribution of onboard recording systems to road safety and accident analysis,” 1998.
- [7] “Advanced driver assistant systems.” <https://www.rosipa.com/rospaweb/docs/advice-services/road-safety/road-crashes-overview.pdf>. Accessed: 2017-11-01.
- [8] “Human error as a cause of vehicle crashes.” <http://cyberlaw.stanford.edu/blog/2013/12/human-error-cause-vehicle-crashes>. Accessed: 2013-12-18.
- [9] “Waymo safety report.” <https://www.mtfchallenge.org/wp-content/uploads/2017/02/waymo-safety-report-2017-10.pdf>. Accessed: 2017-10-01.
- [10] T. Holstein, G. Dodig-Crnkovic, and P. Pelliccione, “Ethical and social aspects of self-driving cars,” *arXiv preprint arXiv:1802.04103*, 2018.
- [11] A. Kunnappillil Madhusudhanan, “Lateral vehicle dynamics control and vehicle state estimation,” 2016.

- [12] “Lane keeping assist systems.” <https://www.vda.de/en/topics/safety-and-standards/lkas/lane-keeping-assist-systems.html>.
- [13] C. Keatmanee, S. Jakborvornphan, C. Potiwanna, W. San-Uml, and M. N. Dailey, “Vision-based lane keeping - a survey,” *2018 International Conference on Embedded Systems and Intelligent Technology & International Conference on Information and Communication Technology for Embedded Systems (ICESIT-ICICTES)*, pp. 1–6, 2018.
- [14] E. E. Nodine, A. H. Lam, W. G. Najm, and J. J. Ference, “Safety impact of an integrated crash warning system based on field test data.,” 2011.
- [15] S. A. Birrell, M. Fowkes, and P. A. Jennings, “Effect of using an in-vehicle smart driving aid on real-world driver performance,” *IEEE Transactions on Intelligent Transportation Systems*, vol. 15, no. 4, pp. 1801–1810, 2014.
- [16] S. Sternlund, J. Strandroth, M. Rizzi, A. Lie, and C. Tingvall, “The effectiveness of lane departure warning systems – A reduction in real-world passenger car injury crashes,” *Traffic injury prevention*, vol. 18, no. 2, pp. 225–229, 2017.
- [17] J. Pohl and J. Ekmark, “A lane keeping assist system for passenger cars - design aspects of the user interface,” 2003.
- [18] Y. Bian, J. Ding, M. Hu, Q. Xu, J. Wang, and K. Li, “An advanced lane-keeping assistance system with switchable assistance modes,” *IEEE Transactions on Intelligent Transportation Systems*, 2019.
- [19] J. M. Snider *et al.*, “Automatic steering methods for autonomous automobile path tracking,” 2009.
- [20] M. A. Sotelo, “Lateral control strategy for autonomous steering of ackerman-like vehicles,” *Robotics and Autonomous Systems*, vol. 45, no. 3-4, pp. 223–233, 2003.
- [21] Z. Lu, B. Shyrokau, B. Boulkroune, S. Van Aalst, and R. Happee, “Performance benchmark of state-of-the-art lateral path-following controllers,” in *2018 IEEE 15th International Workshop on Advanced Motion Control (AMC)*, pp. 541–546, IEEE, 2018.
- [22] G. Collares Pereira, “Model predictive control for autonomous driving of over-actuated research vehicle,” 2016.
- [23] N. H. Amer, H. Zamzuri, K. Hudha, and Z. A. Kadir, “Modelling and control strategies in path tracking control for autonomous ground vehicles: a review of state of the art and challenges,” *Journal of Intelligent & Robotic Systems*, vol. 86, no. 2, pp. 225–254, 2017.
- [24] B. Paden, M. Čáp, S. Z. Yong, D. Yershov, and E. Frazzoli, “A survey of motion planning and control techniques for self-driving urban vehicles,” *IEEE Transactions on intelligent vehicles*, vol. 1, no. 1, pp. 33–55, 2016.
- [25] J. Jiang and A. Astolfi, “Lateral control of an autonomous vehicle,” *IEEE Transactions on Intelligent Vehicles*, vol. 3, no. 2, pp. 228–237, 2018.
- [26] H. B. Pacejka, “Tyre and vehicle dynamics, 2002,” *Butterworth-Heinemann, ISBN 0*, vol. 7506, no. 5141, p. 5, 2006.

-
- [27] M. Abe, *Vehicle handling dynamics: theory and application*. Butterworth-Heinemann, 2015.
- [28] IPGAutomotive, *IPG CarMaker Reference Manual*, 2018.
- [29] R. Rajamani, *Vehicle dynamics and control*. Springer Science & Business Media, 2011.
- [30] S. Pendleton, H. Andersen, X. Du, X. Shen, M. Meghjani, Y. Eng, D. Rus, and M. Ang, “Perception, planning, control, and coordination for autonomous vehicles,” *Machines*, vol. 5, no. 1, p. 6, 2017.
- [31] S. Thrun, M. Montemerlo, H. Dahlkamp, D. Stavens, A. Aron, J. Diebel, P. Fong, J. Gale, M. Halpenny, G. Hoffmann, *et al.*, “Stanley: The robot that won the darpa grand challenge,” *Journal of field Robotics*, vol. 23, no. 9, pp. 661–692, 2006.
- [32] A. Schmeitz, J. Zegers, J. Ploeg, and M. Alirezaei, “Towards a generic lateral control concept for cooperative automated driving theoretical and experimental evaluation,” in *2017 5th IEEE International Conference on Models and Technologies for Intelligent Transportation Systems (MT-ITS)*, pp. 134–139, IEEE, 2017.
- [33] K. J. Aström and R. M. Murray, *Feedback systems: an introduction for scientists and engineers*. Princeton university press, 2010.
- [34] G. Tagne, R. Talj, and A. Charara, “Immersion and invariance control for reference trajectory tracking of autonomous vehicles,” in *16th International IEEE Conference on Intelligent Transportation Systems (ITSC 2013)*, pp. 2322–2328, IEEE, 2013.
- [35] A. Astolfi, D. Karagiannis, and R. Ortega, *Nonlinear and adaptive control with applications*. Springer Science & Business Media, 2007.
- [36] J. A. Acosta, R. Ortega, A. Astolfi, and A. D. Mahindrakar, “Interconnection and damping assignment passivity-based control of mechanical systems with underactuation degree one,” *IEEE Transactions on Automatic Control*, vol. 50, no. 12, pp. 1936–1955, 2005.
- [37] G. Tagne, R. Talj, and A. Charara, “Design of passivity-based controllers for lateral dynamics of intelligent vehicles,” in *2015 IEEE Intelligent Vehicles Symposium (IV)*, pp. 1044–1049, IEEE, 2015.
- [38] G. Tagne, R. Talj, and A. Charara, “Design and comparison of robust nonlinear controllers for the lateral dynamics of intelligent vehicles,” *IEEE Transactions on Intelligent Transportation Systems*, vol. 17, no. 3, pp. 796–809, 2015.
- [39] Y. Shtessel, C. Edwards, L. Fridman, and A. Levant, *Sliding mode control and observation*. Springer, 2014.
- [40] K. Holkar and L. M. Waghmare, “Sliding mode control with predictive pid sliding surface for improved performance,” 2013.
- [41] A. Sorniotti, P. Barber, and S. De Pinto, “Path tracking for automated driving: A tutorial on control system formulations and ongoing research,” in *Automated Driving*, pp. 71–140, Springer, 2017.

- [42] F. Muñoz, M. Bonilla, I. González-Hernández, S. Salazar, and R. Lozano, “Super twisting vs modified super twisting algorithm for altitude control of an unmanned aircraft system,” in *2015 12th International Conference on Electrical Engineering, Computing Science and Automatic Control (CCE)*, pp. 1–6, IEEE, 2015.
- [43] F. Muñoz, E. S. Espinoza, I. González-Hernández, S. Salazar, and R. Lozano, “Robust trajectory tracking for unmanned aircraft systems using a nonsingular terminal modified super-twisting sliding mode controller,” *Journal of Intelligent & Robotic Systems*, vol. 93, no. 1-2, pp. 55–72, 2019.
- [44] F. Munoz, M. Bonilla, E. S. Espinoza, I. González, S. Salazar, and R. Lozano, “Robust trajectory tracking for unmanned aircraft systems using high order sliding mode controllers-observers,” in *2017 International Conference on Unmanned Aircraft Systems (ICUAS)*, pp. 346–352, IEEE, 2017.
- [45] J. A. Moreno, “Lyapunov function for levant’s second order differentiator,” in *2012 IEEE 51st IEEE Conference on Decision and Control (CDC)*, pp. 6448–6453, IEEE, 2012.

Glossary

List of Acronyms

ASIRT	Association of Safe International Road Travel
DARPA	Defense Advanced Research Projects Agency
ADAS	Advanced Driver Assistant Systems
ACC	Adaptive Cruise Control
ABS	Anti-lock Braking Systems
CA	Collision Avoidance
LKS	Lane Keeping Systems
HMI	Human Machine Interface
GCS	Global Coordinate System
LCS	Local Coordinate System
CoG	Center of Gravity
RRT	Rapidly exploring Random Trees
RRT*	Optimal Rapidly Exploring Random Trees
PRM	Probabilistic Road Maps
PCwP	Path Control with Preview
LQR	Linear Quadratic Regulator
II	Immersion and Invariance
PBC	Passivity Based Control
SMC	Sliding Mode Control

STA	Super Twisting Algorithm
MSTA	Modified Super Twisting Algorithm